LD

AFWAL-TR-81-4070
ADA111397

MECHANICAL SPECTROSCOPY FOR EPOXY RESINS

UNIVERSITY OF PITTSBURGH
DEPARTMENT OF MECHANICAL ENGINEERING
PITTSBURGH, PA 15261

AUGUST 1981

FINAL REPORT FOR PERIOD 26 SEPTEMBER 1977 - 2 JANUARY 1981

Approved for public release; distribution unlimited

AIR FORCE MATERIALS LABORATORY
AIR FORCE WRIGHT AERONAUTICAL LABORATORIES
AIR FORCE SYSTEMS COMMAND
WRIGHT-PATTERSON AIR FORCE BASE, OHIO 45433

Best Available Copy

20040223019

NOTICE

When Government drawings, specifications, or other data are used for any purpose other than in connection with a definitely related Government procurement operation, the United States Government thereby incurs no responsibility nor any obligation whatsoever; and the fact that the government may have formulated, furnished, or in any way supplied the said drawings, specifications, or other data, is not to be regarded by implication or otherwise as in any manner licensing the holder or any other person or corporation, or conveying any rights or permission to manufacture use, or sell any patented invention that may in any way be related thereto.

This report has been reviewed by the Office of Public Affairs (ASD/PA) and is releasable to the National Technical Information Service (NTIS). At NTIS, it will be available to the general public, including foreign nations.

This technical report has been reviewed and is approved for publication.

WILLIAM B. JONES, JR., PhD, Matls Rsch Engr.
Composites, Adhesives & Fibrous Matls Br
Nonmetallic Materials Division

THEODORE J. REINHART, JR., Chief
Composites, Adhesives & Fibrous Matls Br
Nonmetallic Materials Division

FOR THE COMMANDER

FRANKLIN D. CHERRY, Chief
Nonmetallic Materials Division

"If your address has changed, if you wish to be removed from our mailing list, or if the addressee is no longer employed by your organization please notify AFWAL/MLBC, W-PAFB, OH 45433 to help us maintain a current mailing list".

Copies of this report should not be returned unless return is required by security considerations, contractual obligations, or notice on a specific document.

AIR FORCE/56780/20 January 1982 — 210

UNCLASSIFIED

SECURITY CLASSIFICATION OF THIS PAGE *(When Data Entered)*

REPORT DOCUMENTATION PAGE		READ INSTRUCTIONS BEFORE COMPLETING FORM
1. REPORT NUMBER AFWAL-TR-81-4070	2. GOVT ACCESSION NO.	3. RECIPIENT'S CATALOG NUMBER
4. TITLE *(and Subtitle)* MECHANICAL SPECTROSCOPY FOR EPOXY RESINS		5. TYPE OF REPORT & PERIOD COVERED Final Report 26 Sept. 1977-02 Jan. 1981
		6. PERFORMING ORG. REPORT NUMBER SETEC-ME-81-035
7. AUTHOR(s) M.L. Williams, N.R. Basavanhally N.H. Wackenhut, E.F.M. Winter R.D. Marangoni, C.C Yates		8. CONTRACT OR GRANT NUMBER(s) F 33615-77-C-5232
9. PERFORMING ORGANIZATION NAME AND ADDRESS University of Pittsburgh Department of Mechanical Engineering Pittsburgh, PA 15261		10. PROGRAM ELEMENT, PROJECT, TASK AREA & WORK UNIT NUMBERS Work Unit Numbers 2419
11. CONTROLLING OFFICE NAME AND ADDRESS Materials Laboratory, (AFWAL/MLBC) Air Force Wright Aeronautical Laboratories Air Force Systems Command Wright-Patterson Air Force Base, OH 45433		12. REPORT DATE August 1981 13. NUMBER OF PAGES 144
14. MONITORING AGENCY NAME & ADDRESS*(if different from Controlling Office)*		15. SECURITY CLASS. *(of this report)* Unclassified 15a. DECLASSIFICATION/DOWNGRADING SCHEDULE

16. DISTRIBUTION STATEMENT *(of this Report)*

Approved for public release; distribution unlimited.

17. DISTRIBUTION STATEMENT *(of the abstract entered in Block 20, if different from Report)*

18. SUPPLEMENTARY NOTES

19. KEY WORDS *(Continue on reverse side if necessary and identify by block number)*

Mechanical Properties
Physiochemical Properties
Mechanical Spectroscopy
Interaction Matrix
Resins
Composites
Epoxy Resins

20. ABSTRACT *(Continue on reverse side if necessary and identify by block number)*

Mechanical characteristics of ten variations of Hercules 3501-5A epoxy resin have been determined to relate their behavior. Tensile properties, failure properties, viscoelastic properties and some physiochemical properties have been investigated. A dilatometer has been developed under this program for the study of cure kinetics.

DD FORM 1 JAN 73 1473 EDITION OF 1 NOV 65 IS OBSOLETE
S/N 0102-LF-014-6601

Unclassified
SECURITY CLASSIFICATION OF THIS PAGE *(When Data Entered)*

PREFACE

This report was prepared by the University of Pittsburgh, Pittsburgh Pennsylvania under Contract No. F 33615-77-C5232, "Mechanical Spectroscopy for Epoxy Resins". The contract was initiated under Project No. 2419 and was administered under the direction of the Materials Laboratory, Air Force Wright Aeronautical Laboratories, Wright-Patterson Air Force Base, with William B. Jones (AFWAL/MLBC) Composites and Fibrous Materials Branch, Non-metallic Materials Division, as the Project Engineer. N. H. Wackenhut, Program Manager directed the program at the University of Pittsburgh with the assistance of R. D. Marangoni. M. L. Williams as Principal Investigator was responsible for the experimental activities. N. R. Basavanhally and E. F. M. Winter provided significant assistance to the project. University of Pittsburgh program administration was provided by C. C. Yates and B. F. Victor.

The report covers the period from 26 September 1977 through 02 January 1981.

The Contractor's report number is SETEK-ME/81-035.

The mention of commercially available products should not be construe in any way as an endorsement by the Government.

TABLE OF CONTENTS

LIST OF ILLUSTRATIONS

LIST OF TABLES

SECTION I

INTRODUCTION

With the continued growth of reinforced epoxy resins in structural applications the intensity of effort placed on mechanical characterization of the components and the interfacial interaction between the two has increased dramatically. The polymeric matrix material is an area of specialized study because of the properties peculiar to it, the most important of which are a) the highly pronounced temperature, time, and moisture dependent mechanical relaxation processes, b) the ability, especially of the elastomer class, to develop large reversible deformations, and c) the intimate coupling of mechanical and chemical processes which affect each other substantially. Mechanical and physiochemical characterization of the resins provide a basis for logical selection and evaluation, for assistance in diagnosing the vulnerability of composites in service environments, and in establishing cost effective specification tolerances for composite.

Substantial progress has been made in establishing standard mechanical tests for composite assemblies by ASTM[1]* and USAF contractors and there is interest by the National Materials Advisory Board in the relation between "off-spec" compositions and performance and cost. Work has also been done in establishing procedures for testing polymers such as outlined by ASTM[1,2] and the Four Volume Series published by Wiley[3].

Quantification of the mechanical-physiochemical characteristics of the resin material presented in two dimensional "Interaction Matrix"[4] can focus on design quantities of interest such as interlaminar shear strength, inherent specific cohesive fracture energy, damping properties and their variation with mechanica, thermal, and aging environments and off-spec conditions as influenced by the chemical kinetics of the mix and cure process.

1. PROGRAM OBJECTIVE

Mechanical spectrographic methodology has been applied to a high performance graphite composite matrix material used in advanced composite primary and secondary aircraft structures. Nine variations of the

---

*Subperscript numbers refer to references listed at the end of this report.

Hercules 3501-5A epoxy resin system consisting of a tetrafunctional resin, an aromatic diamine curing agent and an organometallic catalyst have been prepared in sub-scale lots (100-150 kilograms; 200-300 lbs.) on standard production equipment. In addition one sub-scale batch has been prepared to Hercules standard specifications. A quantity of production resin has also been set aside for this program. Formulations of these variations have been prepared to provide design variations and off-spec variations as designated in Table 1.

TABLE 1

HERCULES 3501-5A RESIN SYSTEM VARIATIONS

Resin Code	Variation
16KV1	High Viscosity Base Resin
8KV2	Low Viscosity Base Resin
8KV3	Brittle Resin
16KV4	Ductile Resin
12KV5	Increased Accelerator & Moisture Content
12KV6	Hardner Concentration, 15% Excess
12KV7	Hardner Concentration, 10% Below Normal
12KV8	Accelerator Concentration, 20% Excess
12KV9	Accelerator Concentration, 20% Below Normal
12KV10	Standard Sub-Scale Batch
12KV11	Production Batch

Approximately eight pounds of each in pre-polymerization form (refrigerated storage at $-40^{\circ}F$) were allocated to this program. Except for the initial variations in compounding, all were treated equally during storage, cure, and testing to obtain comparative property data providing a basis for logical selection and evaluation, for assistance in diagnosing the vulnerability of composites in service environments, and in establishing cost effective specification tolerances for composites.

To achieve the program objective a series of tasks were undertaken which can be generally categorized as:

1. The elastic properties as a function of temperature and time.
2. The cohesive fracture energy characteristics as a function of temperature and time.
3. The rheological nature and temperature-time equivalence.
4. Limited physiochemical behavior and cure kinetics.

2. SUMMARY

From an overall point of view it would appear that within the limits of compounding of the H3501-5A epoxy resin system as outlined in Table 1 that very little differences can be observed among the variations using the mechanical spectrographic testing techniques described in this report. Data spread in general was fairly large. Any subtle variations in mechanical properties caused by variation in chemical batching may have been lost because of an insufficient number of data points to provide statistical information.

Mechanical response obtained from tensile tests at constant strain rate are presented in the form of log secant modulus as a function of log time (Figures 5.a, 5.b, 5.c thru 14.a, 14.b, 14.c). The modulus decreases with an increase in time, temperature, and moisture and for a fixed time decreases with an increase in strain rate. None of the ten variations show distinctive elastic properties which sets one apart from the other. The tangent modulus represents small deformation elastic properties and may be approximated from the above set of curves at the ordinate intercept or more precisely read from Table 3. A plot of tangent modulus versus temperature (see Figure 15) produced a broad band over 15% wide because of data crossover with the mean decreasing from about 0.670×10^6 lb_f/in^2 at 77^oF to 0.440×10^6 lb_f/in^2 at 350^oF for the dry state and from 0.497×10^6 lb_f/in^2 at 77^oF to 0.024 lb_f/in^2 at 350^oF in the wet state, both at a cross head speed of 0.02 inches per minute. Strain rate does not appear to have much effect on the tangent modulus.

Poisson's ratio also decreases with temperature with strain rate having no measurable effect. Using biaxial strain gages, Poisson's ratio was found to be about 0.359 at 77^oF decreasing approximately linearly to about 0.327 at 350^oF for the dry state.

The Smith Plot, Figures 5.d thru 14.d, represents failure properties in tension (see also Table 3). A comparison of this plot among all ten variations does seem to indicate that the Standard Sub-Scale variation 12KV10 in the dry state has somewhat different characteristics. The Smith Plot of this variation shows a rather steep slope indicating higher tensile strengths at lower extension throughout the range of temperatures and strain rates.

This variation does not however stand out from the other nine in the wet state. Table 5 is a judgment evaluation of the Smith Plot based on a low, moderate, or high sensitivity of stress or strain to temperature, time and moisture. It is interesting to note that 8KV3, the "brittle" resin, and 16KV4, the "ductile" resin which should show some differences have been rated the same.

The strain energy of failure in tension is also very erratic within a particular variation again resulting in a broad band of data as a function of temperature when all ten variations are collected on a single set of coordinates. Figure 16 summarizes this data. It is difficult to infer much from this curve except the notable loss in failure energy for the wet state specimens. Again using an averaging process over all ten variations indicates little change in fracture energy up to a temperature of 275°F at which time it increases for dry specimens but decreases for wet specimens. For the dry state the strain energy at failure averages about 124 lb-in/in^3 at 77°F increasing to 216 lb-in/in^3 at 350°F. In the wet state the failure energy averages about 33 lb-in/in^3 at 77°F falling to about 18 lb-in/in^3 at 350°F.

The material behaves in a brittle fashion and with these relatively low values of fracture energy it would be expected that fracture mechanics considerations would greatly influence the strength of the material. Investigation of critical stress intensity factors by Mode I again indicate only trends for the epoxy resin H3501-5A as a whole but not by individual variations. K_{IC} increases from an average value of 624 lb-in$^{-3/2}$ at -67°F to 785 at 350°F in the dry state but decreases from an average value of 622 at -67°F to 155 lb-in$^{-3/2}$ at 350°F. Note that the average critical stress intensity factor is very nearly identical for both the dry and wet states at -67°F.

In a very limited study of critical flaw size a reasonable correlaction between measured and calculated values was observed. At -67°F the critical flaw size for the dry state, was calculated to be about 0.0035 inches at -67°F increasing about five fold at 350°F. See Table 8.

A more detailed study into the viscoelastic nature of a single variation of the H3501-5A epoxy resin, i.e., the standard formulation, indicates that a Maxwell-Weichert chain models this material reasonably well. The resulting model for shear and tensile relaxation modulii are respectively

$$G(t) = G_o + \sum_{i=1}^{n} G_i \exp(-t/\tau_i) \quad (1)$$

$$E(t) = E_o + \sum_{i=1}^{n} E_i \exp(-t/\tau_i) \quad (2)$$

which as a four term Dirichlet series were used to curve fit both shear and tensile relaxation data determined by experiments. The coefficients G_i, E_i and τ_i for the first four terms at several temperatures are tabulated in Appendix B, Table B1. This along with the viscoelastic constitutive equation

$$\sigma(t) = \int_o^t E(t - \tau) \frac{d\varepsilon(\tau)}{d\tau} d\tau \quad (3)$$

was used to generate stress strain curves from the tensile relaxation function. Figures B-3 and B-4 of Appendix B compare relaxation generated stress-strain properties for various temperatures. The correlation is remarkably good.

Using the basic postulate of temperature-time equivalence for rheological materials and the Suh-Turner form of the shift function where

$$\log_{10}(a(t)) = -\lambda \left(\frac{1}{T_o} - \frac{1}{T}\right) \quad (4)$$

the value for λ was determined to be 658.8 for this material. This function was then used to shift the normalized tensile relaxation modulus which when compared with actual experimentally determined tensile relaxation data gave good correlation. See Appendix B, Figure B-5.

Under dynamic conditions the complex modulus of the H3501-5A resin system indicated no marked difference among the ten variations. The storage modulus in flexure for all variations was about 0.65×10^6 lb/in^2 at 77°F in the dry state and about 0.50×10^6 lb/in^2 at 77°F in the wet state at 10 Hz frequency dropping about 10% at 1 Hz frequency over the full range of temperatures. In both the wet and dry state the storage modulus is reduced approximately 50% from room temperature to 200°C. The material has low damping characteristics over the entire temperature range in either the dry or wet state. The loss tangent was no greater 0.10 at high temperature falling off to as low as .01 or less at low temperatures, dry state.

Significantly the standard sub-scale variation 12KV10 has very nearly the lowest permeability coefficient (12KV10 at 0.948 x 10^{-7} gcm/sec m^2 mm Hg and 12KV8 at 0.946, the lowest) which would indicate the highest degree of crosslinking. The brittle variation 8KV3 and the ductile variation 16KV4 have the highest permeability coefficient at 2.304 x 10^{-7} and 1.786 x 10^{-7} gcm/sec m^2 mm Hg respectively which would indicate the lowest level of crosslinking of the ten variations. See Table 8.

Thermal Gravimetric Analysis of the standard sub-scale 12KV10 variation indicates that degredation of the cured material begins at about 239°C (462°F) at a heating rate of 2.5°C/min and that the activation energy of chemical degredation is 41.3 Kcal/mole.

Cure rheological studies were also made on the standard sub-scale variation using a torsion pendulum technique. It was found that the glass transition temperature, T_g, rises from below 90°C to 180°C on heating to 180°C and that isothermal cure at 180°C raises T_g only slightly. On heating to 275°C at 1.5°C/min a distinct T_g was observed at 267°C. The maximum glass transition is above the maximum temperature of isothermal cure (180°C). The apparent activation energy was found to be 18 Kcal/mole.

3. RECOMMENDATIONS

To mechanically characterize a brittle material such as this, sampling should be in sufficiently large quantities to provide statistical information. Fracture mechanics plays an important role and should be taken into account before attempting to assign too much credibility to the ultimate properties. Anomalies such as impurities, voids, surface scratches or cracks influence ultimate properties but do not reflect material properties. Additional work in the area of fracture should be:

1. To develop a molding technique for quantity casting round (or flat) tensile specimens to provide a well ordered near stress free molecular structure with cast-in surface molecular structure rather than a partially machined surface structure including a method for minimizing internal and surface stresses caused by cure shrinkage. To investigate the effect of machined surface conditions and cast surface conditions on failure properties.

2. To take advantage of the birefringent nature of this material and other similar viscoelastic polymeric materials in an attempt to predict Mode I critical stress intensities from non-critical levels.
3. To extend the work on cohesive fracture energies to include Mode II as well as Mode I using the Brazil test technique.
4. To extend the work on critical stress intensities to a study of critical flaw size.
5. To investigate the mechanical dilatometric nature of the cure process as related to the development of cast in residual stresses caused by the cure shrinkage.

SECTION II

TECHNICAL DISCUSSION

To accomplish the program objectives, four specific tasks have been investigated and are reported here as 1. Tensile Properties, 2. Failure Properties, 3. Viscoelastic Properties, 4. Physiochemical Properties.

Emphasis was given the first three mechanical property tasks.

1. TENSILE PROPERTIES

a. Casting and Specimen Preparation

A basis for making castings of the H-3501-5A resin variations has been outlined by W. Ragland[5] however some minor changes were made to the recommended mold and cure cycle as outlined in the following paragraphs.

(1) The Sheet Mold - A simple mold (See Figure 1) was assembled by clamping together two 8 inch x 15 inch x 1/4 inch thick pyrex glass plates spaced apart by a 1/8 inch thick gasket. Three 3/4 inch broad gaskets were cut from 1/8 inch thick teflon sheet sized to the outer periphery of the glass plate. The gaskets were U-shaped open along one long edge. Heavy duty one inch capacity binder clips were placed side by side continuously around two short and one long edge of the glass plate assembly using two of the gaskets as padding between clips and glass. Each glass plate had one long edge ground to a 45^{o} bevel which when assembled inward provided a full length funnel. The mold is easily assembled and disassembled. The gaskets were reused many times.

In addition a trough-like funnel, which spanned the long dimension opening of the assembled mold, was fabricated of heavy sheet metal. The bottom of the trough had a 1/8 inch opening the full length. At each end a round rod somewhat less than 1/8 inch diameter projects down from the funnel about 1-1/2 inches permitting the funnel to be quickly dropped into place or removed.

Prior to pouring the resin into the mold all surfaces contacting or likely to come into contact with the resin were coated several times with a mold release, Frekote 34 supplied in a 16 oz. aerosol spray can, following the recommended instructions. (Frekote Inc., Boca Raton, Florida.) Clean-up of all parts was easily accomplished using a scraper after going through the cure cycle. The glass plates were reused by removing leftover resin with a razor blade and residual Frekote with a mild cleanser.

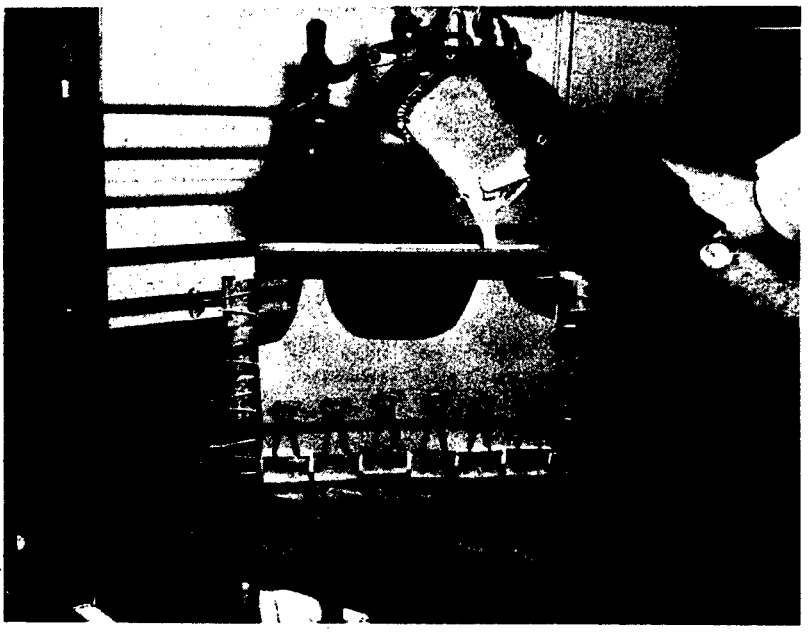

Fig. 1 Sheet Mold, Funnel and Debulk/Pour Pan

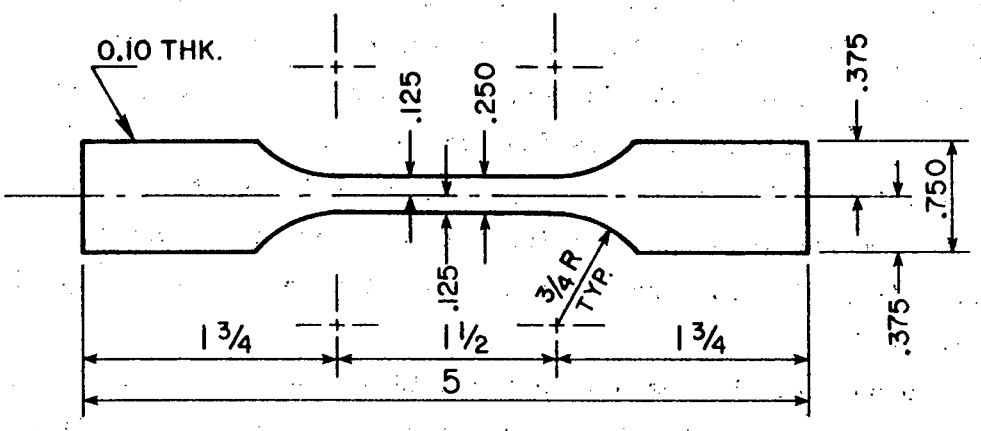

Fig. 2 Tensile Specimen Template

(2) Casting and Cure Procedure - The 11 variations of the H-3501-5A epoxy resin system were batched by Hercules. To extend the liquid shelf life the material was shipped and stored in a frozen state. Storage was at -40°C (-40°F) in a Kelvinator Model UC-744, five cubic foot freezer.

The casting and cure cycle recommended in reference 5 has been altered slightly at the debulking (outgassing) and pour stage. It was observed that if the debulk and pour were done at 93°C (200°F) resulting in a lower viscosity liquid instead of the recommended 80°C (180°F) that all variations of the H-3501-5A resin system would debulk faster and pour into the mold easier. After pour additional debulking in the mold was completed much faster. The net reduction in time to accomplish debulk, pour and mold debulk far outweighs the increase in polymerization rate caused by the higher temperature. Further, debulk periods for the various H-3501-5A variations had to be altered, in some cases considerably, depending on their batching, i.e., viscosity, hardener, accelerator, or moisture concentration. The prepour debulk stage was therefore terminated when the resin lost its milky appearance and became a clear amber color at which time the liquid resin was removed from the oven and quickly poured into the cavity of the preheated mold. Regardless of debulk duration the temperature-time cure sequence was strictly followed. Table 2 outlines the debulk, cast, cure, and postcure procedure. This was done manually in a Cole Parmer Model 5054-40 vacuum oven with Precision Model 69151 vacuum pump. Preheat and post cure was done in an atmospheric laboratory type oven (K.H. Huppert Co. Model 5700 or equivalent). Appropriate quantities of resin were chipped from the solid frozen stated and placed in Kaiser Aluminum 13 ounce, 6 inch x 4-3/8 inch x 1-1/16 inch deep rigid foil containers (catalogue no. 1017-30 with L 1017 cardboard lid) for initial debulk and pour. The resin was no more than about 1/4 inch deep in the bottom of the pan to allow for foaming during early debulk stages. Tongue blades made useful throw-a-way spatulas for transferring the resin from pan to mold.

(3) Specimen Preparation - All tensile specimens were fabricated to dimension prior to post cure on the presumption that they were slightly less brittle than after post cure. Immediately on removal of the cast sheet

TABLE 2

DEBULK, CAST AND CURE SCHEDULE

H-3501-5A EPOXY RESIN SYSTEM

Hour	Event	Temp. Status	Pressure Status
	Storage	-40 C (-40 F)	Atmospheric
-10	Remove from freezer storage. Place in aluminum pans. Approx. 100 gm per pan. Cover.	25 C (77 F) Thaw overnight	Atmospheric
0	Place in cold vacuum oven. Debulk in pans until surface bubbles (foam) under full vacuum vanish. Resin should be clear amber liquid.	25 C (200 F) Raise temp. to 93 C ±2° at 1-1/2 C°/min. max. rate of rise. Do not exceed 95 C.	Full vacuum (29" Hg). Jog between full vac. and atm. periodically and as necessary to prevent spill.
	Quickly pour into mold preheated to 93 C. Place mold in vacuum oven. Remove large pour bubbles by vacuum. Stop vacuum as soon as casting is reasonably clear of bubbles.	93 C (200 F) Hold	Partial vac. (15-20" Hg). Jog as necessary to bring bubbles to top. Avoid too much vacuum.
+4-1/2	Discontinue vacuum	93 C Hold	Atmospheric
+5	Continue cure	93 C (200 F) Raise temp. to 121 C ±2°C at 1-1/2 C°/min. max. rate or rise.	Atmospheric
+6	Continue cure	121 C (250 F) Raise temp. to 177 C ±2°C @ 1-1/2 C°/min. max. rate of rise.	Atmospheric
+6-1/2	Remove mold from oven and quickly remove casting from mold. Mild prying may be required. Casting is cheesy. Return casting to oven flat between same glass plates clean outside surface next to casting. Handle with care. Cover cold sheet with protective tape.	177 C (350 F) Oven power off. Cool to 25°C @ normal oven cool-down rate.	Atmospheric
	Specimen preparation	25 C (77 F) Room temp.	Atmospheric
0 (+6-1/2)	Place specimen between Frekoted glass plates and into cold oven. Oven power on.	25 C Raise temp. to 177 C @ 3 C°/min. max. rate of rise.	
1 (+6-1/2)	Begin postcure	177 C (350 F) Hold	Atmospheric
8 (+6-1/2)	Being cooldown	177 C (350 F) Oven power off cool to 25 C (77 F) @ normal oven cooldown rate	Atmospheric

from the cure cool-down they were covered with 3M Transparent Protective Tape (No. 335) in the form of 8 inch wide by 144 yard roll of adhesive backed film. The film protected the casting surface during specimen roughing out operations.

Roughing was done on an ordinary bench type Model 113,2990,40 Sears 10 inch, 3600 rpm, circular saw using their Khromedge (No. 9 32534) 7 inch diameter, hollow ground, thin rim, satin cut blade, (200 teeth about 1/8 pitch). A hardwood insert was fitted in the blade clearance slot completely closing up the slot. With the blade set at its lowest point and the blade plate fixed in place the power was turned on and the blade slowly raised. In this manner the blade cut a close fitting clearance slot in the wood. The blade was raised only slightly more than 1/8 inch above the bed plate so that when cutting the 1/8 inch thick cast sheet the blade cut at a very flat angle. This very nearly eliminated edge chipping.

A steel template Figure 2 was attached to the roughed out coupon using double sided masking tape. The tensile specimen was then finished to shape on a routing table, Photoelastics, Inc., Model HSR-1 or equivalent, using a Precise Products Corporation Super 40, 1/4 HP, 45000 rpm router equipped with an M.A. Ford No. 41250020 1/4 inch cylindrical, flat end, standard cut, solid carbide burr. To minimize surface stresses at the routed edge the router burrs were frequently replaced. To keep the routed surface cool at all times a light pressure stroking technique was used to remove material. The finished tensile specimen was slightly larger all around than the template because the template follower button must be slightly larger in diameter than the router burr.

After finishing to final shape the tensile specimens were post cured between the pyrex glass plates laying flat. Post cure duration was 8 hours. Refer to Table 2. Following post cure five specimens for each condition were placed, as appropriate, in desiccator cabinets for room temperature drying or in distilled water in wide mouth Mason Jars held at 160°F in laboratory ovens for wet conditioning. Drying to asymtotic minimum weight required 25 days. Moisture asymtotic saturation required soaking for 55 days at the elevated temperature.

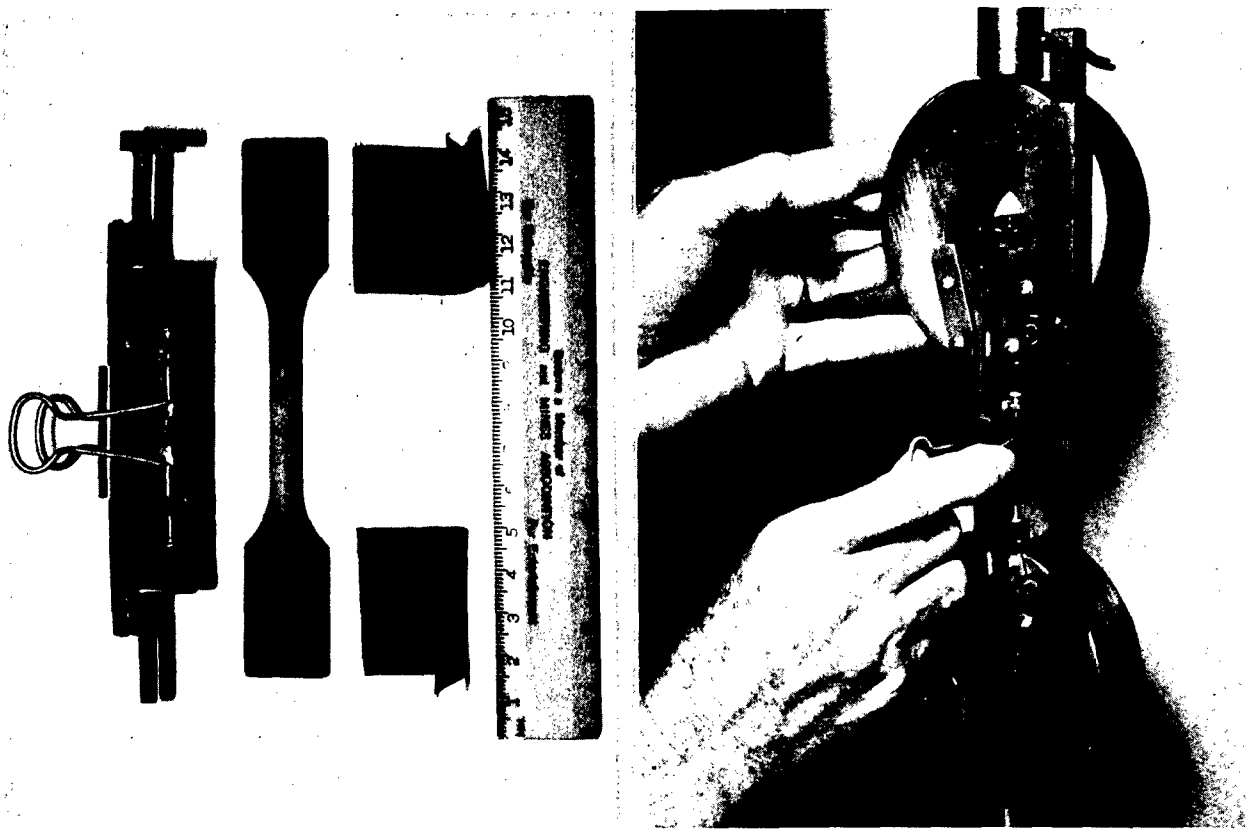

a. b.

Fig. 3 Tensile Specimen Placement Fixture

Fig. 4 Stress Field by Photoelastic Technique (Plane Polarized) of Routinely Mounted Specimen. Load Approximately 57 lbs. (σ = 1824 psi)

b. Equipment and Fixtures

All tensile testing was performed on a calibrated 10,000 pound capacity Tinius Olsen Universal Testing Machine equipped with digital cross head control, Bristol Strip Chart Recorder, and an H. Koch and Son Division of Conrad-Missimer Products, Model FTU 1.8 environmental chamber having a range of -100°F using CO_2 to +600°F. At high cross head speeds of 2.0 inches per minute the slew rate of the Bristol Recorder was inadequate. This necessitated feeding the output of the load cell and the extensometer into a Hewlett Packard Model 320 two channel recorder with sufficiently high response (DC to 50 cycles at 50 mm peak to peak). A Tinius Olsen Model S-500-1 extensometer was used for all tensile tests. The unit makes use of an LVDT transducer applicable in environments from -100°F to +500°F and has a one inch gage length with an elongation range up to 8%.

Gripping a glassy polymeric material of this type was difficult. Tinius Olsen 2500 lb. capacity type KR "self-aligning" grips with double cut diamond serration, hardened, 8-1/2° wedge angle were used. To further assure alignment a precision machined spline (square) was fixed to each grip such that a close fitting slip rod (square) could be used to tie the grips together during placement of the specimen and quickly dropped out of place during pull. See Figure 3h. To eliminate slipping of the specimen in the grips it was necessary to rough-up the glazed gripping surface of each specimen and then to fold over this surface a tab of 120 grit aluminum oxide production grit cloth (plumbers roll, 1-1/2 inch x 25 yards) with the grit side against the specimen before placing between the jaws of the grip. In addition to the alignment tie rod a fixture was also developed to facilitate placement of the tensile coupon and grit tabs consistantly and quickly on the testing machine centerline of action (Figure 3a).

The grip and specimen alignment fixtures minimize moments of unknown magnitude caused by eccentric loading and which would be superimposed on the measured axial load. Once a pull is started it was recognized that non-symmetric settling of the specimen to the grit paper and to the grip wedge could still cause bending moments which are very difficult to evaluate and which have a marked effect on the breaking strength. On the other hand taking advantage of the birefringent nature of the H-3501-5A

epoxy resin, a specimen was routinely placed in the testing machine grips and a load of 57 lbs. applied (σ = 1824 psi). Figure 4 shows a uniform stress distribution through the test section. A slight edge effect of about one fringe order is typical. These small surface stresses are caused by the high speed router shaping of the specimen despite the careful fabrication techniques which were followed.

e. Tensile Modulus

Tensile tests were performed on each of the ten variations of the H-3501-5A epoxy resin system under dry and wet conditions at cross head speeds of 0.02, 0.20, and 2.00 inches per minute (5×10^{-4}, 5×10^{-3}, and 5×10^{-2} meters per minute) and at temperatures of -55 C (-67 F), 25 C (77 F), 93 C (200 F), 135 C (275 F), and 177 C (350 F). Because of the broad scope of the program and the limited quantities available only five specimens were fabricated for each category precluding any statistical approach to data reduction. Except where otherwise noted all data points reported are the average of five test specimens.

The basic data obtained was a continuous load versus elongation record at the various constant strain rates, temperatures and moisture conditions previously mentioned. In all cases the loads have been reduced to engineering stress.

To generate some sort of averaging process for each of the five tensile specimens of a particular set of parameters the data for all five load-displacement sets was least square fit to an exponential curve in the form of a simple Maxwell model,

$$\sigma = A\,(1 - \exp(-B\varepsilon)) \tag{5}$$

This model is not to be construed as representing the viscoelastic temperature-time characteristics of this material. It is a stress-strain curve fit of five specimens at a particular set of parameters. Coefficients for this model for each data set are tabulated in Appendix A, Table A-1.

(1) Secant Modulus - It can be shown that

$$\text{Extensometer strain} = \frac{\text{Cross Head Speed x Time}}{\text{Gage Length}}$$

or

$$\varepsilon = \frac{(CHS)\ t}{(GL)} \tag{6}$$

and since the Secant Modulus E_s is

$$E_s = \frac{\sigma}{\varepsilon} \tag{7}$$

on substituting equations (5) and (6) into (7)

$$E_s = \frac{(GL)\ A\ (1 - \exp Bt\ (CHS)/(GL))}{(CHS)\ t} \tag{8}$$

On the basis of a gage length of 2.50 inches this equation was used to generate the set of curves Log Secant Modulus versus Log Time at the three cross head speeds 0.02 in/min, 0.20 in/min, and 2.00 in/min, up to the time of fracture determined from the mean fracture strain. See Figures 5.a through 14.a, Figures 5.b through 14.c, Figures 5.c through 14.c respectively. The curves behave in general as one would expect with the simple Maxwell Model curve fit used. A comparison among the ten variations does not indicate any distinctive trends which separate one from the other. All show a loss of rigidity with temperature, time and moisture.

(2) Tangent Modulus - A property which should be a material characteristic is the tangent modulus E_T. This quantity has been tabulated in Table 3. It was evaluated by determining the slope of the stress-strain characteristic equation evaluated at zero strain, thus from equation (5)

$$E_T = \left.\frac{d\sigma}{d\varepsilon}\right|_{\varepsilon=0} = AB \tag{9}$$

Here again the values of E_T show the dependence of this material properties on temperature, and moisture state, however, no discernible strain rate dependence. Figure 15 shows this dependence for one strain rate. The plot also shows the considerable crossover of the ten variations making it impossible to single out this particular mechanical characteristic as associated with the batching of ingredients.

(3) Poisson's Ratio - A limited number of experiments were run to determine Poisson's Ratio. Bi-axial self-temperature compensating strain gages were mounted on standard tensile specimens. The output of each gage

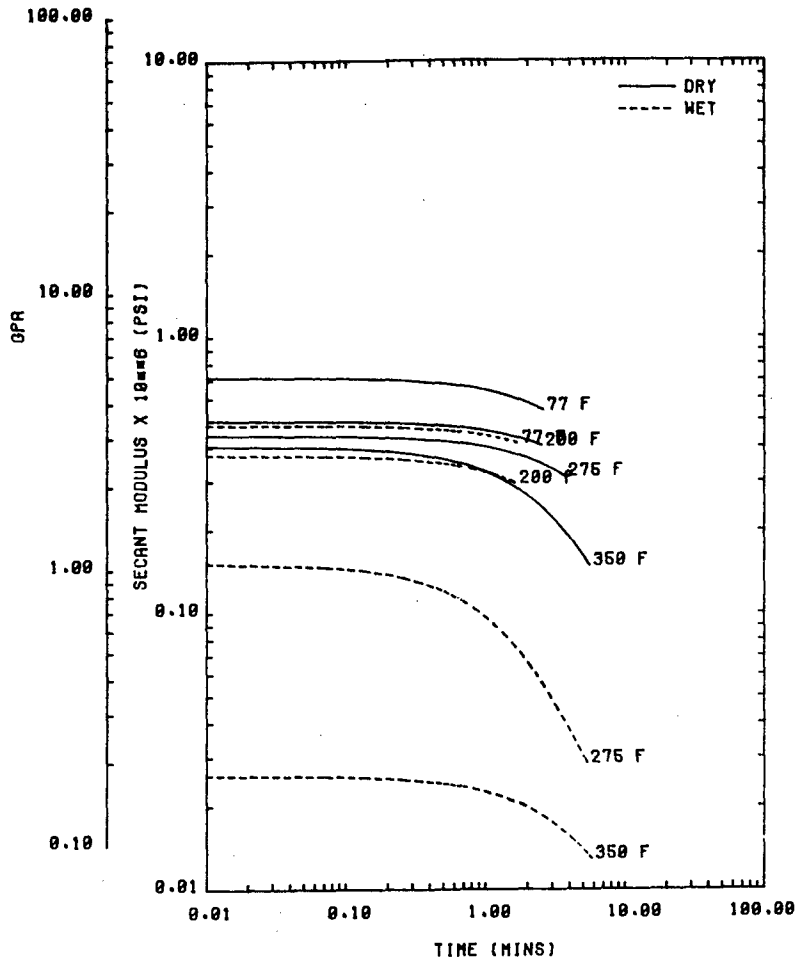

FIG. 5.a Secant Modulus vs Time

3501-5A Epoxy Resin
16KV1 Variation
0.02 in/min C.H.S.

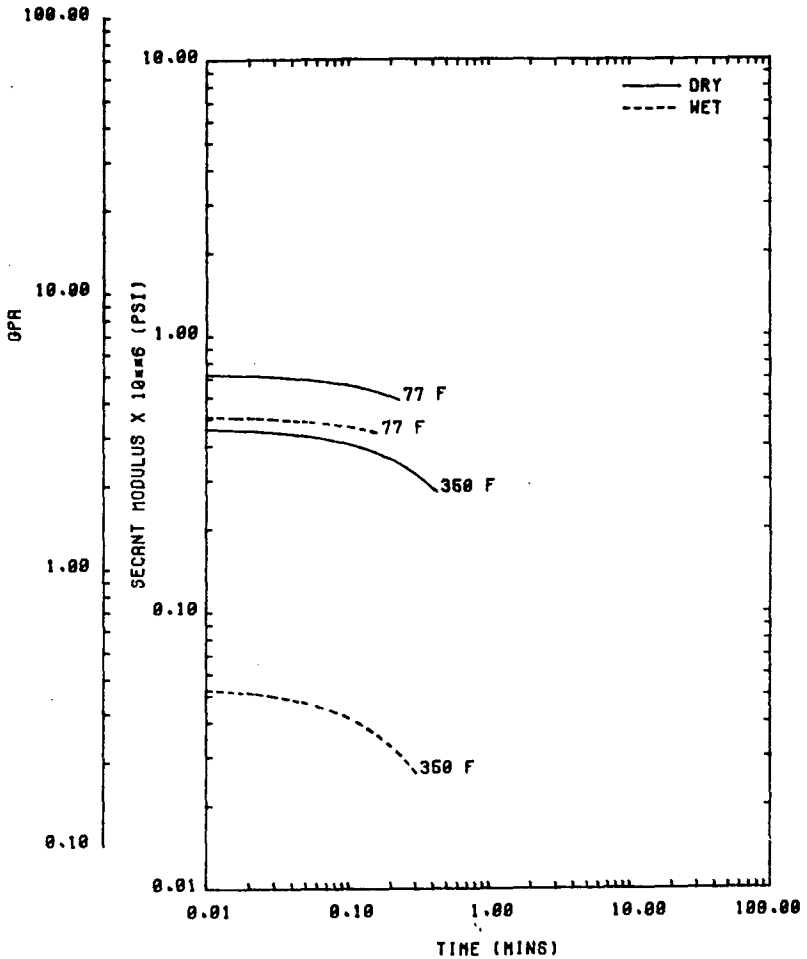

FIG. 5.b Secant Modulus vs Time

3501-5A Epoxy Resin
16KV1 Variation
0.20 in/min C.H.S.

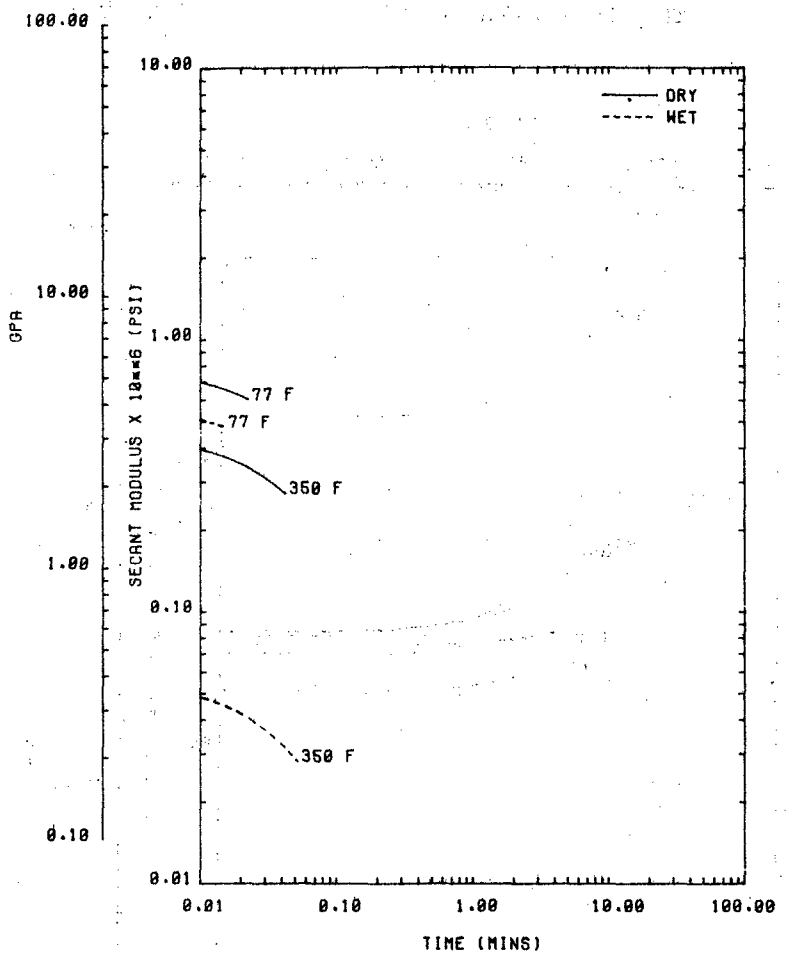

FIG. 5.c Secant Modulus vs Time
3501-5A Epoyx Resin
16KV1 Variation
2.0 in/min C.H.S.

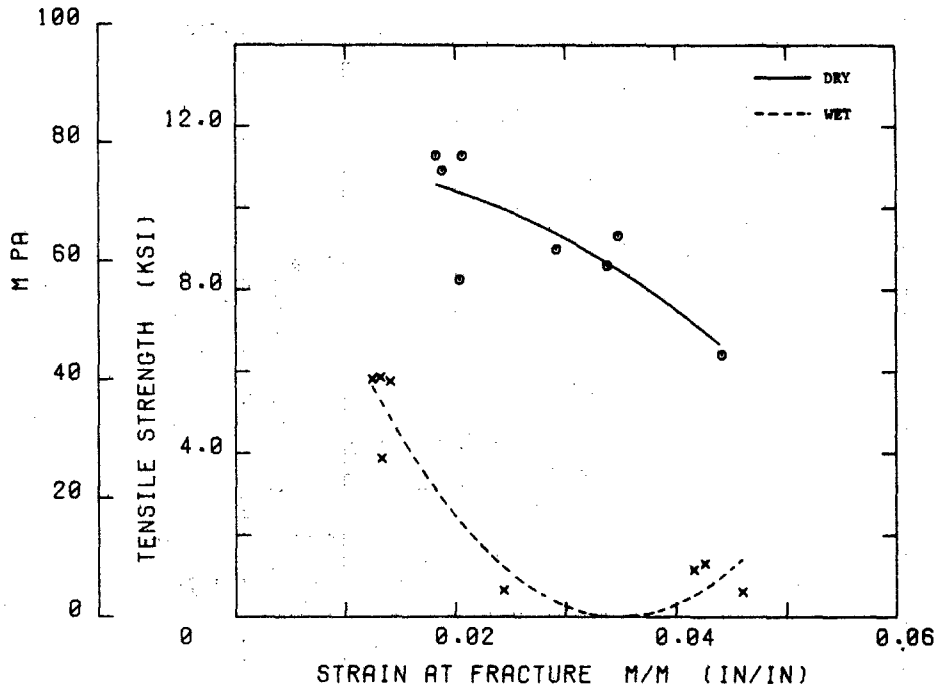

FIG. 5.d Smith Plot
3501-5A Epoxy Resin
16KV1 Variation

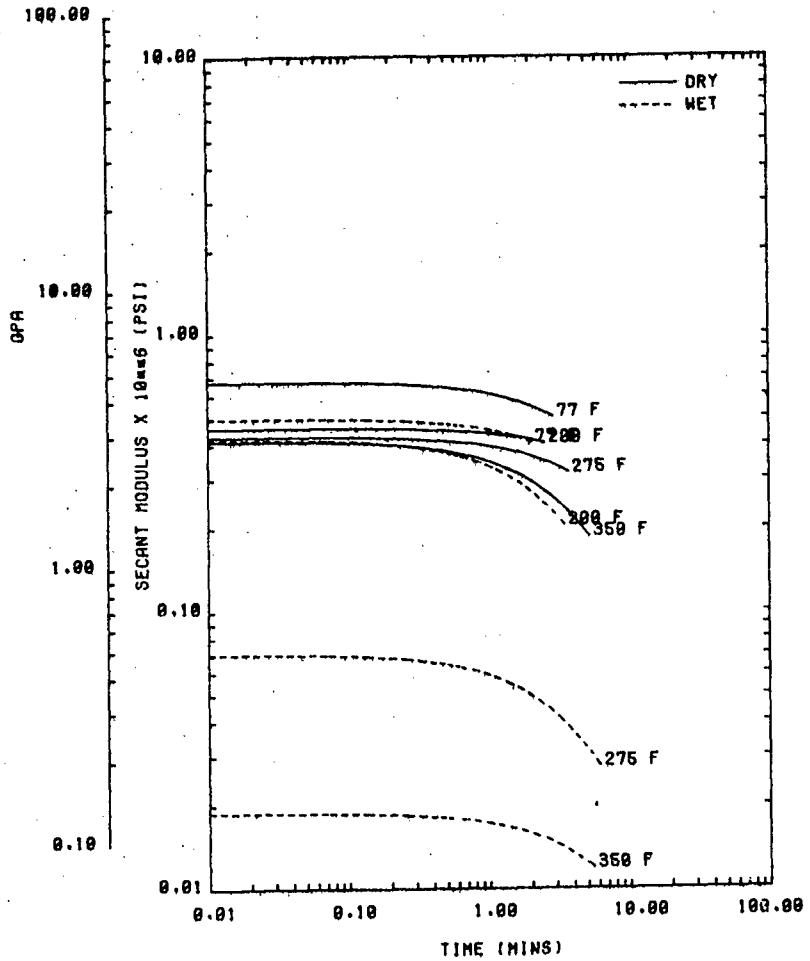

FIG. 6.a Secant Modulus vs Time

3501-5A Epoxy Resin
8KV2 Variation
0.02 in/min C.H.S.

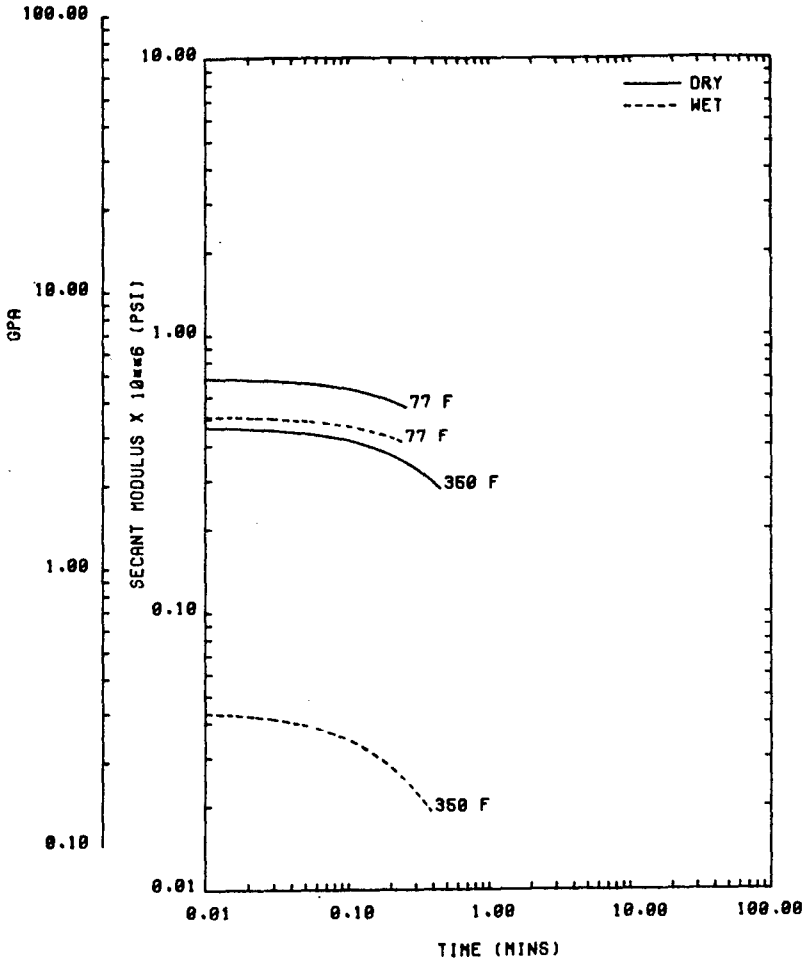

FIG. 6.b Secant Modulus vs Time

3501-5A Epoxy Resin
8KV2 Variation
0.20 in/min C.H.S.

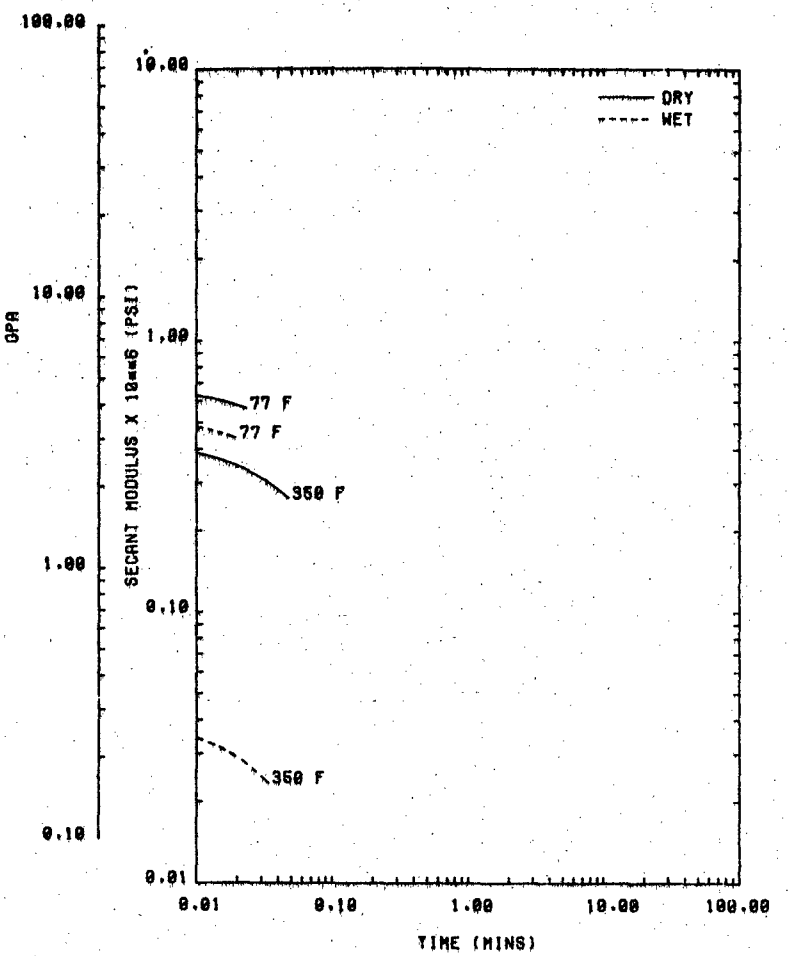

FIG. 6.c Secant Modulus vs Time

3501-5A Epoxy Resin
8KV2 Variation
2.00 in/min C.H.S.

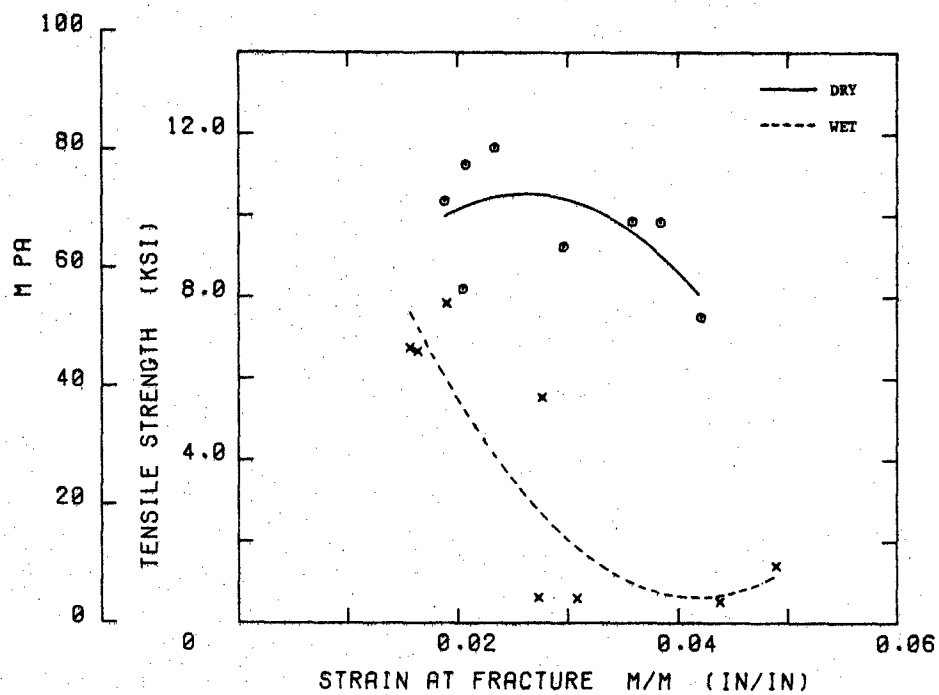

FIG. 6.d Smith Plot

3501-5A Epoxy Resin
8KV2 Variation

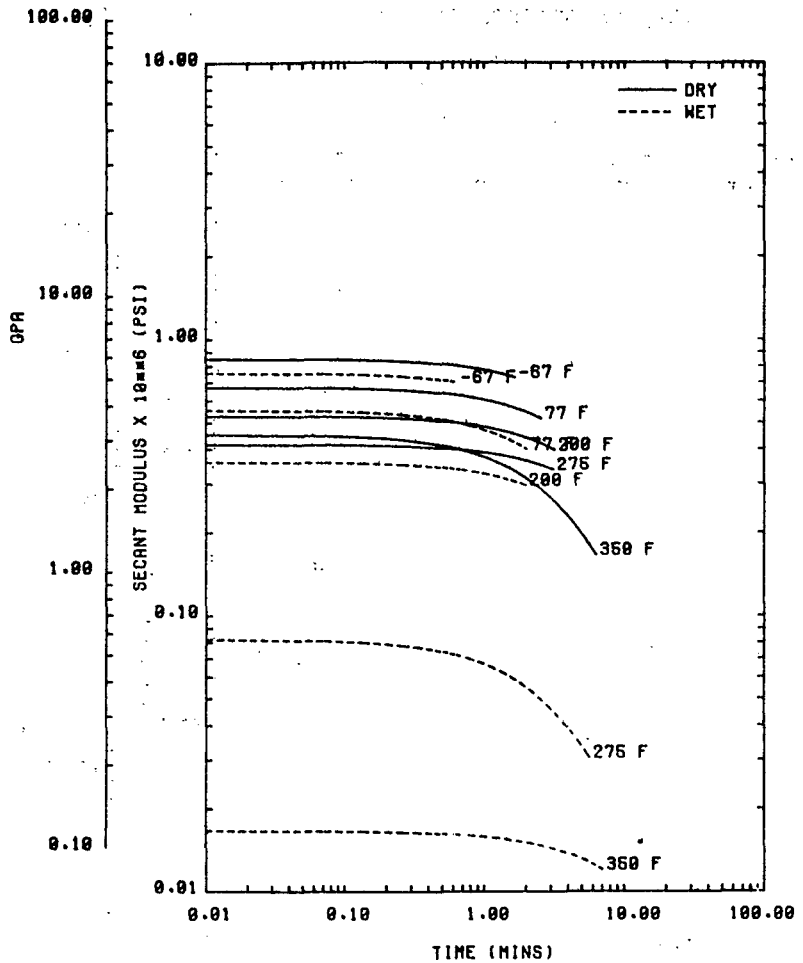

FIG. 7.a Secant Modulus vs Time

3501-5A Epoxy Resin
8KV3 Variation
0.02 in/min C.H.S.

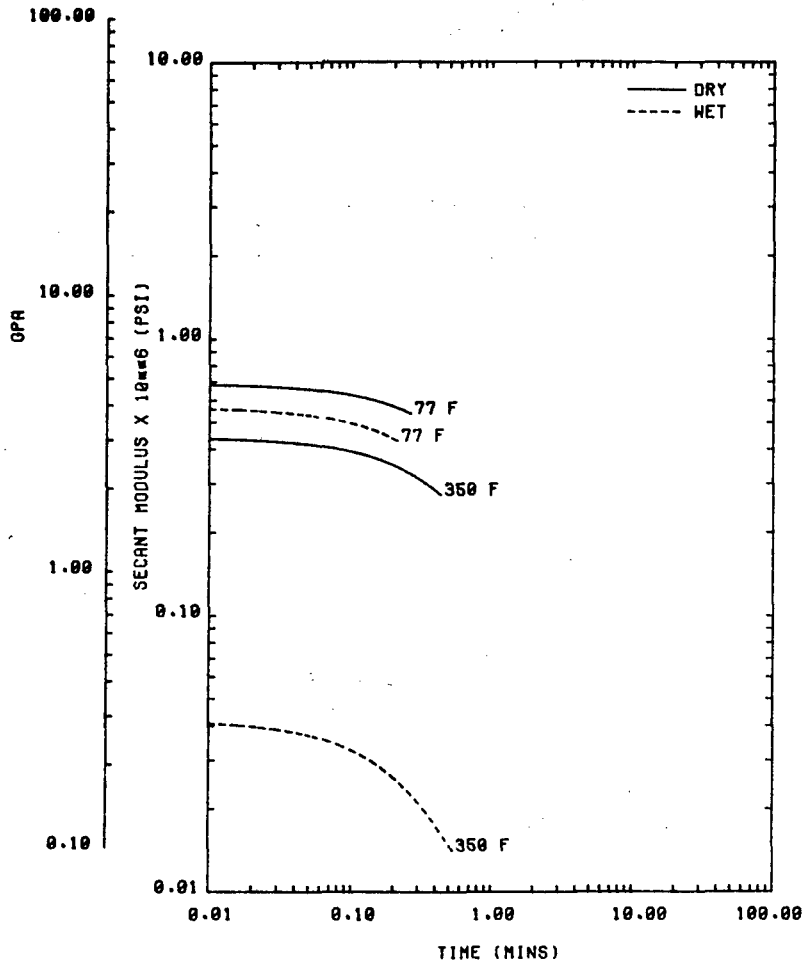

FIG. 7.b Secant Modulus vs Time

3501-5A Epoxy Resin
8KV3 Variation
0.20 in/min C.H.S.

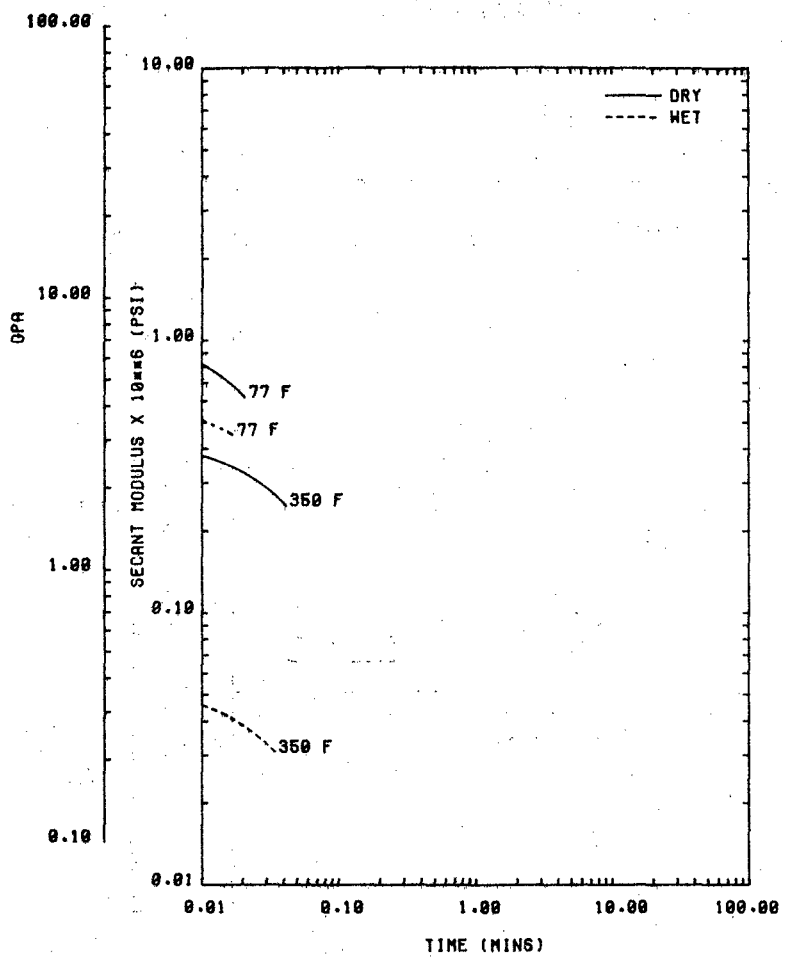

FIG. 7.c Secant Modulus vs Time

3501-5A Epoxy Resin
8KV3 Variation
2.00 in/min C.H.S.

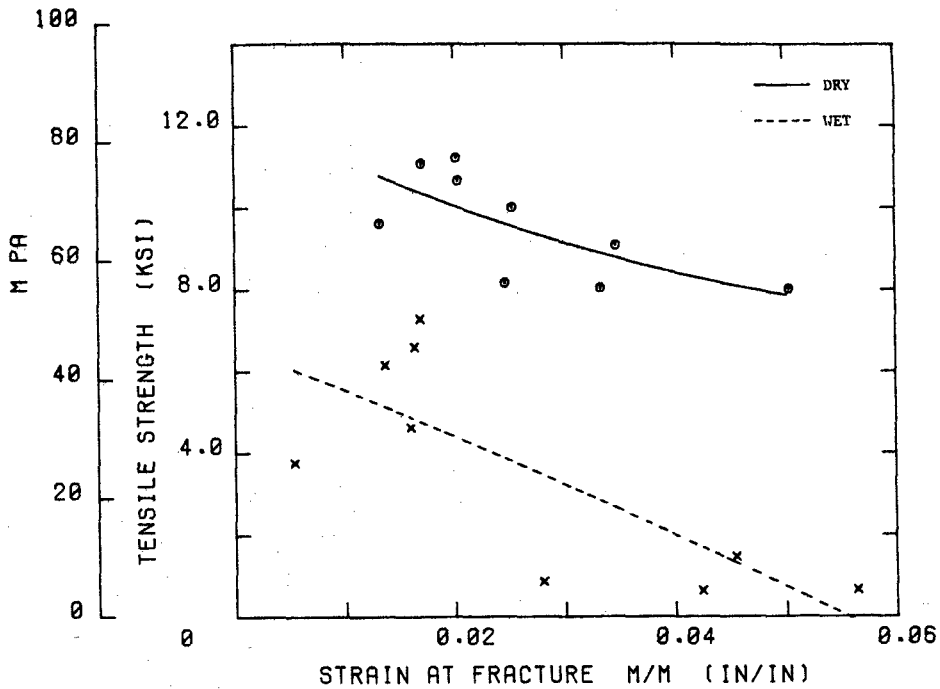

FIG. 7.d Smith Plot

3501-5A Epoxy Resin
8KV3 Variation

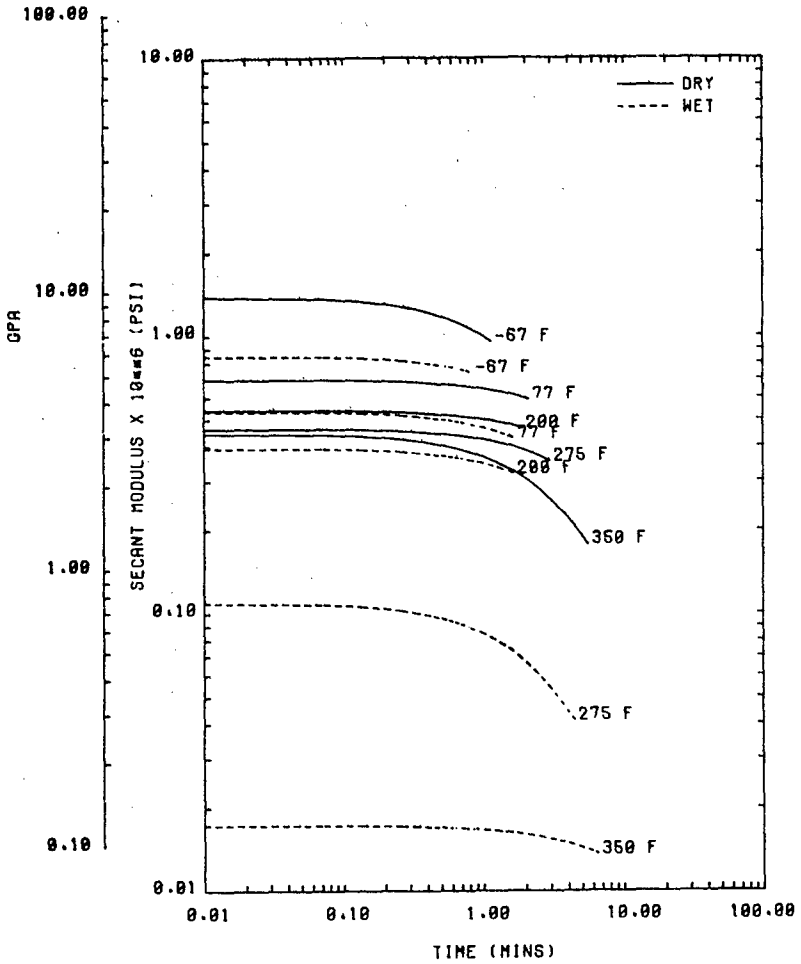

FIG. 8.a Secant Modulus vs Time
3501-5A Epoxy Resin
16KV4 Variation
0.02 in/min C.H.S.

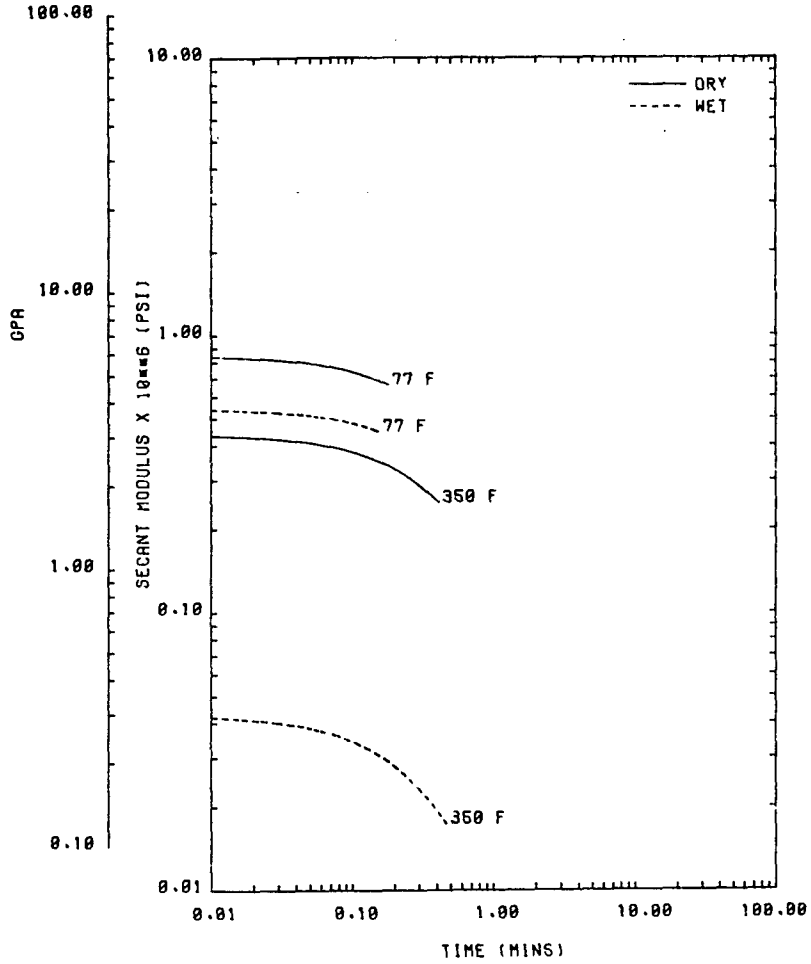

FIG. 8.b Secant Modulus vs Time
3501-5A Epoxy Resin
16KV4 Variation
0.20 in/min C.H.S.

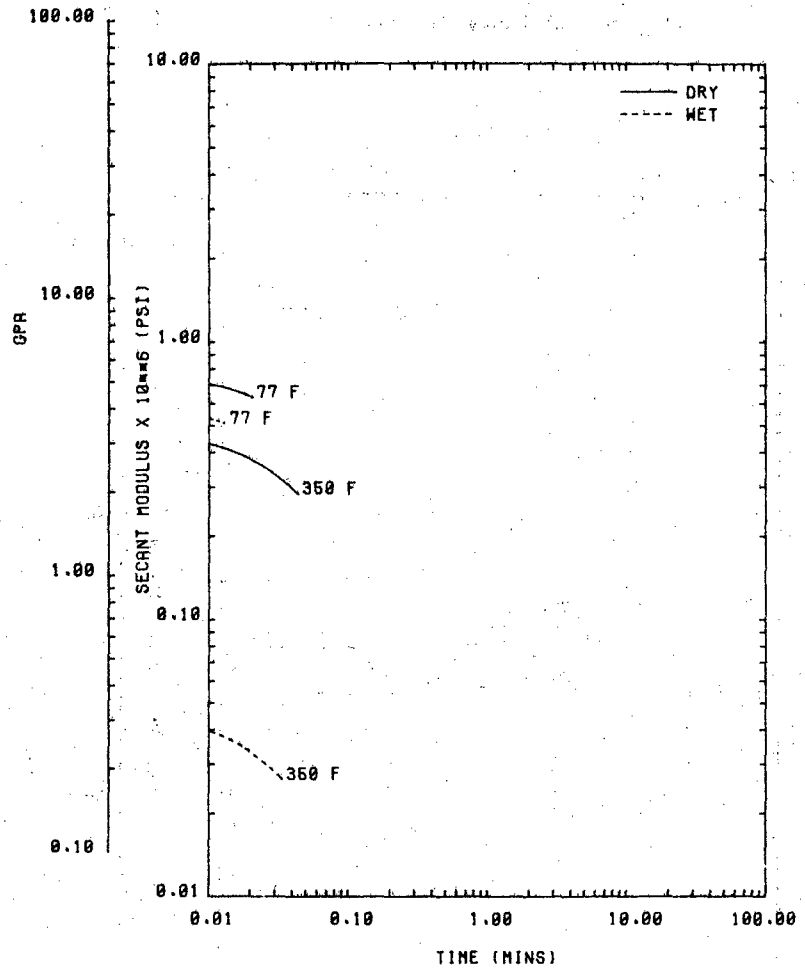

FIG. 8.c Secant Modulus vs Time

3501-5A Epoxy Resin
16KV4 Variation
2.00 in/min C.H.S.

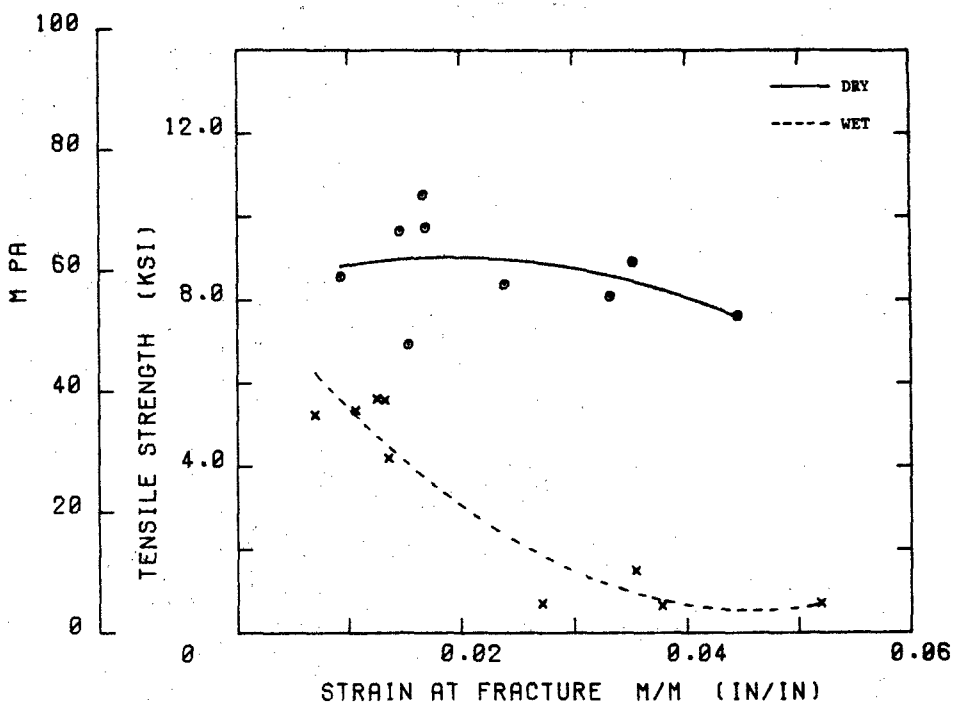

FIG. 8.d Smith Plot

3501-5A Epoxy Resin
16KV4 Variation

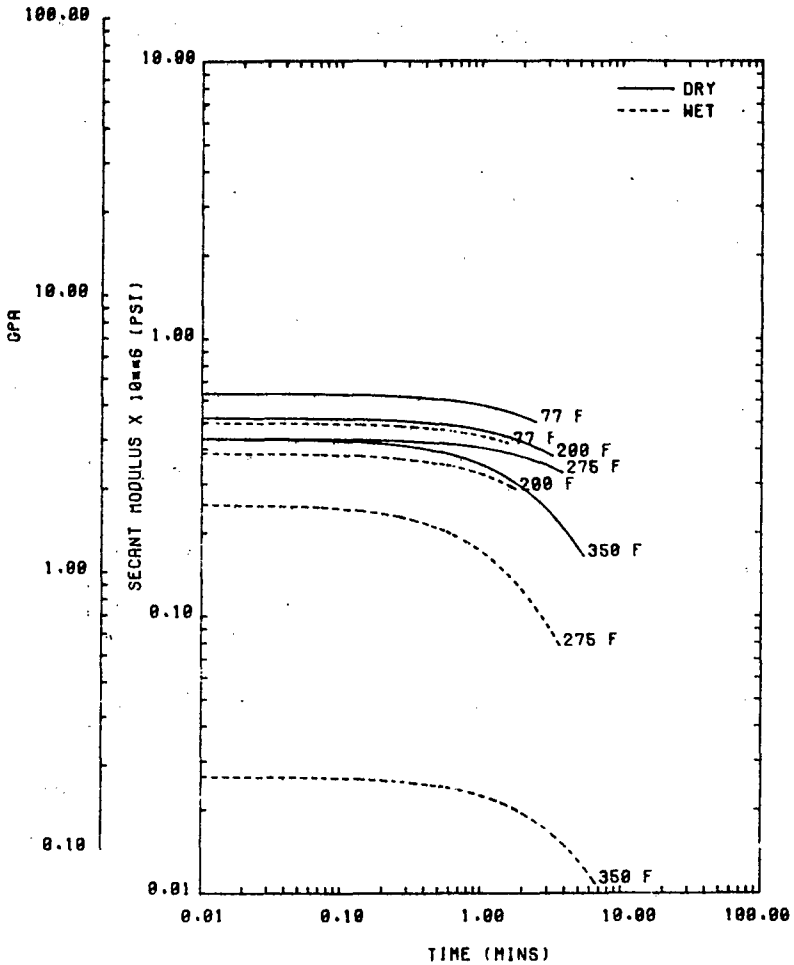

FIG. 9.a Secant Modulus vs Time

3501-5A Epoxy Resin
12KV5 Variation
0.02 in/min C.H.S.

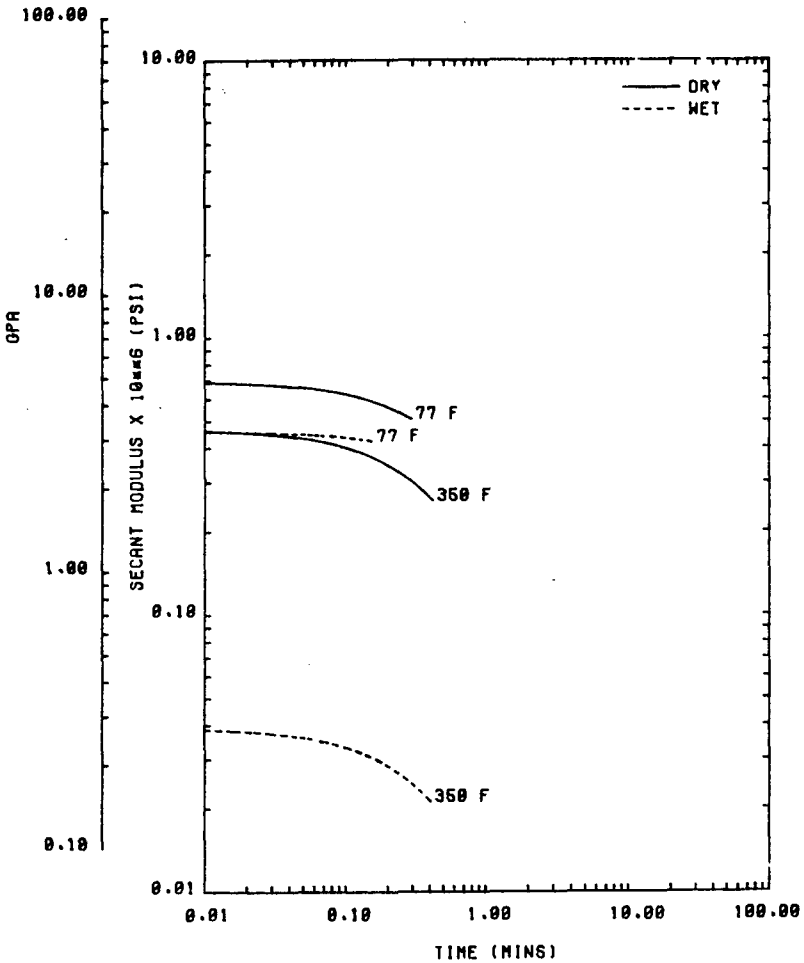

FIG. 9.b Secant Modulus vs Time

3501-5A Epoxy Resin
12KV5 Variation
0.20 in/min C.H.S.

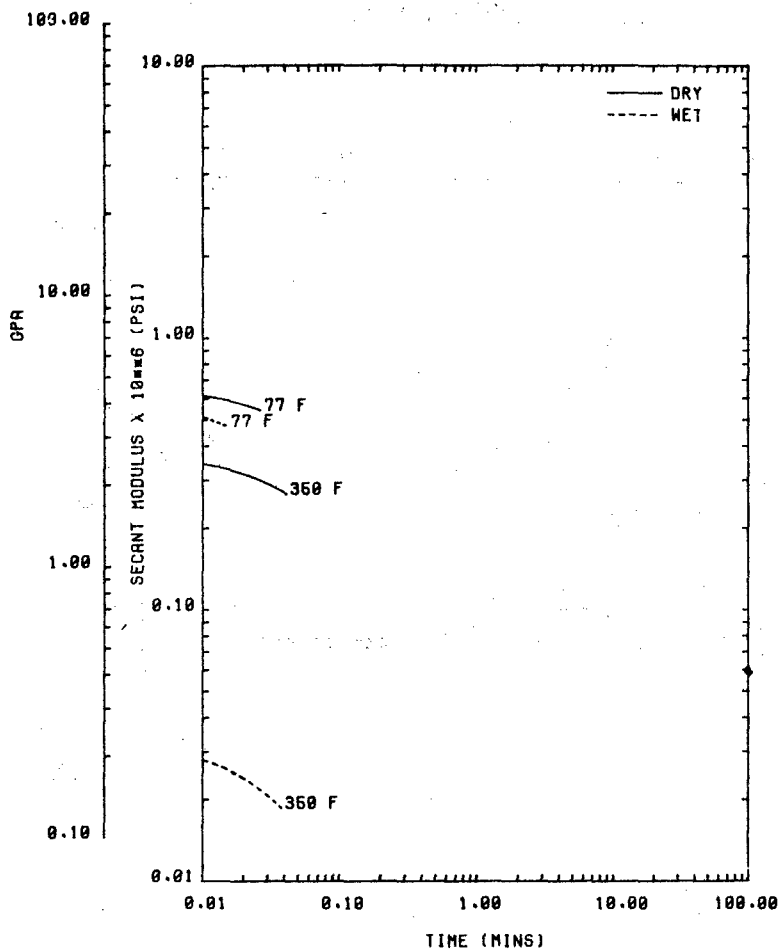

FIG. 9.c Secant Modulus vs Time

3501-5A Epoxy Resin
12KV5 Variation
2.00 in/min C.H.S.

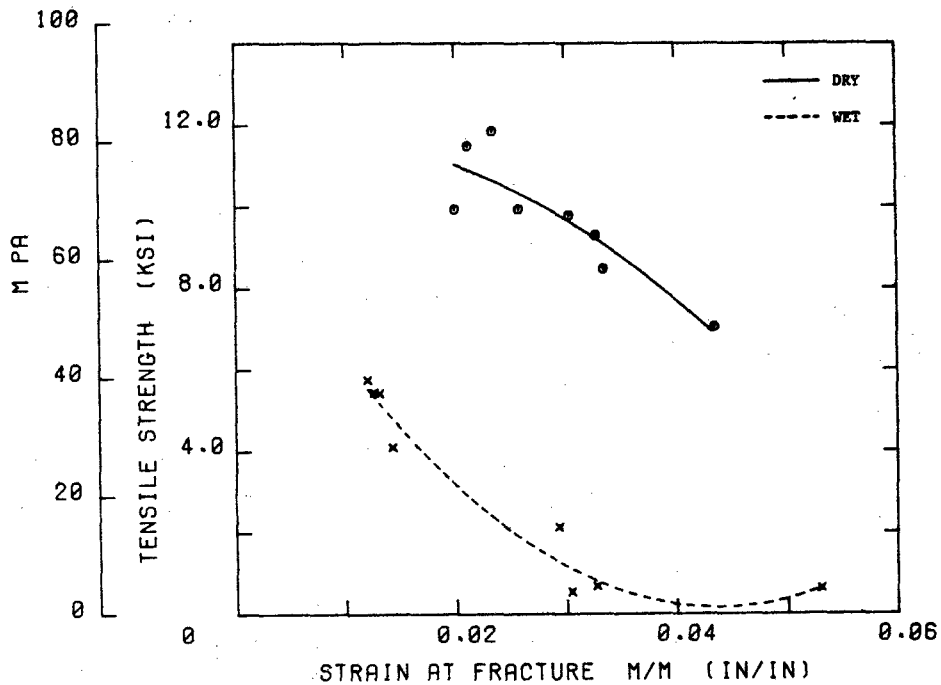

FIG. 9.d Smith Plot

3501-5A Epoxy Resin
12KV5 Variation

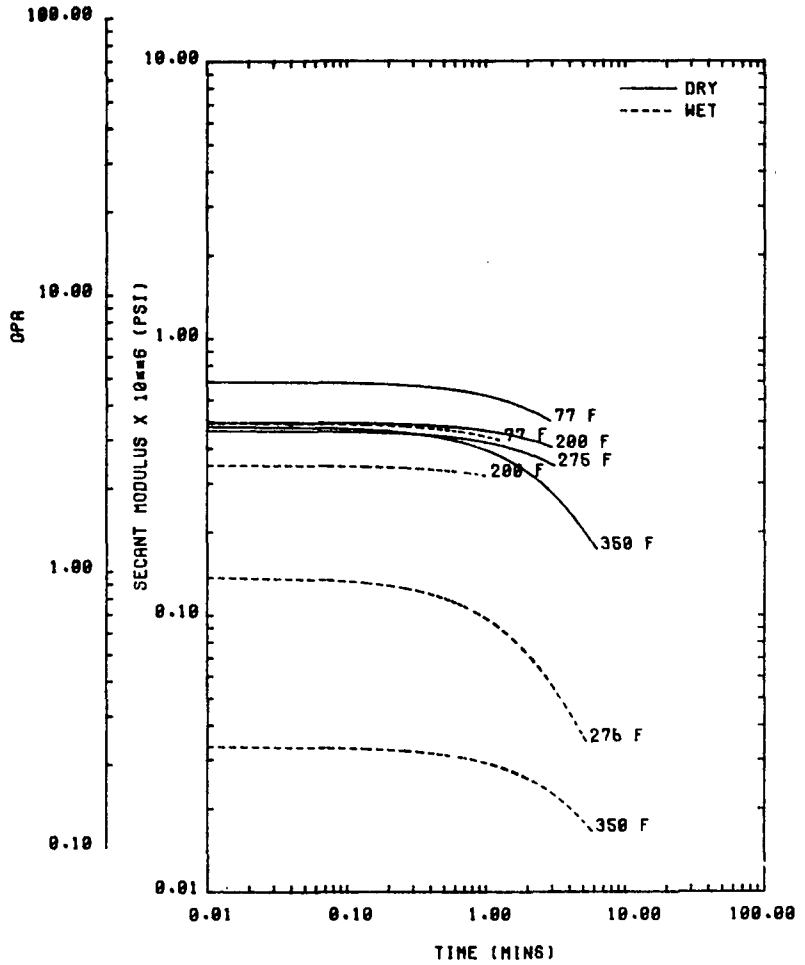

FIG. 10.a Secant Modulus vs Time

3501-5A Epoxy Resin
12KV6 Variation
0.02 in/min C.H.S.

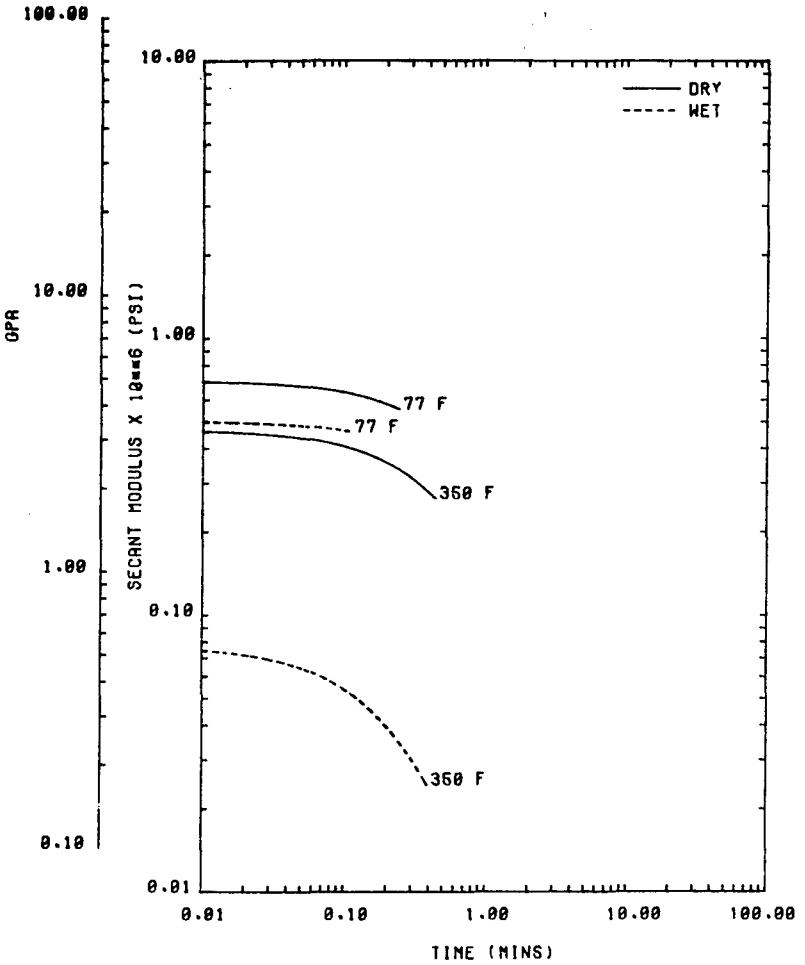

FIG. 10.b Secant Modulus vs Time

3501-5A Epoxy Resin
12KV6 Variation
0.20 in/min C.H.S.

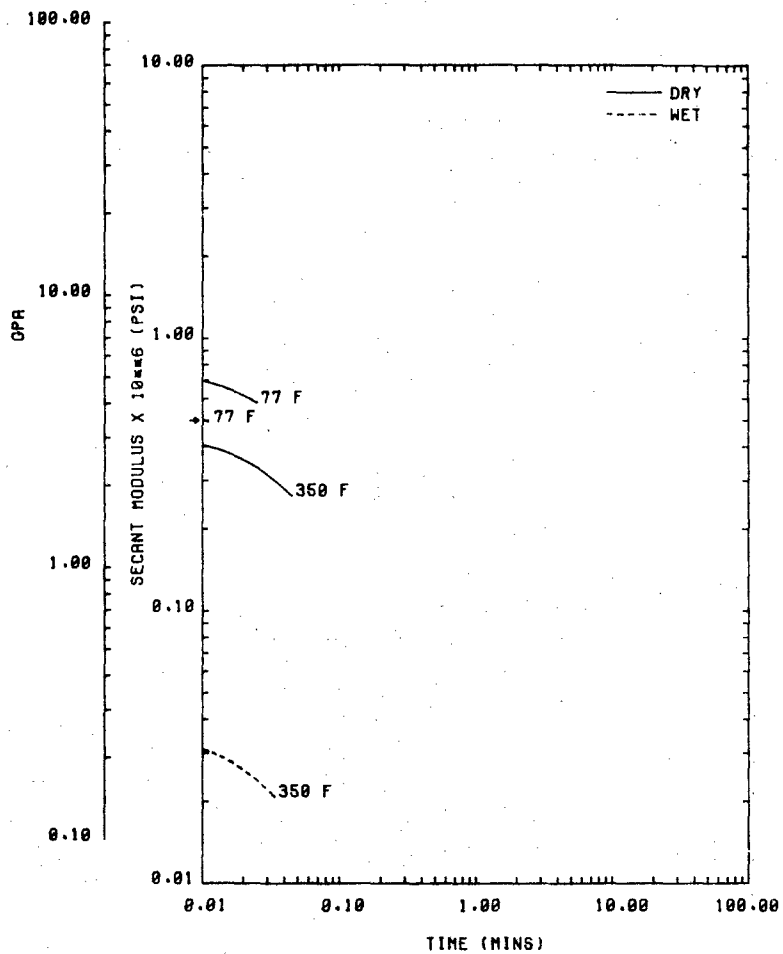

FIG. 10.c Secant Modulus vs Time

3501-5A Epoxy Resin
12KV6 Variation
2.00 in/min C.H.S.

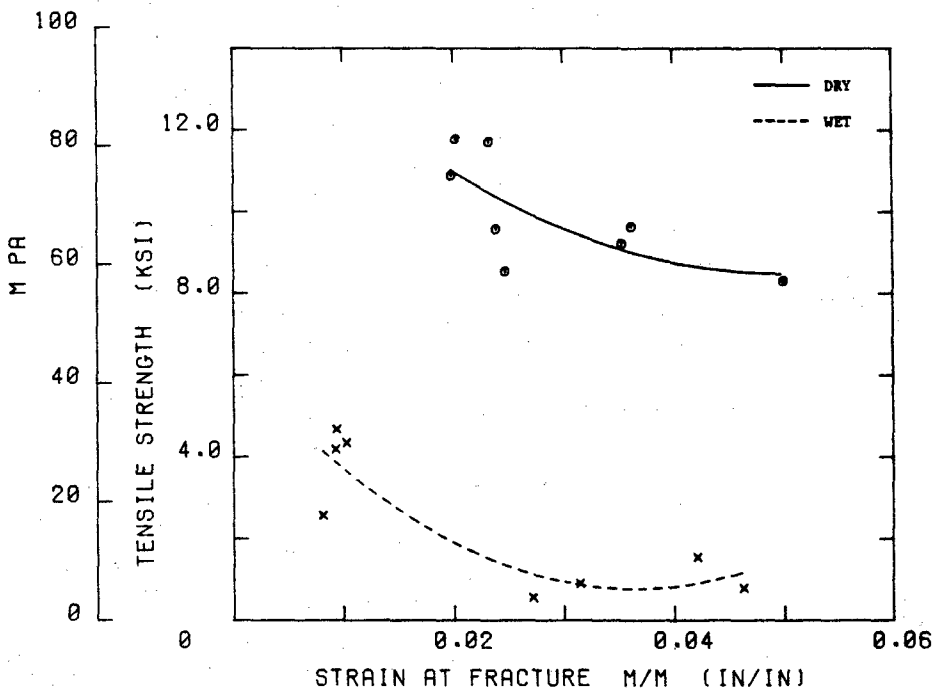

FIG. 10.d Smith Plot

3501-5A Epxoy Resin
12KV6 Variation

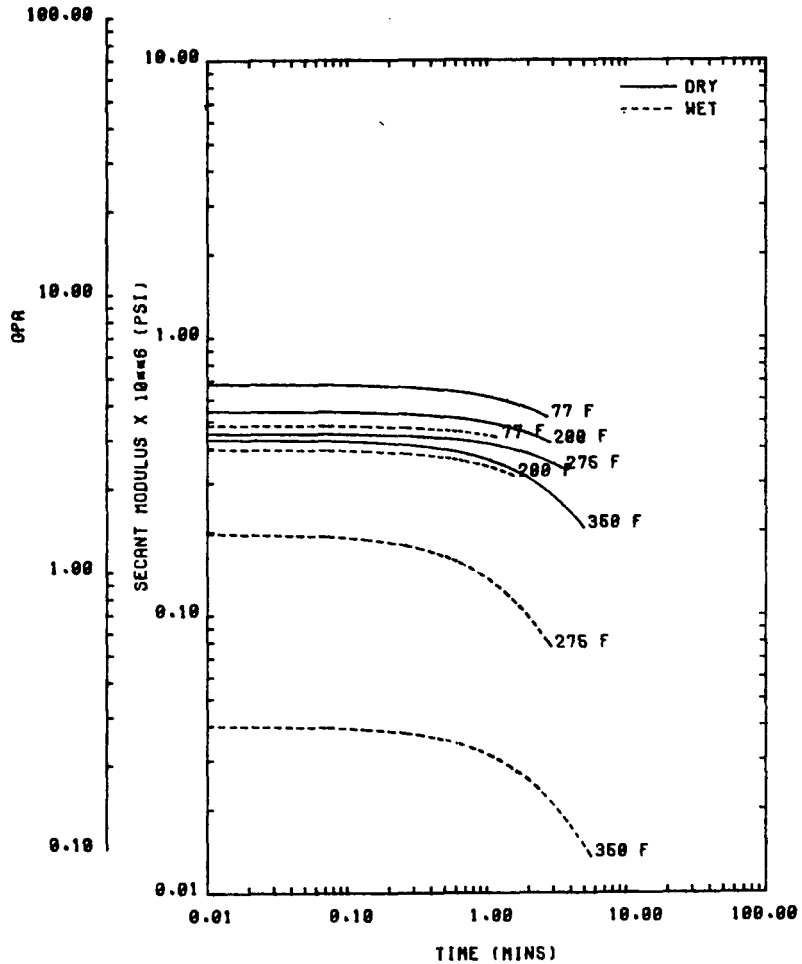

FIG. 11.a Secant Modulus vs Time
3501-5A Epoxy Resin
12KV7 Variation
0.02 in/min C.H.S.

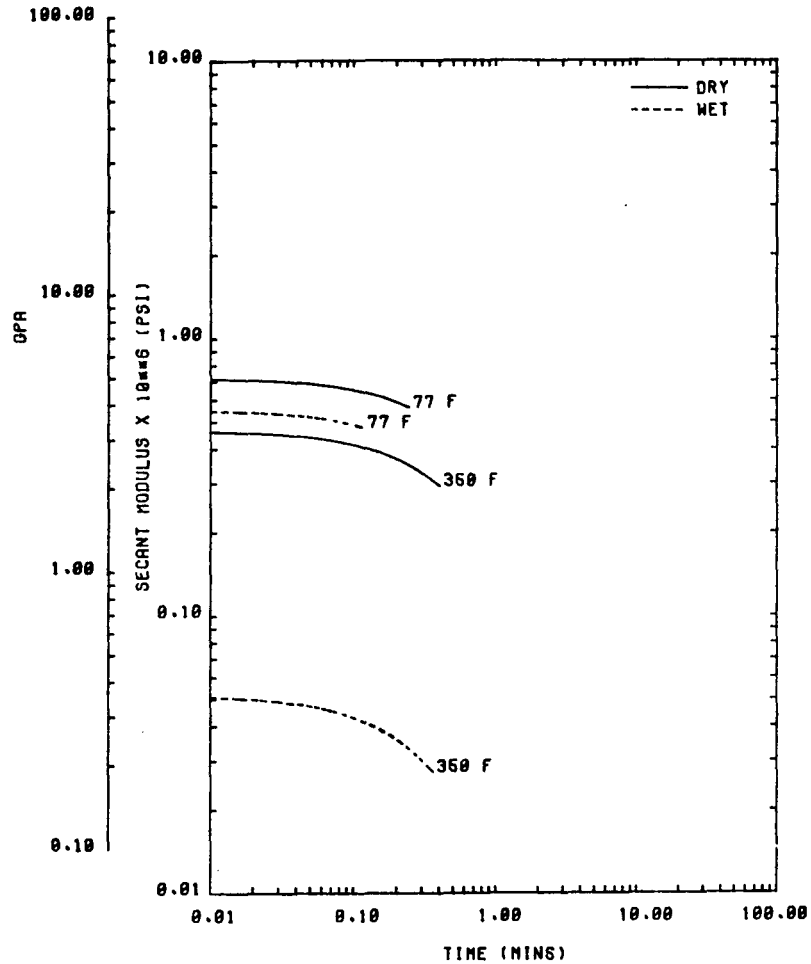

FIG. 11.b Secant Modulus vs Time
3501-5A Epoxy Resin
12KV7 Variation
0.20 in/min C.H.S.

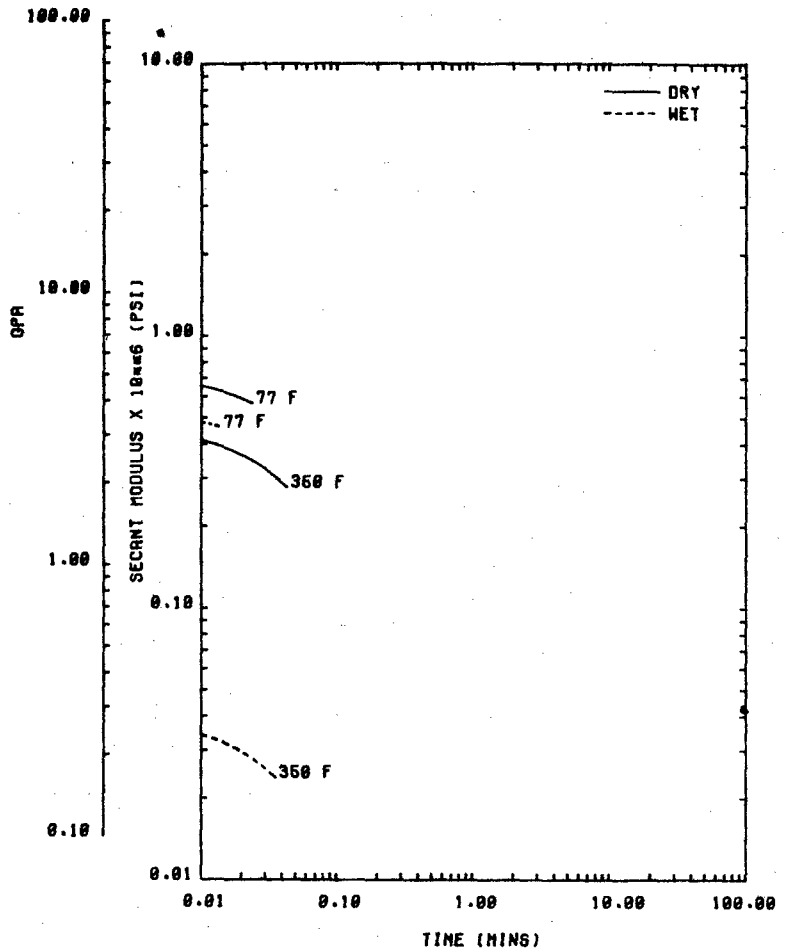

FIG. 11.c Secant Modulus vs Time

3501-5A Epoxy Resin
12KV7 Variation
2.00 in/min C.H.S.

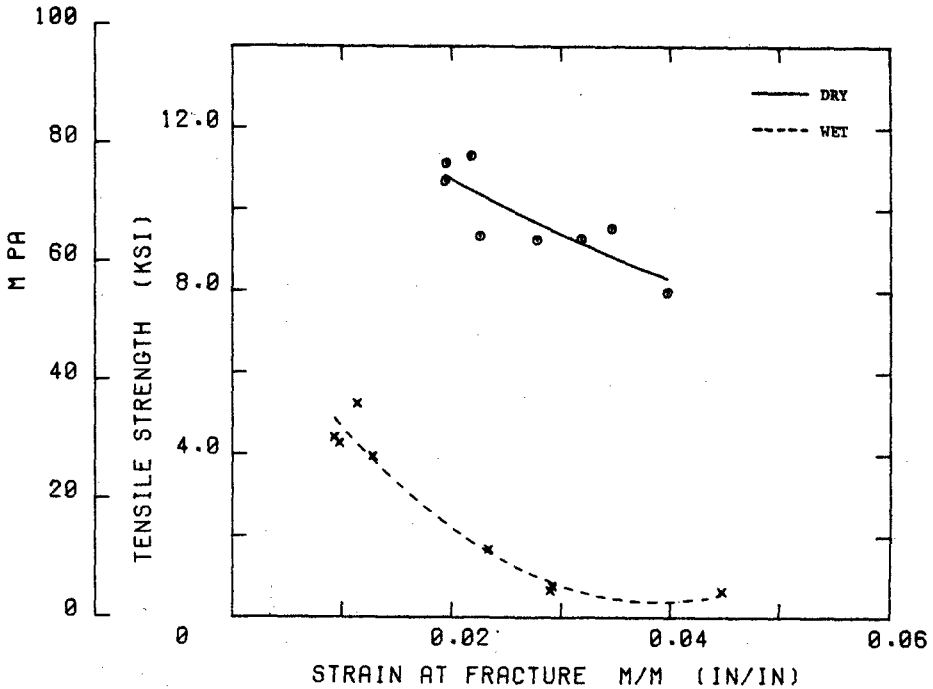

FIG. 11.d Smith Plot

3501-5A Epoxy Resin
12KV7 Variation

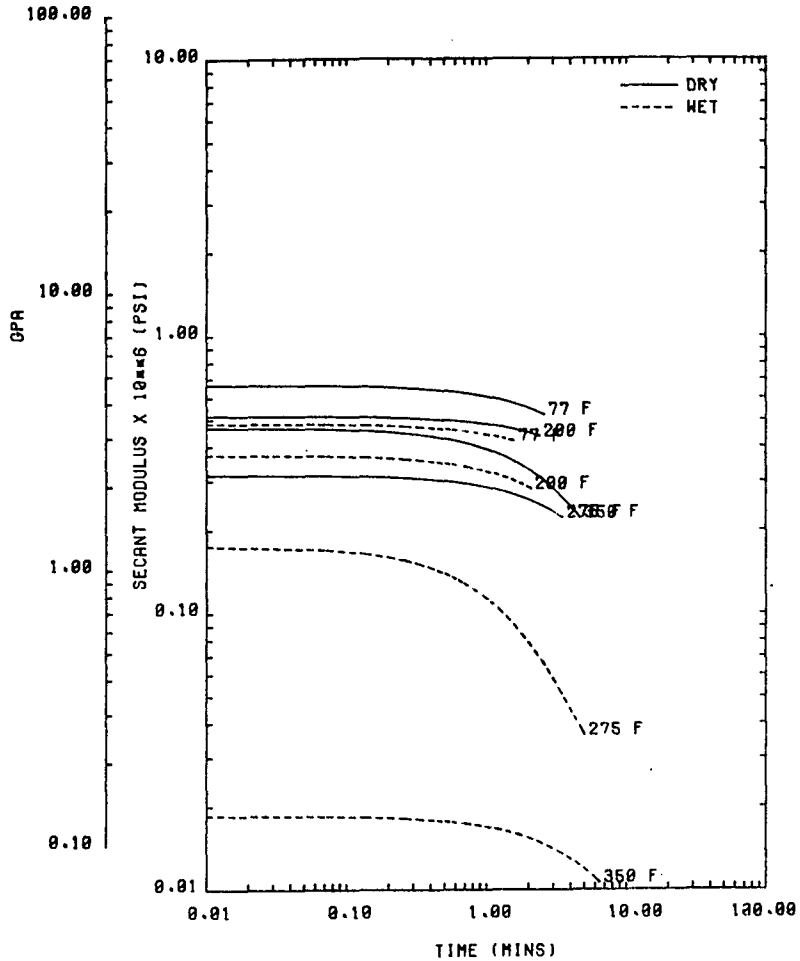

FIG. 12.a Secant Modulus vs Time

3501-5A Epoxy Resin
12KV8 Variation
0.02 in/min C.H.S.

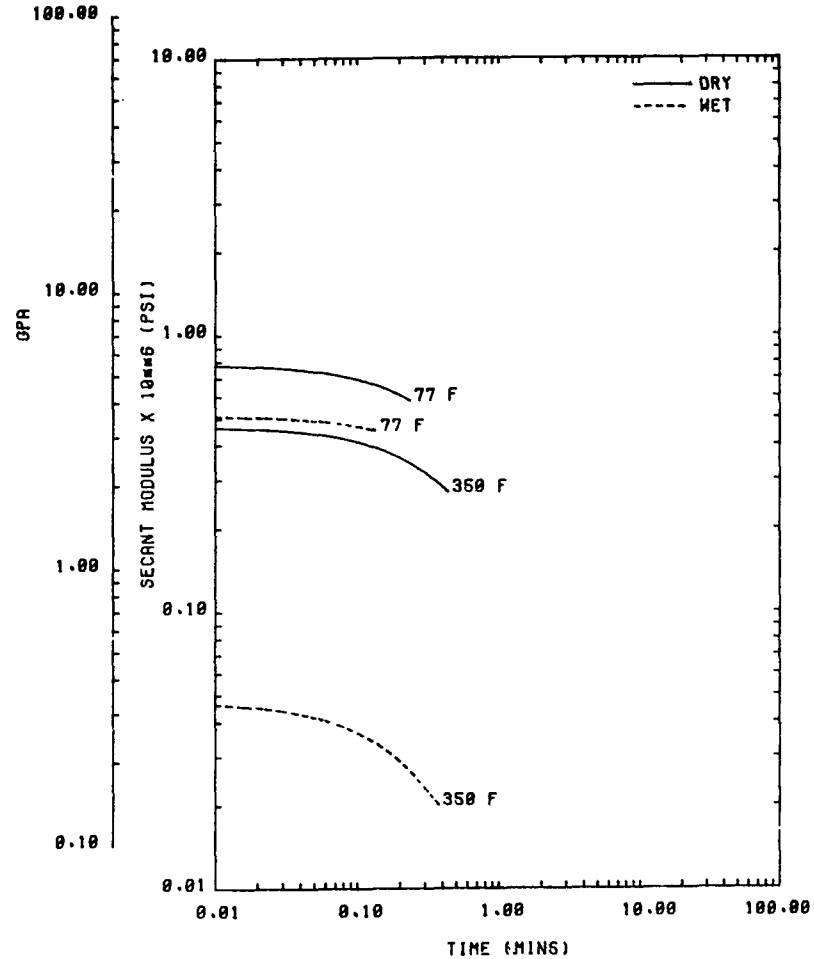

FIG. 12.b Secant Modulus vs Time

3501-5A Epoxy Resin
12KV8 Variation
0.20 in/min C.H.S.

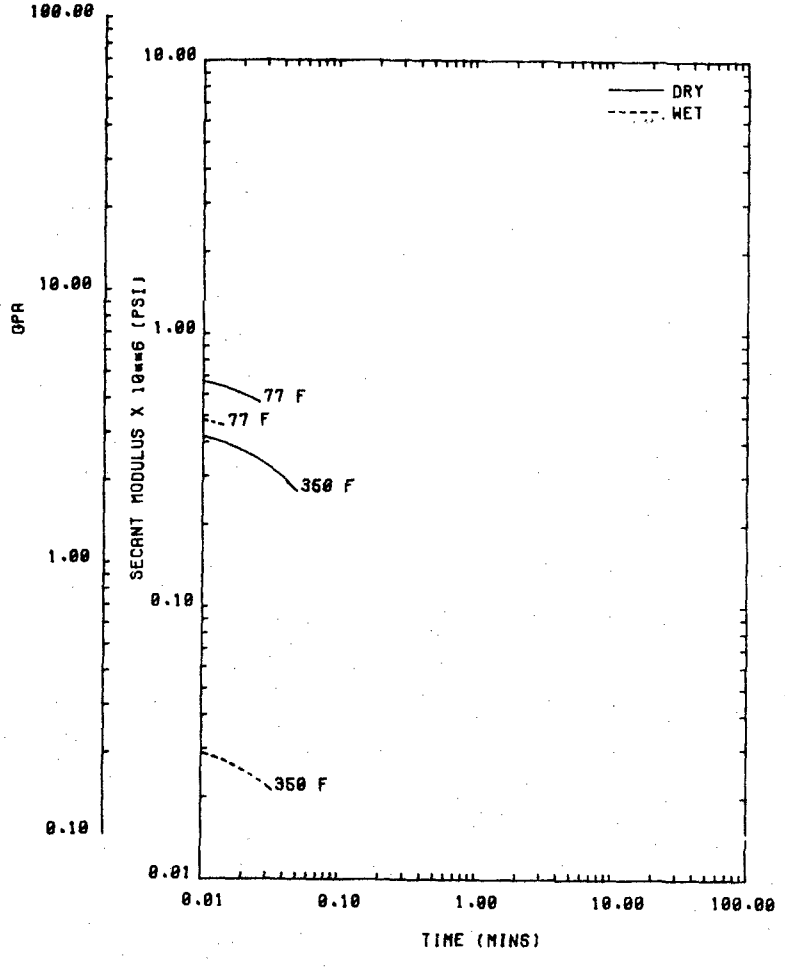

FIG. 12.c Secant Modulus vs Time

3501-5A Epoxy Resin
12KV8 Variation
2.00 in/min C.H.S.

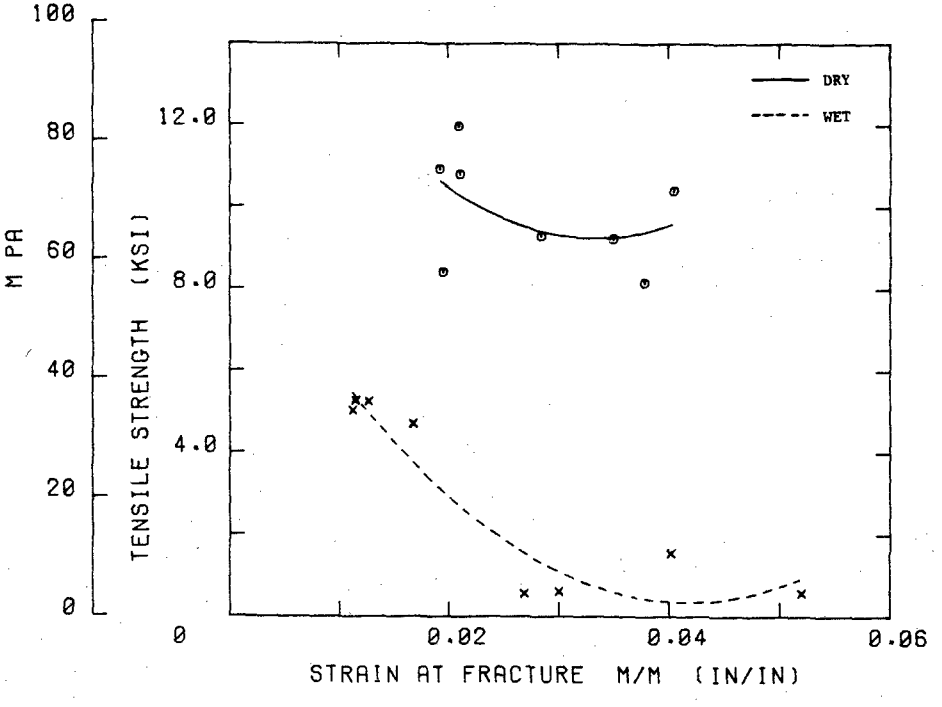

FIG. 12.d Smith Plot

3501-5A Epoxy Resin
12KV8 Variation

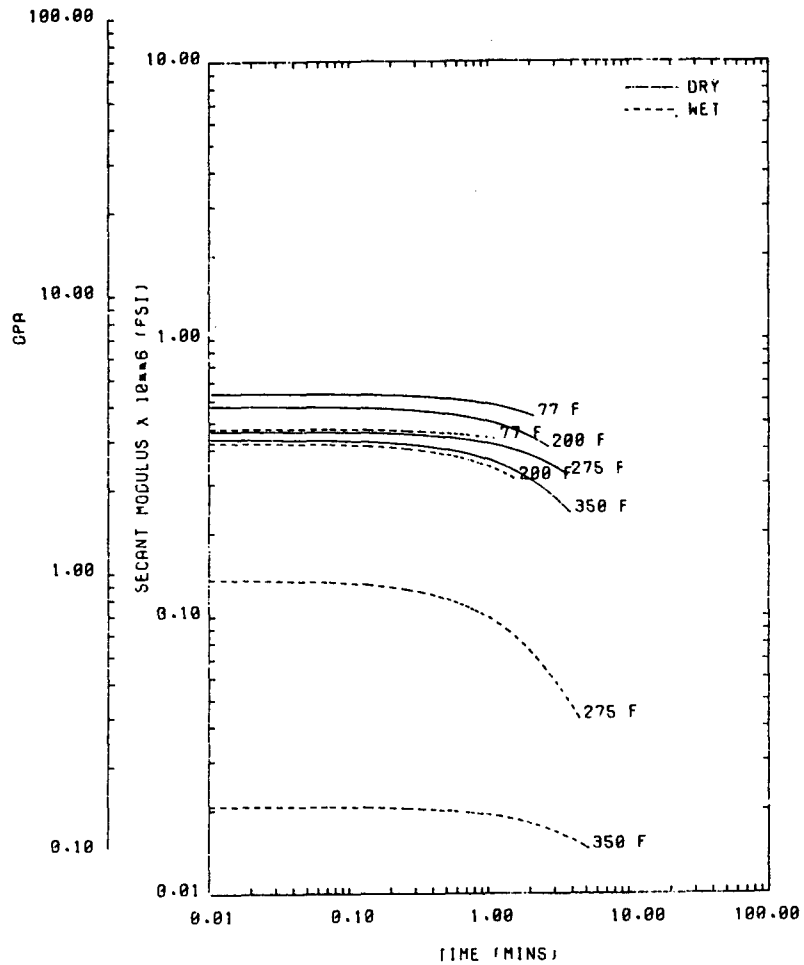

FIG. 13.a Secant Modulus vs Time

3501-5A Epoxy Resin
12KV9 Variation
0.02 in/min C.H.S.

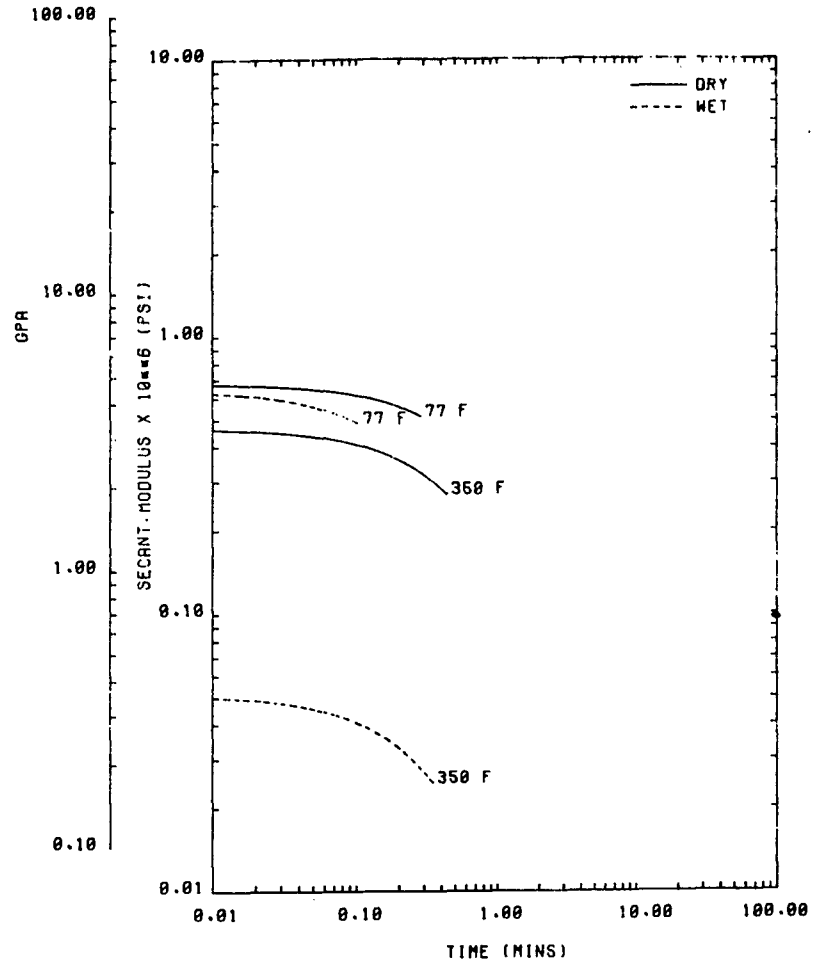

FIG. 13.b Secant Modulus vs Time

3501-5A Epoxy Resin
12KV9 Variation
0.20 in/min C.H.S.

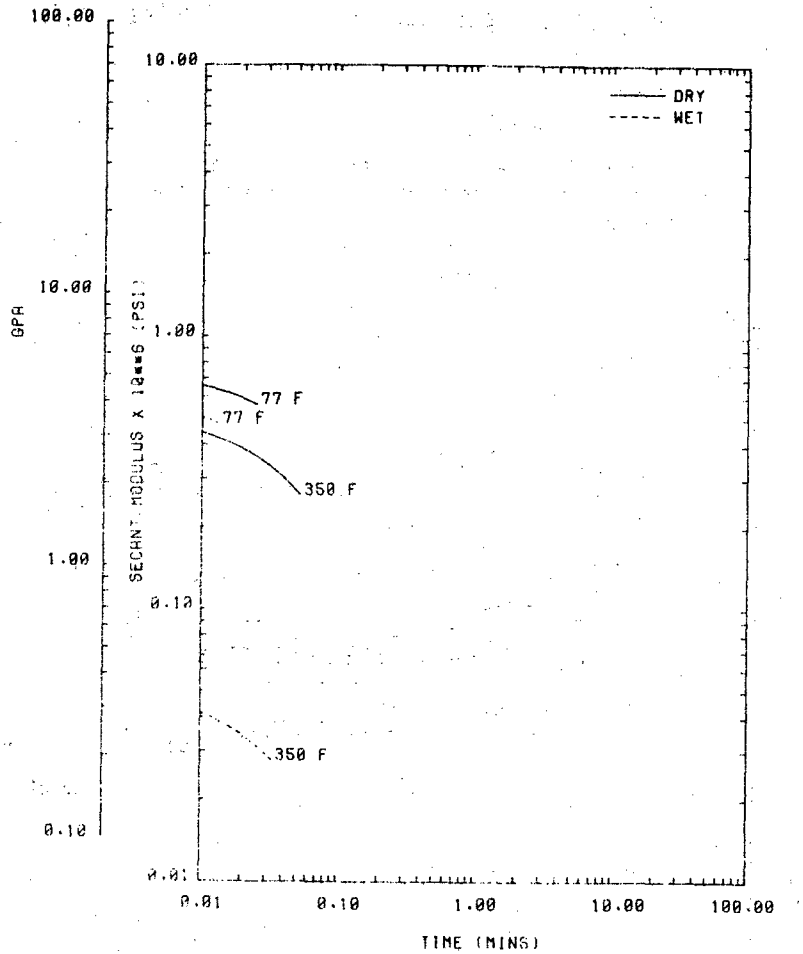

FIG. 13.c Secant Modulus vs Time

3501-5A Epoxy Resin
12KV9 Variation
2.00 in/min C.H.S.

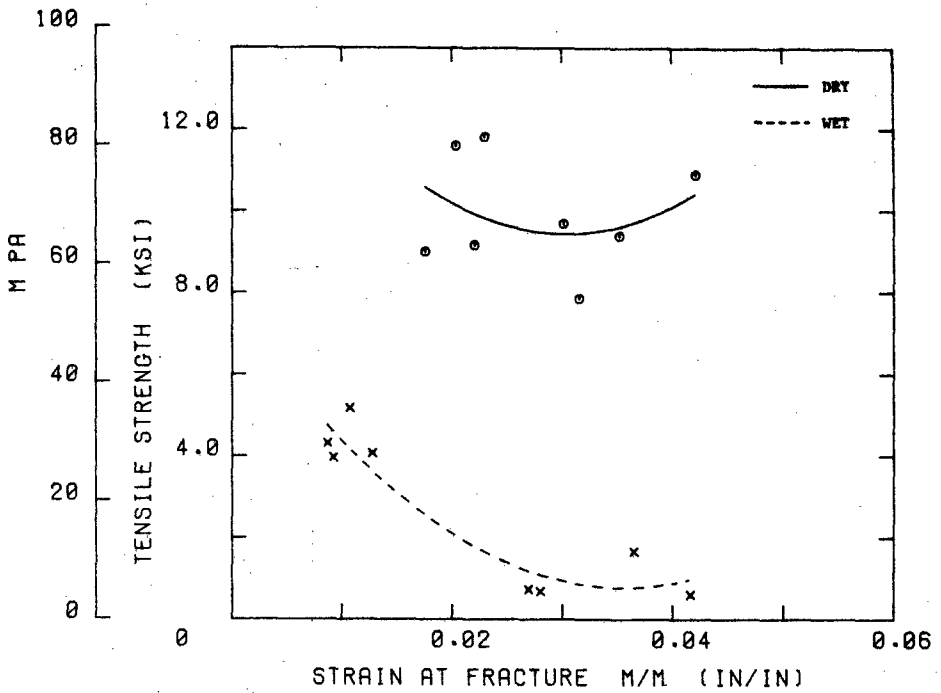

FIG. 13.d Smith Plot

3501-5A Epoxy Resin
12KV9 Variation

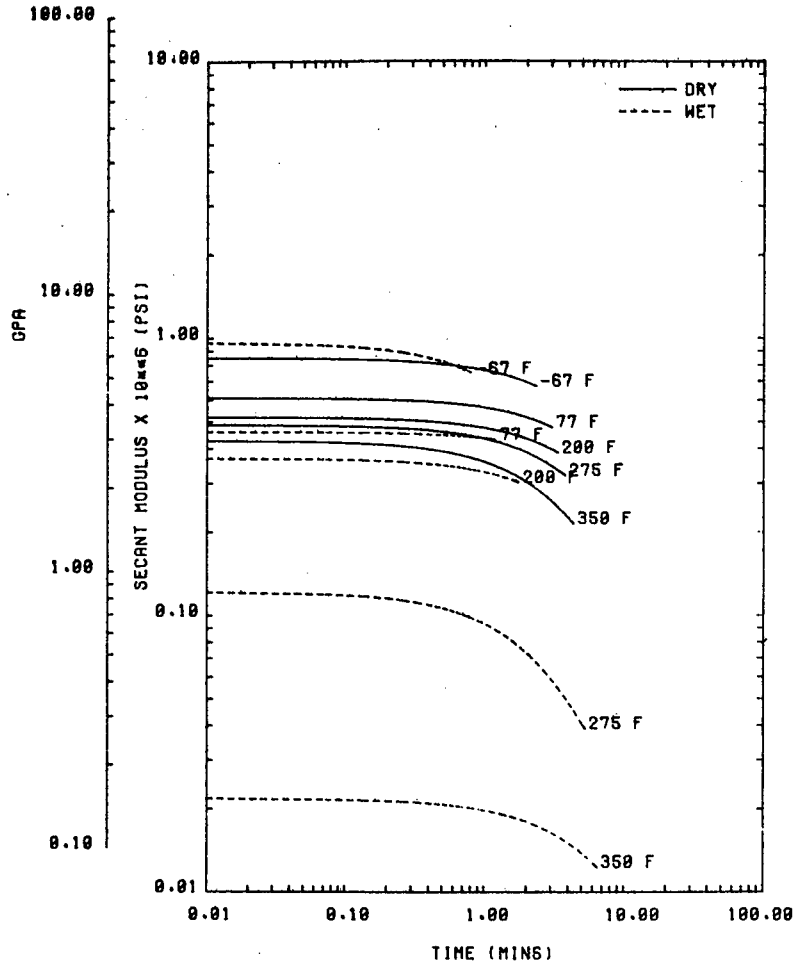

FIG. 14.a Secant Modulus vs Time

3501-5A Epoxy Resin
12KV10 Variation
0.02 in/min C.H.S.

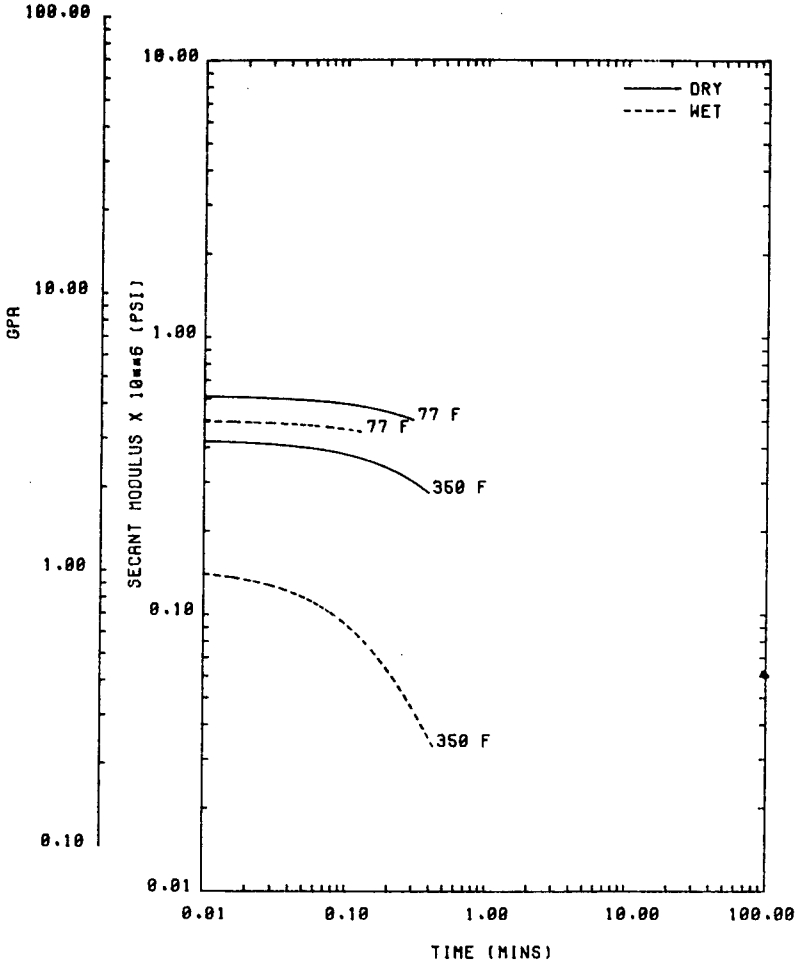

FIG. 14.b Secan Modulus vs Time

3501-5A Epoxy Resin
12KV10 Variation
0.20 in/min C.H.S.

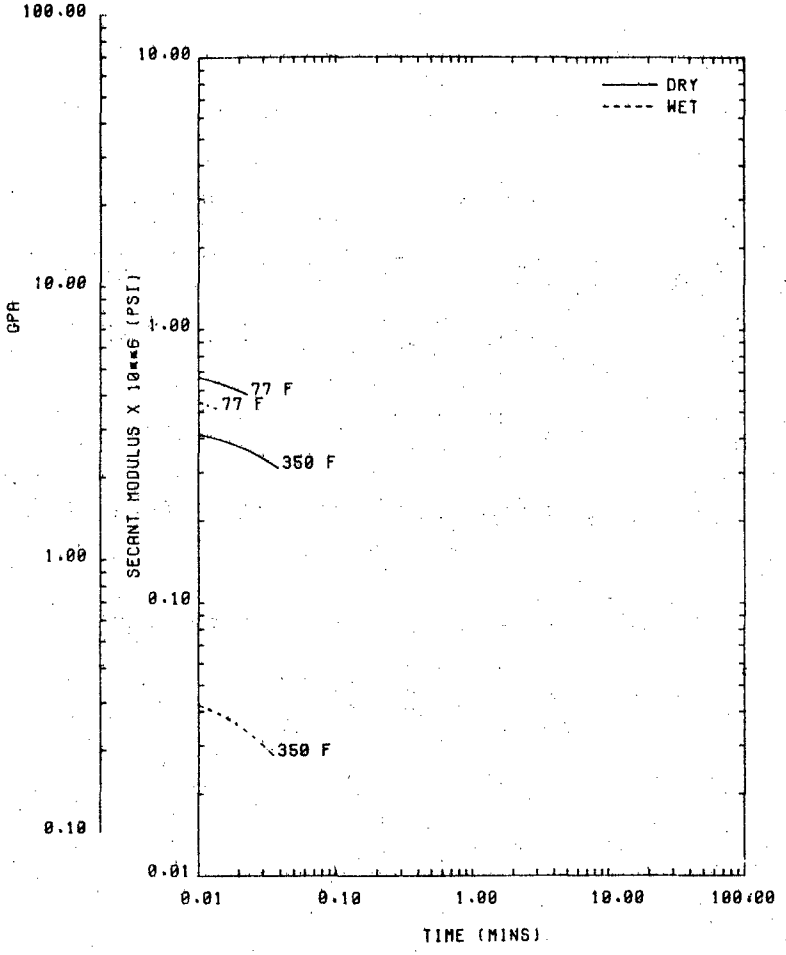

FIG. 14.c Secant Modulus vs Time

3501-5A Epoxy Resin
12KV10 Variation
2.00 in/min C.H.S.

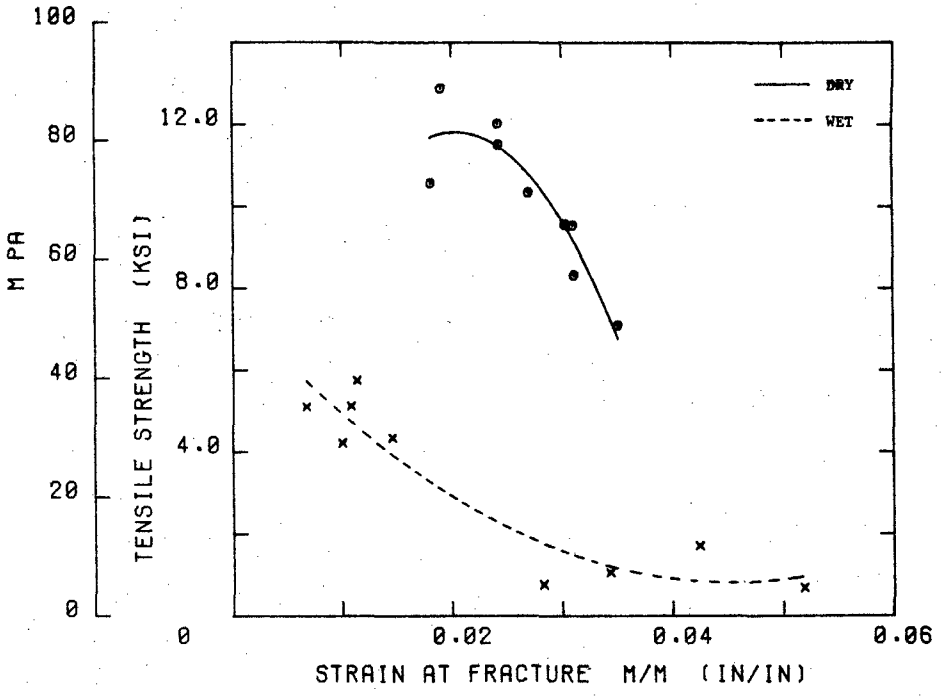

FIG. 14.d Smith Plot

3501-5A Epoxy Resin
12KV10 Variation

TABLE 3

SUMMARY OF MECHANICAL PROPERTIES H-3501-5A EPOXY RESIN

(MEAN VALUES OF FIVE SPECIMENS)

Variation	Condition	Cross Head Speed (in/min)	Temperature °F (°C)	Tangent Modulus $\varepsilon_r = 0$ (10^6 psi)	Strain Energy $0<\varepsilon<.01$ (lb-in/in^3)	Failure			
						Stress (psi)	Strain (in/in)	Secant Modulus (10^6 psi)	Fracture Energy, U_f (lb-in/in^3)
16 KV 1 (High Viscosity Base Resin)	Dry	0.02	-67(-55C)	-	-	-	-	-	-
			77(25C)	.717	32.8	11290	.0206	.547	127
			200(93C)	.499	23.3	8263	.0204	.410	90
			275(135C)	.442	20.4	9000	.0292	.312	150
			350(177C)	.405	16.9	6421	.0442	.149	200
		0.20	77	.729	33.6	10921	.0188	.588	110
			350	.465	20.8	9329	.0347	.269	195
		2.00	77	.792	35.3	11285	.0182	.621	109
			350	.451	20.3	8600	.0338	.266	183
	Wet	0.02	-67	-	-	-	-	-	-
			77	.482	22.4	5765	.0141	.412	42.9
			200	.375	16.6	3880	.0133	.298	28.2
			275	.152	5.2	1311	.0426	.031	42.3
			350	.026	1.1	616	.0460	.014	17.1
		0.20	77	.512	23.8	5866	.0132	.445	40.4
			350	.054	2.8	648	.0244	.027	9.8
		2.00	77	.577	26.0	5821	.0124	.472	39.2
			350	.056	2.5	1161	.0416	.028	30.6
8 KV 2 (Low Viscosity Base Resin	Dry	0.02	-67	-	-	-	-	-	-
			77	.676	30.9	11661	.0233	.501	151
			200	.461	22.1	8198	.0205	.401	98
			275	.429	20.0	9239	.0296	.316	134
			350	.414	17.9	7503	.0421	.180	213
		0.20	77	.705	32.4	11250	.0208	.544	128
			350	.472	21.2	9857	.0359	.276	214
		2.00	77	.690	32.0	10253	.0188	.530	106
			350	.434	19.7	9842	.0384	.260	228
	Wet	0.02	-67	-	-	-	-	-	-
			77	.498	22.9	6665	.0164	.407	58.4
			200	.420	17.4	3536	.0277	.202	99.1
			275	.071	3.0	1402	.0489	.028	44.5
			350	.019	.9	524	.0438	.012	13.2
		0.20	77	.515	23.8	7841	.0190	.414	80.3
			350	.045	1.8	603	.0309	.020	12.1
		2.00	77	.536	24.6	6756	.0157	.469	57.8
			350	.401	1.8	622	.0273	.023	10.5
9 KV 3 (Brittle Resin)	Dry	0.02	-67	.850	39.2	9609	.0131	.720	66
			77	.670	30.6	10660	.0203	.510	116
			200	.528	24.4	10002	.0253	.397	139
			275	.416	19.6	8163	.0246	.336	109
			350	.453	19.3	8012	.0504	.163	289
		0.20	77	.688	31.7	11210	.0211	.531	129
			350	.440	19.9	9086	.0346	.266	191
		2.00	77	1.109	43.3	11076	.0170	.718	107
			350	.440	19.4	8044	.0332	.248	163
	Wet	0.02	-67	.756	34.0	3751	.0053	.703	10.2
			77	.535	24.1	6594	.0163	.415	58.5
			200	.360	16.5	4621	.0139	.292	39.8
			275	.082	3.5	1458	.0453	.033	43.3
			350	.017	0.8	646	.0564	.012	21.3
		0.20	77	.565	25.2	7280	.0168	.434	56.6
			350	.042	1.7	624	.0424	.015	17.9
		2.00	77	.617	26.3	6147	.0136	.460	46.1
			350	.055	2.4	848	.0280	.030	14.6
16 KV 4 (Ductile Resin)	Dry	0.02	-67	1.393	52.8	8561	.0091	.976	46
			77	.698	32.6	9731	.0168	.584	88
			200	.541	25.3	6931	.0153	.460	57
			275	.463	21.4	3376	.0238	.353	110
			350	.446	18.9	7624	.0445	.175	236
		0.20	77	.850	37.8	9644	.0145	.674	76
			350	.441	19.5	8089	.0332	.250	165
		2.00	77	.794	36.2	10519	.0166	.636	94
			350	.495	22.0	9914	.0352	.287	211
	Wet	0.02	-67	.850	36.9	5240	.0070	.789	18.6
			77	.536	23.8	5598	.0132	.428	40.3
			200	.395	17.7	4201	.0135	.319	31.1
			275	.110	4.6	1504	.0354	.044	35.1
			350	.017	0.8	717	.0519	.014	19.8
		0.20	77	.345	24.5	5630	.0125	.451	37.4
			350	.043	1.8	655	.0377	.018	16.5
		2.00	77	.621	27.4	5351	.0106	.509	30.3
			350	.048	2.1	707	.0271	.026	11.8

TABLE 3 (cont.)

SUMMARY OF MECHANICAL PROPERTIES H-3501-5A EPOXY RESIN

(MEAN VALUES OF FIVE SPECIMENS)

Variation	Condition	Cross Head Speed (in/min)	Temperature °F (°C)	Tangent Modulus $\varepsilon \to 0$ (10^6 psi)	Strain Energy $0<\varepsilon<.01$ (lb-in/in^3)	Failure: Stress (psi)	Failure: Strain (in/in)	Failure: Secant Modulus (10^6 psi)	Fracture Energy, U_f (lb-in/in^3)
12 KV 5	Dry	0.02	-67(-55C)	-	-	-	-	-	-
(Increase			77(25C)	.634	29.2	9931	.0200	.499	107
Accelerator			200(93C)	.518	23.8	9939	.0258	.431	139
& Moisture			275(135C)	.436	20.4	9783	.0303	.326	166
Content)			350(177C)	.436	18.4	7046	.0434	.164	211
		0.20	77	.697	31.8	11845	.0234	.513	155
			350	.468	20.6	8470	.0334	.261	175
		2.00	77	.664	31.1	11484	.0212	.545	130
			350	.426	19.6	9292	.0328	.287	176
	Wet	0.02	-67	-	-	-	-	-	-
			77	.498	22.6	5429	.0131	.418	37.6
			200	.386	16.7	4103	.0142	.294	31.8
			275	.254	9.2	2143	.0292	.084	48.3
			350	.026	1.2	612	.0530	.012	20.3
		0.20	77	.460	22.0	5447	.0125	.439	34.1
			350	.039	1.7	680	.0327	.021	13.8
		2.00	77	.600	26.3	5761	.0120	.483	36.8
			350	.033	1.4	540	.0304	.018	10.4
12 KV 6	Dry	0.02	-67	-	-	-	-	-	-
(Hardener			77	.698	31.6	11706	.0232	.506	151
Concentration			200	.498	23.4	9569	.0238	.402	123
15% Excess)			275	.464	21.4	8535	.0246	.349	116
			350	.480	20.4	8306	.0499	.172	298
		0.20	77	.705	32.4	10874	.0197	.555	117
			350	.469	20.8	9218	.0353	.265	199
		2.00	77	.799	35.8	11771	.0201	.586	131
			350	.467	20.8	9626	.0362	.267	208
	Wet	0.02	-67	-	-	-	-	-	-
			77	.496	22.5	4352	.0103	.428	23.5
			200	.348	16.1	2566	.0081	.323	10.7
			275	.137	5.2	1544	.0421	.037	47.0
			350	.033	1.5	783	.0463	.017	22.3
		0.20	77	.304	23.5	4188	.0093	.453	20.3
			350	.078	2.9	891	.0314	.035	17.4
		2.00	77	.610	26.0	4681	.0094	.509	23.1
			350	.038	1.6	556	.0271	.021	9.3
12 KV 7	Dry	0.02	-67	-	-	-	-	-	-
(Hardener			77	.681	31.2	11320	.0218	.531	134
Concentration			200	.543	25.1	9352	.0226	.422	116
10% Below			275	.453	21.0	9257	.0278	.334	144
Normal)			350	.430	18.7	7986	.0397	.205	207
		0.20	77	.721	33.0	10695	.0194	.566	115
			350	.467	21.0	9281	.0318	.293	173
		2.00	77	.735	33.4	11131	.0195	.572	117
			350	.474	21.2	9541	.0346	.276	199
	Wet	0.02	-67	-	-	-	-	-	-
			77	.484	22.5	4275	.0098	.437	21.7
			200	.398	17.6	3953	.0128	.316	28.0
			275	.198	7.2	1682	.0234	.082	28.2
			350	.040	1.6	642	.0447	.015	19.0
		0.20	77	.554	24.9	4412	.0094	.476	21.9
			350	.052	2.2	777	.0292	.027	14.4
		2.00	77	.546	24.7	5244	.0115	.463	31.9
			350	.040	1.8	668	.0290	.023	11.8

TABLE 3 (cont.)

SUMMARY OF MECHANICAL PROPERTIES H-3501-5A EPOXY RESIN

(MEAN VALUES OF FIVE SPECIMENS)

Variation	Condition	Cross Head Speed (in/min)	Temperature °F (°C)	Tangent Modulus $\varepsilon = 0$ (10^6 psi)	Strain Energy (sec.01 (lb-in/in^3)	Failure			
						Stress (psi)	Strain (in/in)	Secant Modulus (10^6 psi)	Fracture Energy, U_f (lb-in/in^3)
12 KV 8 (Accelerator Concentration 20% Excess)	Dry	0.02	-67(-55C)	-	-	-	-	-	-
			77(25C)	.667	30.7	10806	.0210	.519	125
			200(93C)	.516	24.3	8411	.0195	.432	87
			275(135C)	.478	21.9	9298	.0284	.334	132
			350(177C)	.468	20.1	8163	.0378	.219	201
		0.20	77	.789	35.3	10928	.0193	.573	118
			350	.470	21.0	9235	.0349	.266	198
		2.00	77	.750	34.1	11981	.0210	.572	137
			350	.480	21.5	10380	.0405	.257	262
	Wet	0.02	-67	-	-	-	-	-	-
			77	.484	22.4	5257	.0127	.422	35.5
			200	.373	16.6	4702	.0168	.284	43.3
			275	.175	6.1	1560	.0402	.039	46.8
			350	.019	0.9	576	.0520	.011	17.2
		0.20	77	1.272	23.7	5040	.0113	.447	29.9
			350	.048	1.9	612	.0300	.021	25.9
		2.00	77	.544	24.6	5278	.0116	.459	32.4
			350	.034	1.5	562	.0269	.021	8.9
12 KV 9 (Accelerator Concentration 20% Below Normal)	Dry	0.02	-67	-	-	-	-	-	-
			77	.637	29.5	9000	.0175	.524	86
			200	.573	25.7	9161	.0220	.420	111
			275	.465	21.4	9682	.0301	.324	165
			350	.437	18.9	7856	.0315	.204	143
		0.20	77	.678	31.2	11817	.0229	.517	148
			350	.468	20.9	9385	.0352	.267	200
		2.00	77	.737	33.6	11595	.0203	.571	126
			350	.511	22.7	10892	.0421	.262	290
	Wet	0.02	-67	-	-	-	-	-	-
			77	.475	22.3	3964	.0092	.434	19.0
			200	.423	17.9	4068	.0128	.325	28.0
			275	.136	5.2	1669	.0365	.046	40.7
			350	.021	1.0	608	.0416	.013	14.1
		0.20	77	.644	25.7	4310	.0087	.523	20.0
			350	.051	2.1	685	.0280	.025	12.2
		2.00	77	.599	26.0	5171	.0173	.492	29.7
			350	.050	2.1	734	.0269	.027	12.2
12 KV 10 (Standard Sub-Scale Batch)	Dry	0.02	-67	.851	39.0	12883	.0190	.678	131
			77	.612	28.5	11500	.0242	.477	152
			200	.522	24.1	10332	.0269	.386	134
			275	.498	22.1	9539	.0302	.320	168
			350	.428	18.5	7091	.0350	.216	164
		0.20	77	.613	29.0	12012	.0242	.498	137
			350	.426	19.3	8314	.0311	.272	153
		2.00	77	.756	34.2	10567	.0180	.587	103
			350	.461	21.1	9536	.0309	.311	159
	Wet	0.02	-67	.967	37.5	5099	.0067	.785	18.1
			77	.461	22.0	4213	.0100	.425	21.9
			200	.370	16.8	4341	.0145	.302	34.0
			275	.122	4.9	1709	.0424	.041	30.1
			350	.022	1.0	681	.0518	.014	20.0
		0.20	77	.500	23.5	5121	.0107	.482	27.0
			350	.147	5.0	1053	.0343	.030	30.5
		2.00	77	.637	27.9	5749	.0113	.521	35.0
			350	.052	2.2	768	.0282	.027	13.5

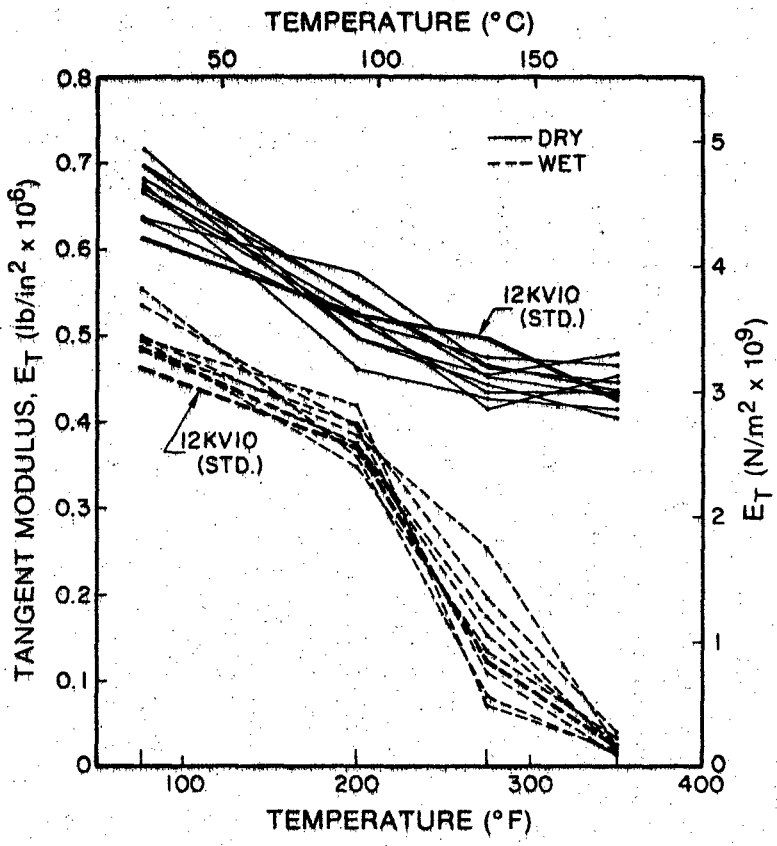

Fig. 15 Tangent Modulus versus Temperature for Ten Variations of H 3501-5A Epoxy Resin 0.02 C.H.S.

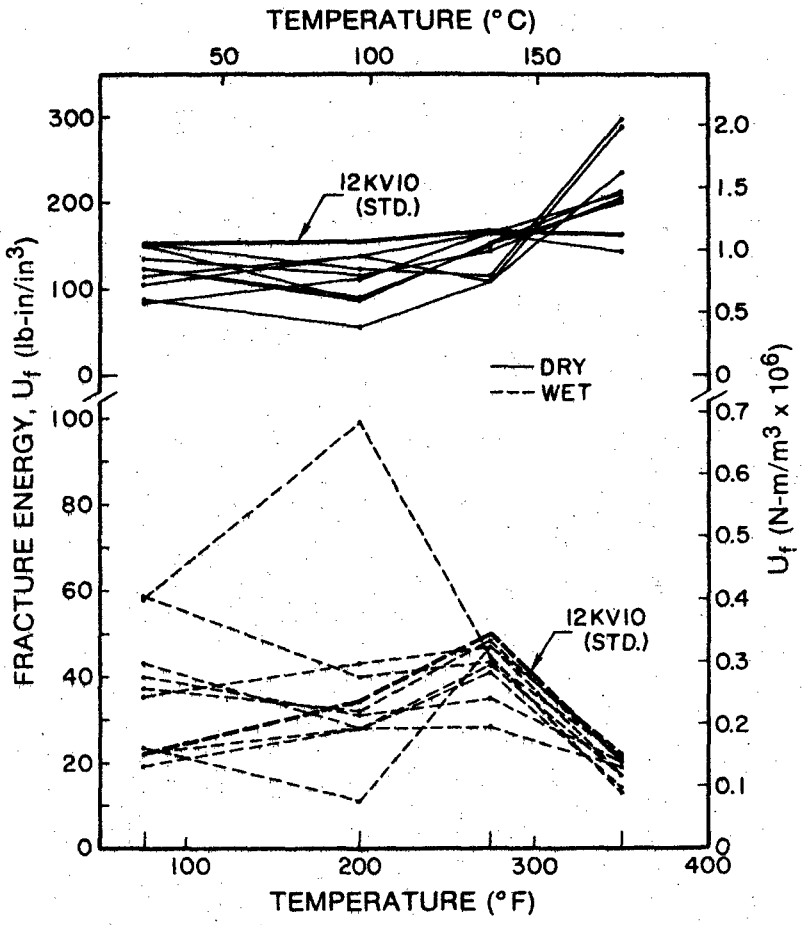

Fig. 16 Strain Energy at Failure in Tension versus Temperature for Ten Variations of H 3501-5A Epxoy Resin 0.02 C.H.S.

was fed through bridge amplifiers which conditioned the signals for simultaneous recording on a two channel oscillograph. Care was observed in calibration and balancing the output of one gage against the other using appropriate cross-over techniques. The gage signals were converted to strains using the calibration values. The axial strain was also monitored during tests using the electro-mechanical extensometer as a check on the axially placed strain gage.

Each test specimen was axially loaded in tension and held at a point well below failure. Both axial and transverse strains were simultaneously recorded during loading and during a relaxation period. Tests were run on only three variations, 8KV3 (Brittle Resin), 16KV4 (Ductile Resin), and 12KV10 (Standard Sub-Scale), at 77 F (25 C), 200 F (93 C), and 350 F (177 C) at a cross head speed of 0.02 and 2.0 inches per minute. Poisson's ratio was evaluated from

$$\nu = -\varepsilon_L/\varepsilon_A \tag{10}$$

where ε_L and ε_A are the lateral and axial strains respectively. Instantaneous recording of strains permitted evaluation of Poisson's ratio during the loading phase or during the relaxation phase. Loading rate had no discernable effect on Poisson's ratio. During relaxation, since the axail strain ε_A was constant ε_L was also constant and Poisson's ratio was constant. Table 4 is a tabulation of Poisson's ratio. Figure 17 indicates that Poisson's ratio is probably very nearly a linear relation with temperature having decreased approximately 10% with increase in temperature over the test range.

(4) Strain Energy - Another parameter which it was felt may reflect material properties is the strain-energy up to 1% strain. This level of strain was chosen because the mean failure strain of all specimen sets was very nearly equal to or greater than 1% and little data extrapolation would be required. Parenthetically there were, of 172 data sets, 4 sets having mean failure strains slightly less than 1%. Where the tangent modulus may be representative of the material rigidity as $\varepsilon \to 0$ and therefore as time $t \to 0$ it does not indicate the elasto-plastic nature of the material with elevated temperature and moisture. This quantity was therefore evaluated by integrating equation (5) to get

$$\int_{0 < \varepsilon < \bar{\varepsilon}}^{U} = A\,\bar{\varepsilon} - \frac{A}{B}\left(1 - \exp(-B\bar{\varepsilon})\right) \tag{11}$$

where $\bar{\varepsilon} = .01$ for all specimen sets and is tabulated in Table 3.

TABLE 4

POISSON'S RATIO
EXPERIMENTALLY DETERMINED FOR THREE VARIATIONS
OF H-3501-5A EPOXY RESIN

Variation	77F (25C)	200F (93C)	350F (177C)
8KV3	0.360	-	0.330
16KV4	0.358	-	0.327
12KV10	0.358	0.341	0.323

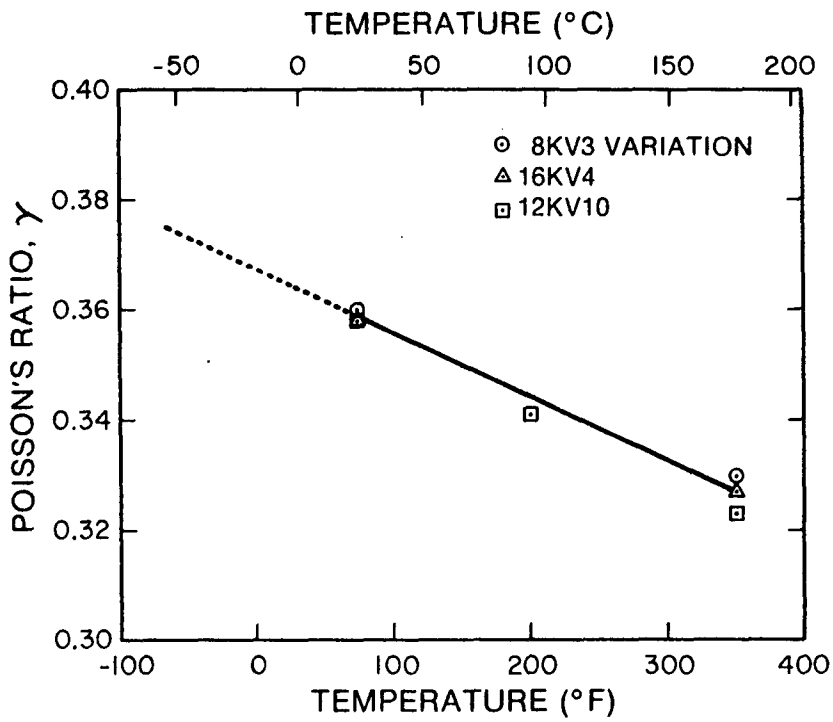

Fig. 17 Poisson's Ratio versus Temperature for Three Variations of H 3501-5A Epoxy Resin

2. FAILURE PROPERTIES

Although great care, cleanliness, and consistancy was observed in preparing specimens through mold preparation to resin pour, resin cure, rough and smooth fabrication and post cure, data scatter was substantial. Cure kinetics may have had an effect on data spread since all specimens of a group did not necessarily come from the same casting of a particular resin variation. A large influence on failure data scatter for a brittle material such as this are cast-in flaws in the form of very small (invisable to the naked eye) bubbles or impurities or molecular anomalies and surface flaws caused during specimen preparation. Tensile failure inconsistancies and fracture toughness data spread emphasize the sensitivity of this material to flaws.

a. Tensile Failure

(1) The Smith Plot - Smith[6] has shown that amorphous polymers have a time-temperature equivalence and that their ultimate tensile strength and ultimate strain over a range of temperatures and strain rates may be reduced to single temperature values. On this basis a representation[7] (now referred to as the "Smith Plot") of the dependence of the stress-strain curves on strain rate and temperature can be developed. The envelope of failure points and the individual stress-strain curves at the various constant strain rates and temperatures forms a region of useful application of the material.

Figures 5.d through 14.d are Smith Plots of the ultimate tensile strength and strain for the ten variations of the H-3501-5A epoxy resin system. The data points represent the average ultimate tensile properties of five specimens of the material in the temperature range -55 C (-67 F) to +177 C (+350 F) and cross head speeds of .02 in/min to 2.0 in/min. (See also Table 3 which summarizes the tensile properties.) Following the curves left to right in each case represents increasing temperature and decreasing strain rate.

The continuous curve for both dry and wet conditions was obtained by a least square polynomial fit. The data scatter is generally large with the data of the standard subscale batch behaving somewhat more orderly

than the rest particularly in the dry state. The data scatter for the dry state for all the variations would suggest that a linear fit may be as justifiable as a polynomial curve fit. On the other hand data for the wet state does seem to justify the polynomial fit and for this reason the same method was applied to both conditions of moisture. Values of stress and strain at failure used to obtain the Smith Plot are tabulated in Table 3.

Table 5 is a comparative summary of the Smith Plot based on the failure sensitivity to temperature-time and to moisture. The tabulation is a judgment evaluation subject to debate. Its purpose is an attempt to develop some form of order to the ten variations. No pattern could be established except perhaps that the standard formulation, 12KV10, seems to stand out from all other nine variations based on a much steeper slope indicating generally higher tensile strengths at smaller strains. For the wet state no differences can be observed.

(2) Strain Energy to Failure - Each stress-strain data averaging equation (Equation (5)) has been integrated (Equation (11)) to the mean strain at failure and the results tabulated in Table 5 as the strain energy U_f at failure. The results are very erratic within a given resin variation. Furthermore when the values for all ten variations are collected on the same Strain Energy - Temperature coordinates as shown in Figure 16, a broad band formed by crossover of data precludes characterization using this parameter. An averaging process seems to indicate an increase in U_f with increasing temperature for dry specimens and a decrease with increasing temperature for wet specimens. It is not apparent why the isolated point occurred at 200°F for the variation 8KV2 (Low Viscosity Resin). The original data was carefully checked. This set of specimens may not have been properly wet conditioned.

This material is brittle in nature. It fails catastrophically. In the dry state the material shows normal viscoelastic behavior with an apparent temperature-time equivalence. In the wet condition the material

takes on a cheezy character with the small H_2O molecule acting as a plasticizer by occupying intermolecular voids and acting as a "lubricant" permitting more mobility between chains. Further hydraulitic degredation may be occurring when the hydrogen ion or the hydroxyl radical sever the long chains into shorter chains, again resulting in more mobility. On the other hand, by forming secondary bonds, viz hydrogen bonding, to the larger polymer molecule and spreading them apart thus reducing the polymer to polymer chain secondary bonding more room is provided for the polymer molecules to move around and past each other providing a more deformable material.

Values of strain energy at failure of a limited number of individual specimens have been integrated using a polar planimeter. These values are tabulated in Table 8. An arithmetical average of the measured strain energy of any set of five specimens which is also tabulated compares very well with the mathematically integrated area to the mean strain at failure of the data averaging equation (5) tabulated in Table 3 and again in Table 8. This strengthens the validity of using this equation as a representation of the data of five specimens of a particular set of parameters.

(3) Fracture Toughness - Fracture toughness of the H-3501-5A epoxy system was carried out using the ASTM procedure E 399-78[8] for metallic materials as a guideline. For this work a test fixture for four point beam loading instead of the recommended three point was fabricated. This provided a uniform moment in the region of the fracture and therefore slight off center alignment of the initiating crack of the specimen in the load frame could be tolerated. Handling of hot specimens in a hot environmental chamber had to be accomplished rapidly. Figure 18 is a full size sketch of the specimen which was used for all fracture toughness tests. To provide a geometry which would accommodate a displacement gage across the crack, two lugs were routed into the beam shape. A crack starter envelope 0.012 inches wide by 0.10 inches deep was milled into the specimen centered between the gage lugs. A razor cut was

TABLE 5

SMITH PLOT COMPARATIVE SUMMARY

	H-3501-5A Variation									
(Rated Low, Moderate, High)	16KV	8KV	8KV	16KV	12KV	12KV	12KV	12KV	12KV	12KV
	1	2	3	4	5	6	7	8	9	10
Dry Strength Sensitivity to temperature-time	M	L	L	L	M	L	M	L	L	H
Dry Strain Sensitivity to temperature-time	M	M	H	H	M	M	L	L	M	L
Wet Strength Sensitivity to temperature-time	H	H	M	M	M	L	M	M	M	M
Wet Strain Sensitivity to temperature-time	M	M	H	H	H	M	M	H	M	H
Moisture Sensitivity	H	M	M	M	H	H	H	H	H	H

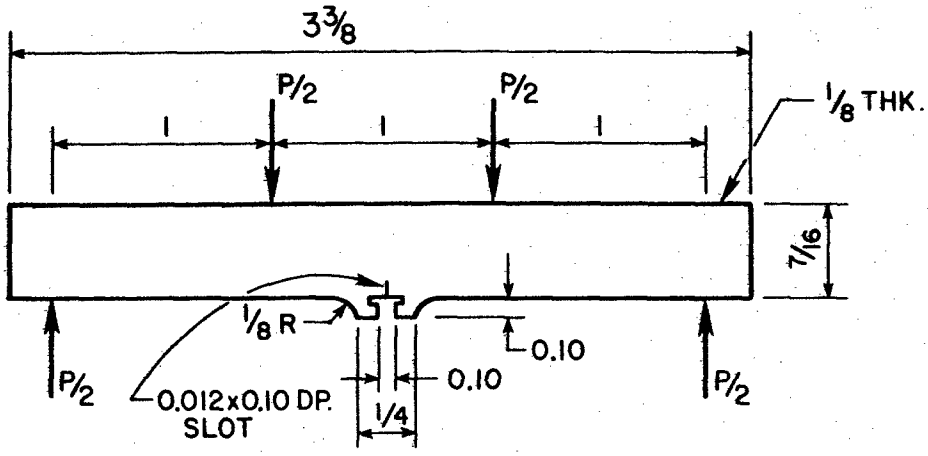

Figure 18 Fracture Toughness Specimen

made at the base of the milled slot to initiate a crack which is then varified as a reasonably well ordered fully developed crack (crack, not razor cut) across the beam thickness by using a 30 power measuring microscope. At the same time crack depth "a" and beam depth "b" were measured to a resolution better than 0.01 mm.

Fracture was by the opening Mode I[9] in which the crack surfaces move directly apart. The plain-strain critical stress intensity factor or fracture toughness K_{IC} for this mode was evaluated by the method summarized by Tada, Paris, and Irwin[9] using the equation valid for a beam in pure bending (4 point) as follows;

$$K_I = \sigma_{xx} \sqrt{\pi a}\ f(a/b) \tag{12}$$

where

$$\sigma_{xx} = \frac{6M}{db^2} \tag{13}$$

and

$$f(a/b) = 1.122 - 1.40\ (a/b) + 7.33\ (a/b)^2 - 13.08\ (a/b)^3 + 14.0\ (a/b)^4 \tag{14}$$

where: K_I = Mode I stress intensity factor

a = crack depth

b = beam depth

d = beam thickness

M = moment

and $f(a/b)$ is 0.2% accurate for $a/b \leq 0.6$

Photoelastic studies of 4X sized models, Figures 19a and 19b were used to confirm that the lugs for the displacement gage did not appreciably alter the stress field at the crack front.

A displacement gage was fabricated following the general configuration described in ASTM E 399-78. The two fingers of the gage were fabricated of bronze shim stack .020 inches thick by 1/4 inch wide by 2 inch cantilever length. Each finger had a tension and compression strain gage mounted at its root. They were separated 3/16 inches by an aluminum spacer block to minimize weight. Assembly of the entire unit was accomplished by using a high temperature epoxy resin commonly used in mounting strain gages. When placed in position on the test specimen the fingers of the displacement gage exerted no more than 50 grams force at the point of application. It is important that this force be held to a minimum or accounted for as part of the moment M in Equation (13). In this case this minor moment was less than 2.5 percent of the major moment, for the worst cases of fracture tests conducted which were at the high temperatures and wet condition. Because of this small influence and the difficulty of actually evaluating this minor moment (as crack deflection increases particularly at high temperatures, wet, the displacement gage force decreases) it was ignored.

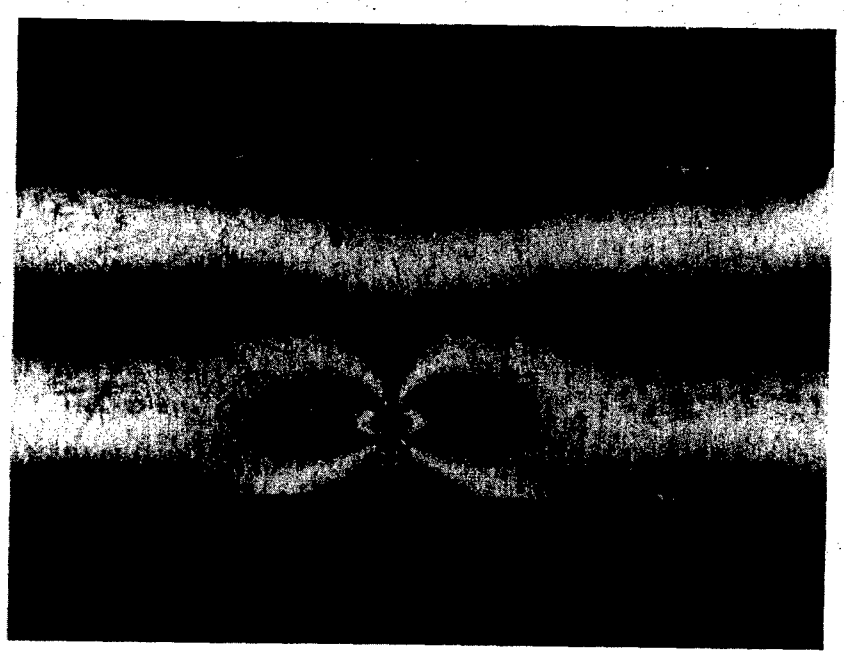

Fig. 19a Photoelastic Model (4X) of Fracture Specimen Without Displacement Gage Lugs

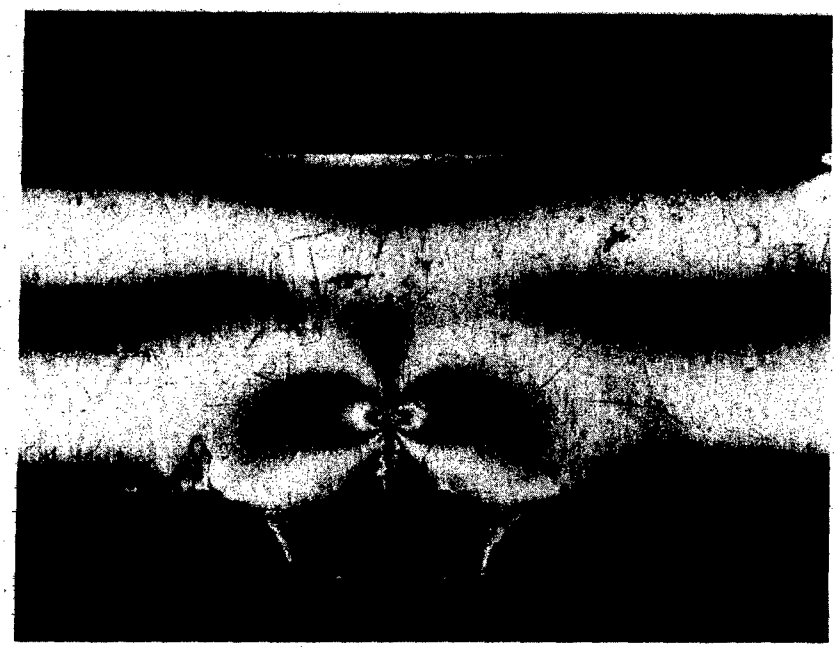

Fig. 19b Photoelastic Model (4X) of Fracture Specimen With Displacement Gage Lugs

Load and diaplacement signals were appropriately conditioned and recorded on an X-Y plotter to monitor any deviation from linearity as specified by the ASTM E 399-78 code.

For these fracture toughness tests in all ranges of temperature and both dry and wet conditions the load-deflection data was linear within the ASTM allowable 5% deviation. All tests were conducted at a cross head speed of 0.02 inches per minute. Again 5 specimens were tested at each condition and reported values are the arithmetical average of five test results. Table 6 summarizes the critical stress intensity factors K_{IC}.

Figure 20 is a point-to-point plot of the fracture toughness of the ten epoxy resin variations as it varies with temperature and moisture state. In the dry state generally K_{IC} increases with temperature over the full span of temperature -67 F (-55 C) to +350 F (177 C) for all variations. This may be predictable on the basis that subcritical crack growth in a polymer is due to thermomechanically activated processes such as chain stretching, plastic deformation, void opening, chain disentanglement and chain breaking[10] and that increasing the temperature increases the molecular mobility increasing the ability of the polymer chains to untangle and slip past one another resulting in a tougher material.

On the other hand the toughness K_{IC} drops off drastically for wet specimens with increasing temperature to 350 F (177 C). The presence of a small molecule such as H_2O could produce the effects of a plasticizer by hydrogen bonding to polar linkages and/or by occupying the free volume. This normally should lower the glass point temperature T_g and therefore increase instead of decrease the toughness of the material. The stress intensity factor K_I is an indication of the intensity of the local stress field at the crack tip and is based on the crack length and the external applied stress σ_o. The fracture toughness K_{IC} or critical stress intensity factor is an indication of the local stress field at the crack tip when catastrophic failure occurs, caused by the external critical stress σ_o. In this case however the behavior of K_{IC} with temperature for wet specimens, normally thought of as the resistance to crack propagation, is totally obscured by the behavior of the modulus with temperature. A more significant

basis for judging the material resistance to fracture therefore is the Griffith criterion which is a measure of the rate of decrease of the total elastic energy with crack extension. Then

$$G_I = -\frac{1}{d}\frac{\partial U_e}{\partial a} \tag{15}$$

where: G_I = strain energy release rate

U_e = elastic energy

a = crack depth

d = material thickness

For the plain strain problem G_I[11] is related to K_I[11][12] by

$$G_I = \frac{\pi a \sigma_o^2}{E(T,t)}(1 - \nu^2) f(a/b) \tag{16}$$

$$= \frac{K_I^2}{E(T,t)}(1 - \nu^2) \tag{17}$$

where: G_I is the energy release rate sometimes referred to as "the crack extension force"

This quantity now accounts for the variation of modulus with temperature and time which is significant for this material and Poisson's ratio with a somewhat lower temperature sensitivity. When the critical stress intensity factor K_{IC} is used in Equation (16) G_I becomes G_{IC}, the critical energy release rate. Table 7 tabulates the G_{IC} values. Modulus values were assumed to be the tangent modulus at the appropriate state taken from Table 3. Poisson's ratio was taken from Figure 17 and is assumed to be a function of temperature only, not of dry or wet condition or strain rate as previously mentioned. The critical energy release rate G_{IC} is plotted point-by-point against temperature, Figure 21. Figure 21 indicates that the resistance to fracture increases with temperature as one would expect and furthermore that the material responds similarly to fracture regardless of its condition, dry or wet.

(4) Flaw Size Correlation - Since this material seems to be highly sensitive to flaws, an attempt was made to correlate flaw size with the strain energy at failure. This study was not used to characterize the

TABLE 6

SUMMARY OF CRITICAL STRESS INTENSITY FACTORS, MODE K_{I_C}
H-3501-5A EPXOY RESIN

	Critical Stress Intensity Factor K_{I_C} (lb-in$^{-3/2}$) (Mean value of five specimens)					
	Dry Condition			Wet Condition		
Variation	-67F (-55C)	77F (25C)	350F (177C)	-67F (-55C)	77F (25C)	350F (177C)
16 KV 1	616	632	739	547	484	175
8 KV 2	619	767	692	548	523	168
8 KV 3	631	787	845	636	513	131
16 KV 4	611	847	853	633	508	175
12 KV 5	642	627	748	580	523	145
12 KV 6	660	787	880	653	552	150
12 KV 7	647	633	746	634	477	137
12 KV 8	606	552	793	600	537	125
12 KV 9	602	645	818	669	531	170
12 KV 10	612	592	734	725	582	169

TABLE 7

SUMMARY OF CRITICAL ENERGY RELEASE RATE G_{I_C}
H-3501-5A EPOXY RESIN

	Critical Energy Release Rate G_{I_C} (lb-in/in^2) (See Note Below)					
	Dry Condition			Wet Condition		
Variation	-67F (-55C)	77F (25C)	350F (177C)	-67F (-55C)	77F (25C)	350F (177C)
16 KV 1	-	.485	1.204	-	.423	1.052
8 KV 2	-	.758	1.033	-	.478	1.327
8 KV 3	.401	.805	1.408	.458	.413	.901
16 KV 4	.230	.895	1.457	.404	.419	1.609
12 KV 5	-	.540	1.146	-	.478	.722
12 KV 6	-	.773	1.441	-	.535	.609
12 KV 7	-	.513	1.556	-	.410	.419
12 KV 8	-	.398	1.200	-	.519	.734
12 KV 9	-	.569	1.367	-	.517	1.229
12 KV 10	.377	.499	1.124	.465	.640	1.159

Note:
G_{I_C} has been evaluated on the basis that Poissons Ratio is a function of temperature only and not dependent on the resin variation or on its condition, dry or wet. The tangent modulus determined at the lowest strain rate (0.02 C.H.S.) has also been used.

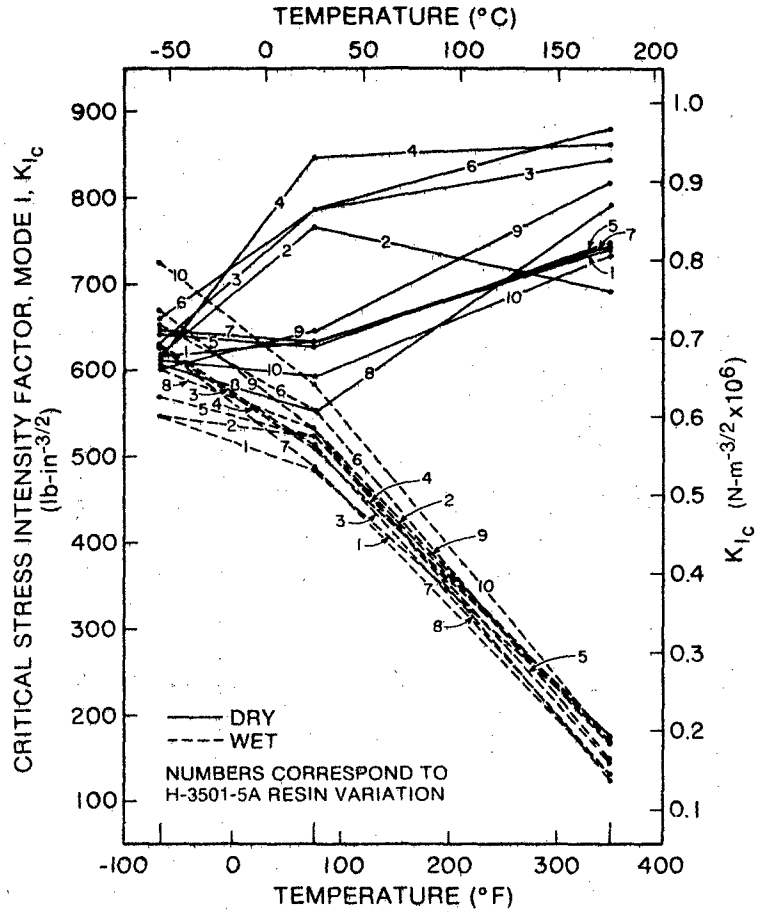

Fig. 20 Critical Stress Intensity Factor K_{I_C} versus Temperature for Ten Variations of H 3501-5A

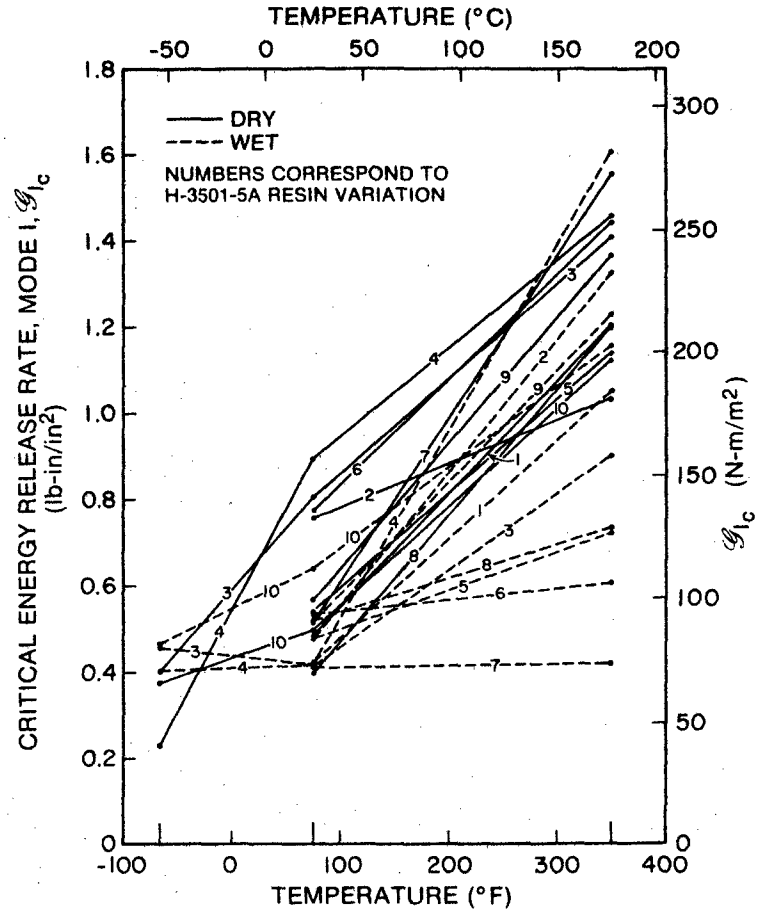

Fig. 21 Critical Energy Release Rate G_{I_C} versus Temperature for Ten Variations of H 3501-5A

variations, however it did tend to confirm that the use of tensile failure properties to characterize a material is not necessarily the best method. Individual specimens from the Standard Sub-Scale variation 12 KV 10 were studied in more detail using a 100 power light reflective/transmition microscope with a measuring eyepiece having a least increment of 0.0005 inches. The fracture surface of each specimen was carefully examined in an attempt to identify and quantify the flaw which initiated failure. In many cases two or more fracture surfaces were formed at specimen failure. It was impossible to determine which fracture initiated failure and which fracture resulted from a reflected stress wave. In other cases a fracture initiating site could be identified but no flaw size could be determined. (See Fig. 22 & Table 8). Numerous specimens displayed a round mirror area of fracture or shiny penny described by Leighton Orr[13] in his work with glass at Pittsburgh Plate Glass Research. He noted that fracture always originates from a finite flaw and radiating out from this origin are concentric wave markings on a smooth fracture face where the fracture velocity is relatively low. As the fracture velocity increases the pattern changes to a narrow frosted band and then to a rough "hackled" surface at high velocity. He correlated the radius of the half penny or the quarter penny with the stress at failure basing his findings on experimental data to obtain the relation

$$\text{Stress at Failure} = 1950/(\text{Penny Radius})^{1/2}$$

Orr's work indicated that only quarter or half pennies would form since failure for glass always initiates from an outside edge or corner.

Sneddon and Lowengrub[14] have treated the shiny penny problem on the basis of classical theory of elasticity. They imbed the penny in the interior of a semi-inifinite cylinder with the axes of each coincident and show that

$$\sigma_{zz}\ (\rho,0) = K_I/\sqrt{2(\rho - C)} \qquad (18)$$

where C is the initial radius of the penny and ρ the radius, a variable with $c \leq \rho \leq c + \delta c$ and K_I the Mode I, tension stress intensity factor.

Solutions to the penny problem (and many other crack configurations) have been solved by various techniques and have been summarized by Tada et al.

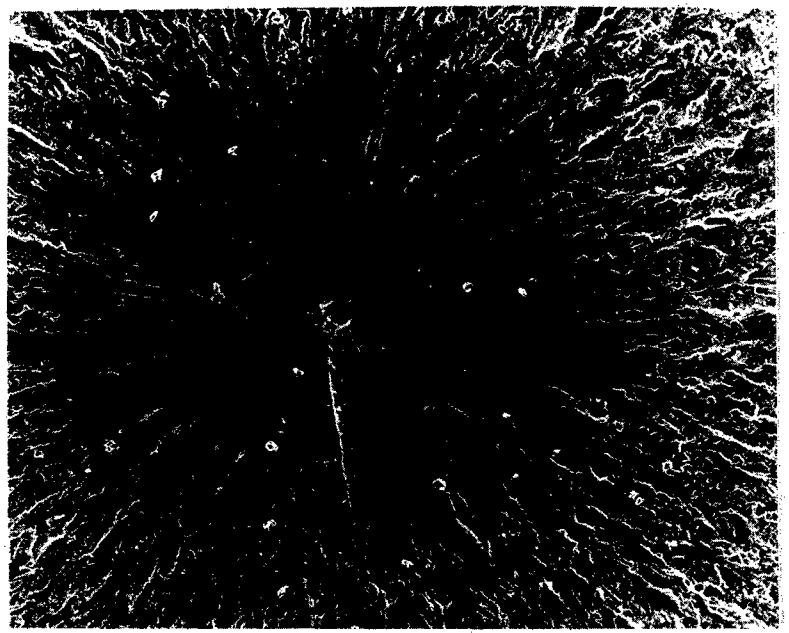

a. 60X

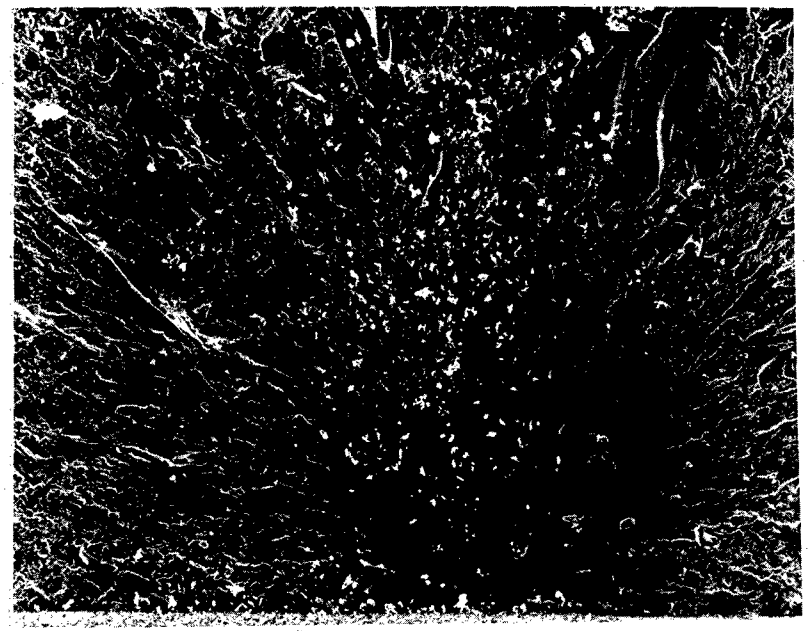

b. 60X

Fig. 22 Tensile Specimen Fracture Surface
Refer to Table 8

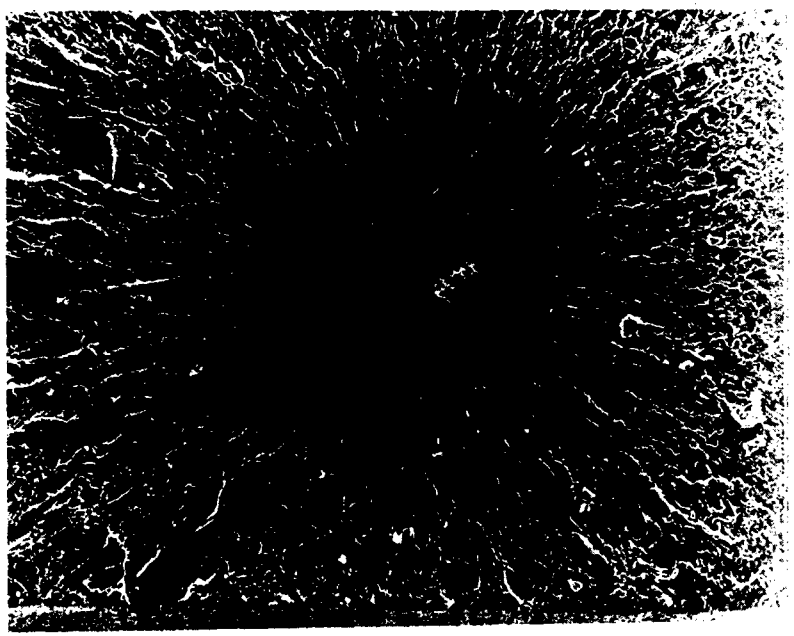

c. 60X

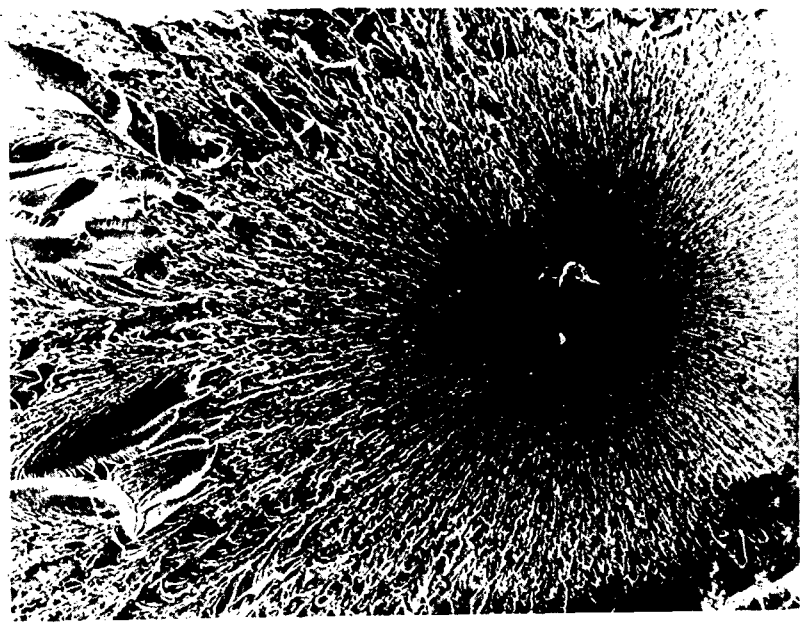

d. 60X

Fig. 22 Tensile Specimen Fracture Surface
Refer to Table 8

e. 60X

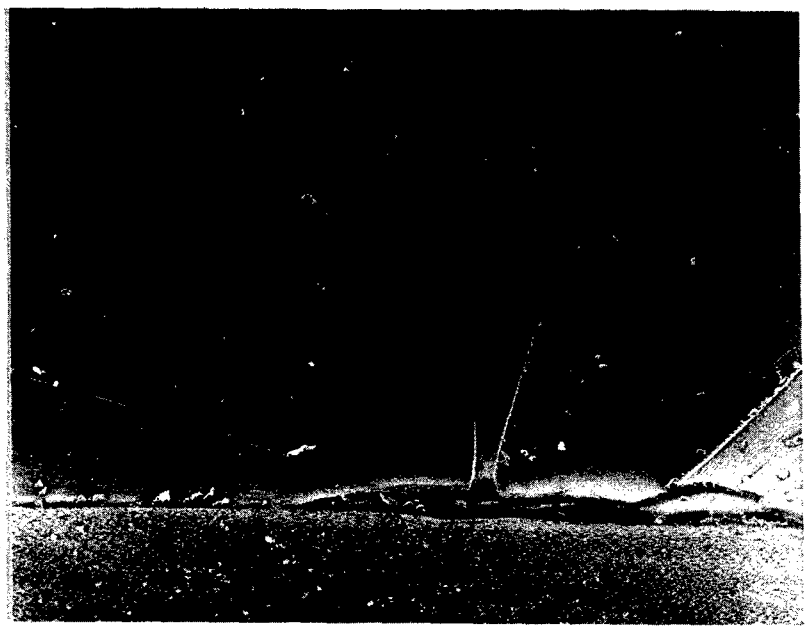

f. 60X

Fig. 22 Tensile Specimen Fracture Surface
Refer to Table 8

g. 60X

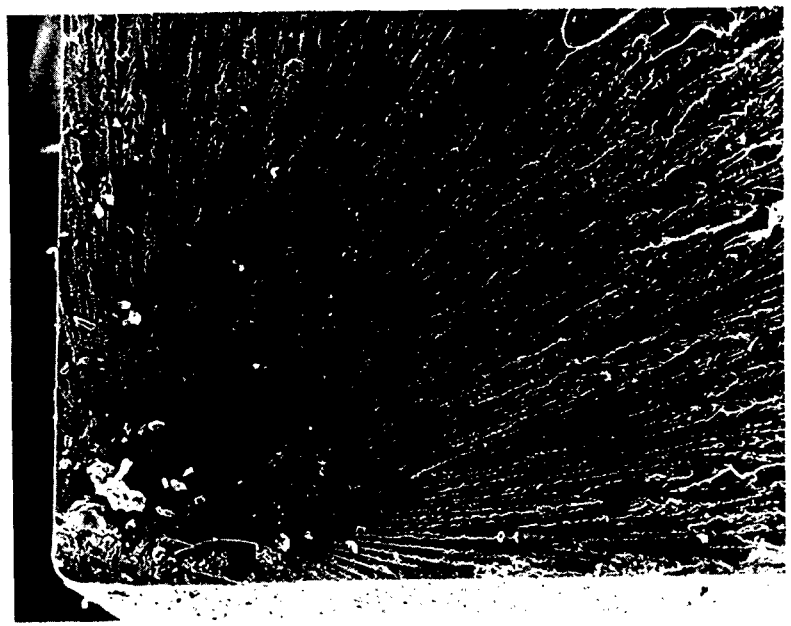

h. 60X

Fig. 22 Tensile Specimen Fracture Surface
Refer to Table 8

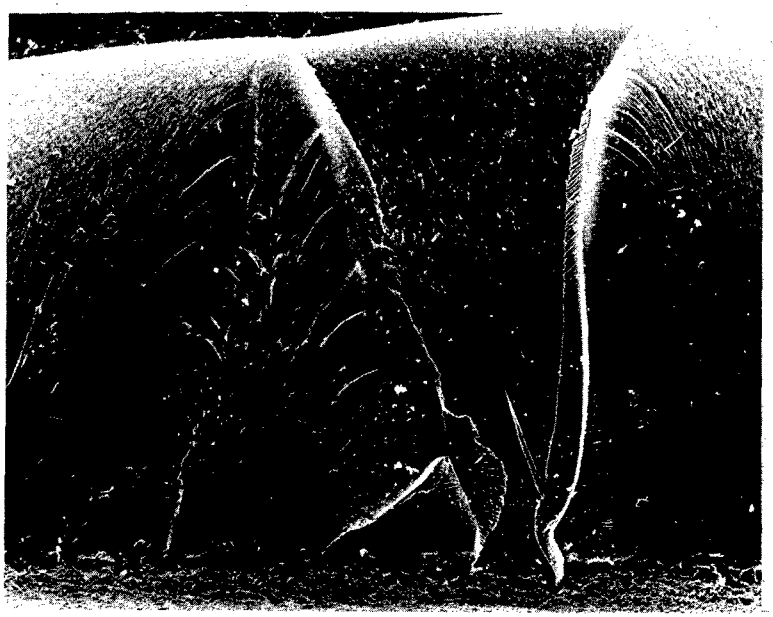

i. 60X

j. 60X

Fig. 22 Tensile Specimen Fracture Surface
Refer to Table 8

None of the configurations fit the problem of a penny crack imbedded eccentrically in a semi-infinite rectangular region. Therefore the penny crack imbedded in an infinite region with uniform stress normal to the face of the penny has been selected as a reasonably close geometry to investigate the correlation between flaw size and tensile strength. Accordingly from Tada[15]

$$K_I = \frac{2}{\pi} \sigma_o \sqrt{\pi a} \tag{19}$$

and therefore at failure

$$a_c = \frac{\pi}{4} \left(\frac{K_{IC}}{\sigma_f} \right)^2 \tag{20}$$

where in this case

a_c = radius of penny crack

σ_f = tensile strength

K_{IC} = critical stress intensity factor determined from four point beam test (see Section 2.a.3)

For a limited number of specimens Table 8 lists a comparison between the calculated flaw size "$2a_c$" using Equation (20) and a measured flaw size "$2a_m$" using the measuring microscope. The correlation is good for those initiation sites which are identifiable.

TABLE 8

SUMMARY OF FLAW SIZE AND TENSILE FAILURE CHARACTERISTICS
OF INDIVIDUAL SPECIMENS OF H3501-5A EPOXY RESIN
VARIATION 12KV10 STANDARD SUBSCALE 0.02 CHS, DRY

Site Key

1. Interior
2. Cast Edge
3. Routed Edge
4. Corner
5. Routed Edge at Extensometer Knife Edge

Temperature: -67 F (-55 C)

Specimen Number	Fracture Surfaces	Site*	Flaw Size, 2a Measured (±.0005 in)	Tensile Strength, σ_f (ksi)	Crit. Stress Intensity Factor, K_{IC} (lb in$^{-3/2}$)	Flaw Size, 2a** Calculated (in)	Fracture Energy***, U_f (lb in/in^3)
1	a	1a	.005	12.49	612	.0038	129
	b	5	.002				
	c						
2	a	1b	.003	13.19	612	.0033	141
	b	5	?				
	c						
3	a	1	.011	12.98	612	.0035	130
	b						
	c						
4	a						
	b						
	c						
5	a						
	b						
	c						
Ave. of Five Specimen Fracture Energy (U_f)							133
Fracture Energy by Integration ****							131

Temperature: 77 F (25 C)

Specimen Number	Fracture Surfaces	Site*	Flaw Size, 2a Measured (±.0005 in)	Tensile Strength, σ_f (ksi)	Crit. Stress Intensity Factor, K_{IC} (lb in$^{-3/2}$)	Flaw Size, 2a** Calculated (in)	Fracture Energy***, U_f (lb in/in^3)
1	a	1c	.004	12.69	592	.0034	198
	b	3	?				
	c						
2	a	5i	?	12.84	592	.0033	199
	b	4g	?				
	c						
3	a	5	?	11.09	592	.0045	140
	b	3	?				
	c						
4	a	1	.005	9.78	592	.0058	103
	b						
	c						
5	a	1d	.010	11.10	592	.0045	137
	b						
	c						
Ave. of Five Specimen Fracture Energy (U_f)							155
Fracture Energy by Integration ****							152

Temperature: 200 F (93 C)

Specimen Number	Fracture Surfaces	Site*	Flaw Size, 2a Measured (±.0005 in)	Tensile Strength, σ_f (ksi)	Crit. Stress Intensity Factor, K_{IC} (lb in$^{-3/2}$)	Flaw Size, 2a** Calculated (in)	Fracture Energy***, U_f (lb in/in^3)
1	a	3	?	10.08			140
	b	2	.005				
	c	3	?				
2	a	1	.001	11.46			204
	b	3	.005				
	c						
3	a	4	?	11.07			185
	b	5	?				
	c						
4	a	1	.006	10.58			156
	b						
	c						
5	a	4	?	8.47			100
	b	3	?				
	c						
Ave. of Five Specimen Fracture Energy (U_f)							157
Fracture Energy by Integration ****							154

Temperature: 275 F (125 C)

Specimen Number	Fracture Surfaces	Site*	Flaw Size, 2a Measured (±.0005 in)	Tensile Strength, σ_f (ksi)	Crit. Stress Intensity Factor, K_{IC} (lb in$^{-3/2}$)	Flaw Size, 2a** Calculated (in)	Fracture Energy***, U_f (lb in/in^3)
1	a	5	?	10.23			195
	b	1	.010				
	c						
2	a	5	?	10.38			192
	b	2	?				
	c						
3	a	4	?	7.78			92
	b						
	c						
4	a	3	?	8.92			139
	b	4	.005				
	c	4	.003				
5	a	5	?	10.48			233
	b	3	?				
	c						
Ave. of Five Specimen Fracture Energy (U_f)							170
Fracture Energy by Integration ****							168

Temperature: 350 F (177 C)

Specimen Number	Fracture Surfaces	Site*	Flaw Size, 2a Measured (±.0005 in)	Tensile Strength, σ_f (ksi)	Crit. Stress Intensity Factor, K_{IC} (lb in$^{-3/2}$)	Flaw Size, 2a** Calculated (in)	Fracture Energy***, U_f (lb in/in^3)
1	a	5	?	7.79	734	.0139	263
	b	5	?				
	c						
2	a	1	?	7.99	734	.0133	188
	b	5j	?				
	c						
3	a	5	?	7.99	734	.0133	250
	b	3	?				
	c						
4	a	2e	.036	5.56	734	.0274	60
	b						
	c						
5	a	4h	?	5.91	734	.0242	73
	b	3f	?				
	c						
Ave. of Five Specimen Fracture Energy (U_f)							167
Fracture Energy by Integration ****							164

* The letter following some site numbers corresponds to the photomicrographs by SEM shown in Figure 22a thru 22j.

** See Equation (2.16).

*** Area under each load-displacement curve of raw data using a Polar Planimeter.

**** Mathematical integration of stress-strain data fit Equation (2.1) (See also Equation (2.7)).

BEST AVAILABLE COPY

3. VISCOELASTIC PROPERTIES

The viscoelastic nature of the ten variations of this material has already been observed throughout earlier discussions. Additional static-mechanical studies in the form of relaxation modulus and dynamic-mechanical studies in the form of complex modulus have been performed. A still more detailed study into the time-temperature dependence of one of the variations viz the standard batch has provided additional insight to the material behavior.

a. Shear Relaxation Modulus Data - Figure 23 is a schematic description of the test apparatus which was used to obtain the shear stress relaxation data. It consists of a cylindrical, split wound, clam shell oven, a loading frame and torque (load) and rotation transducers. The oven is capable of maintaining the internal temperature to within $\pm 0.5^{o}F$. The load frame contains an upper grip, fixed in rotation but free to move axially, and a lower grip, fixed axially but attached to a torque arm. Load is measured via a strain gaged double flexure beam, while the applied angle of rotation and deviation due to load transducer deflection are determined by fixed graduation on the loading frame and a high precision, low friction potentiometer, respectively.

Cylindrical epoxy specimens 1-1/2" long with a diameter of 0.20" were placed between the grips (Figure 24). A steel shield, placed over the specimen and grips was used to minimize the radiation effects from the furnace resistance coils. During the heating and stabilization period, the transducers were calibrated by use of a known force applied to the torque arm. Upon completion of stabilization, the desired angle of rotation was rapidly applied, fixed, and the resulting angular rotation and torque signals were recorded as functions of time. From these quantities, the shear relaxation modulus was determined as a function of time.

For a cylindrical specimen displaced in torsion the shear modulus may be expressed in terms of the various parameters by the well known relation

$$G = \frac{TL}{\theta J}$$

where: G = shear modulus
T = torque
L = length of specimen
θ = angular twist over length L
J = polar moment of inertia

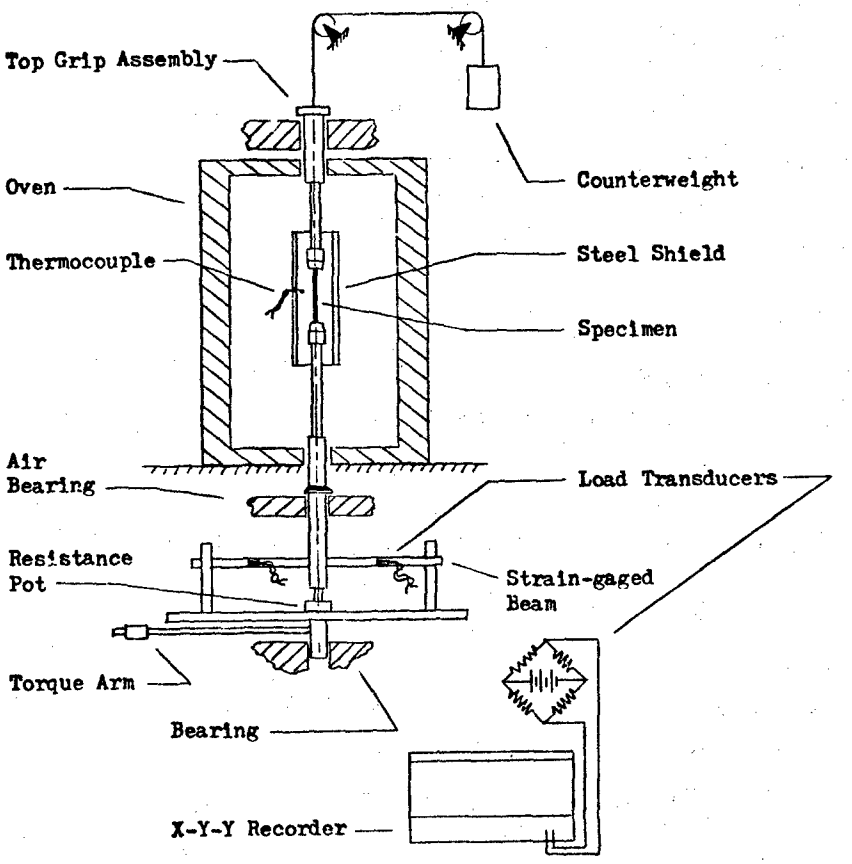

Figure 23 Schematic of Shear Relaxation Apparatus

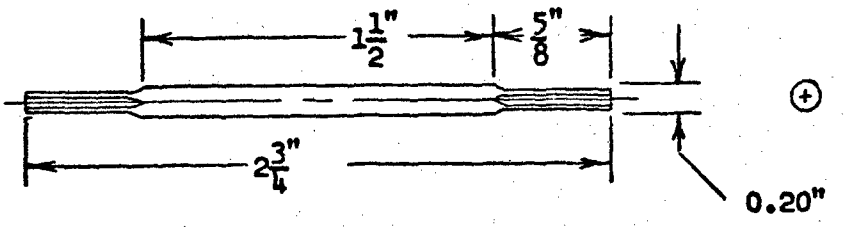

Figure 24 Shear Specimen

As relaxation occurs with time (t) then the shear modulus response is

$$G(t) = \frac{T(t)L}{\theta(t)J}$$

and to normalize the instataneous shear modulus to the initial shear modulus we may write

$$\frac{G(t)}{G_o} = \frac{\theta_o}{T_o} \cdot \frac{T(t)}{\theta(t)}$$

But $\theta(t) = (\theta_o - \Delta\theta(t))$ where $\Delta\theta(t)$ is the relative angle between the flexure beam and the torque arm. Then

$$\frac{G(t)}{G_o} = \frac{T(t)}{T_o} \cdot \frac{1}{1 - \frac{\Delta\theta(t)}{\theta_o}} \tag{21}$$

As displacement approaches zero the torque-angular displacement is approximately linear and it may then be said that

$$G_o = G_{(\theta \to o)}$$

which may then be evaluated using the linear relationship

$$G_o = \frac{E_T}{2(1 + \nu)} \tag{22}$$

where the tangent modulus E_T and Poisson's ratio ν may be determined from previously presented data.

Figures 25.a through 25.j are Log $G(t)/G_o$ versus Log time curves for the ten variations of H-3501-5A epoxy resin at 25 C (77 F), 93 C (200 F) and 177 C (350 F). All were run at the same initial angular displacement sufficiently large to provide a fairly high initial stress level but below the failure stress. All specimens were in a dry state.

The shear relaxation characteristics of KV5, KV8, and KV9 are almost identical to the standard batch KV10 for all observed time and temperatures. Variations KV2, KV4 and KV6 are also very comparable to KV10 except at the high temperature at time greater than 500 minutes when they tail off at a greater rate. KV1 is also comparable but starts to tail off after only about 10 minutes time at 177 C (350 F). $G(t)/G_o$ for variation KV7 at 177 C (350 F) begins to tail off after only one minute elapsed time. After three thousand minutes under essentially constant strain all variations

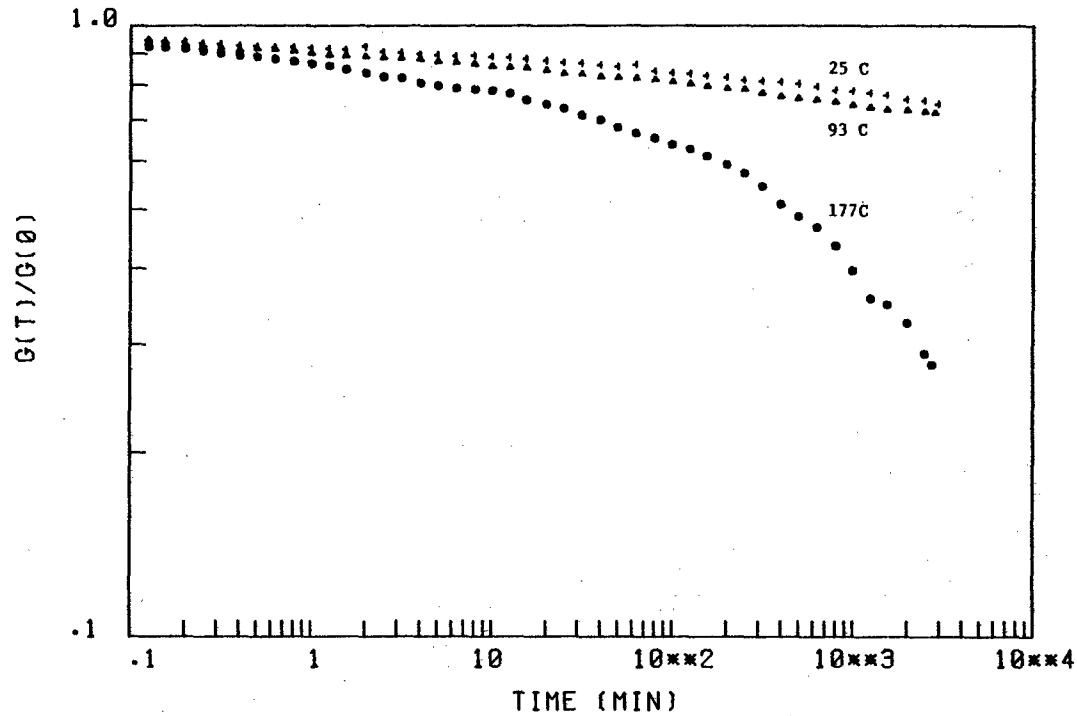

Fig. 25.a Torsional Relaxation Curve For 3501-5A (16KV1) Epoxy Resin

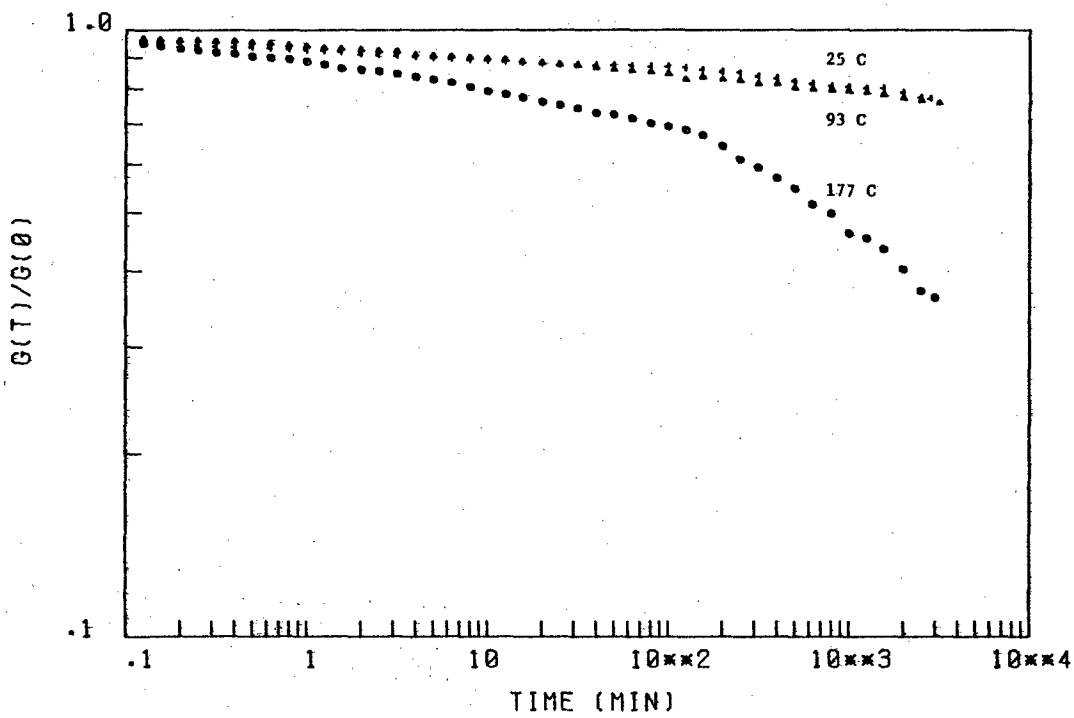

Fig. 25.b Torsional Relaxation Curve For 3501-5A (8KV2) Epoxy Resin

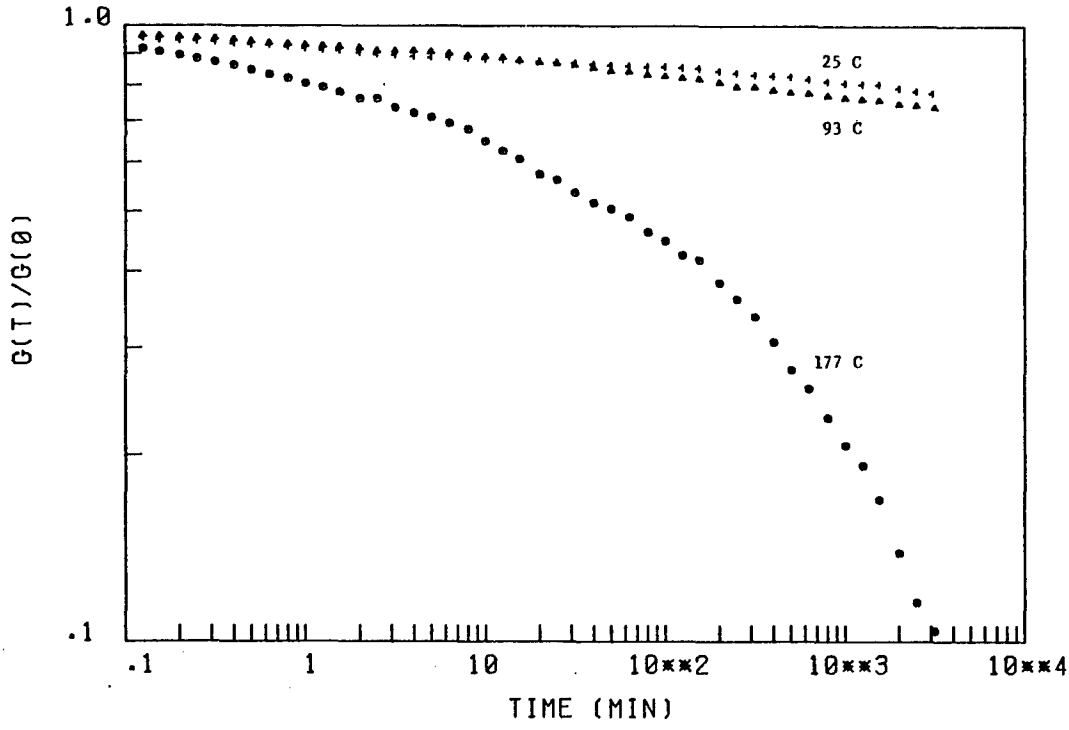

Fig. 25.c Torsional Relaxation Curve For 3501-5A (8KV3) Epoxy Resin

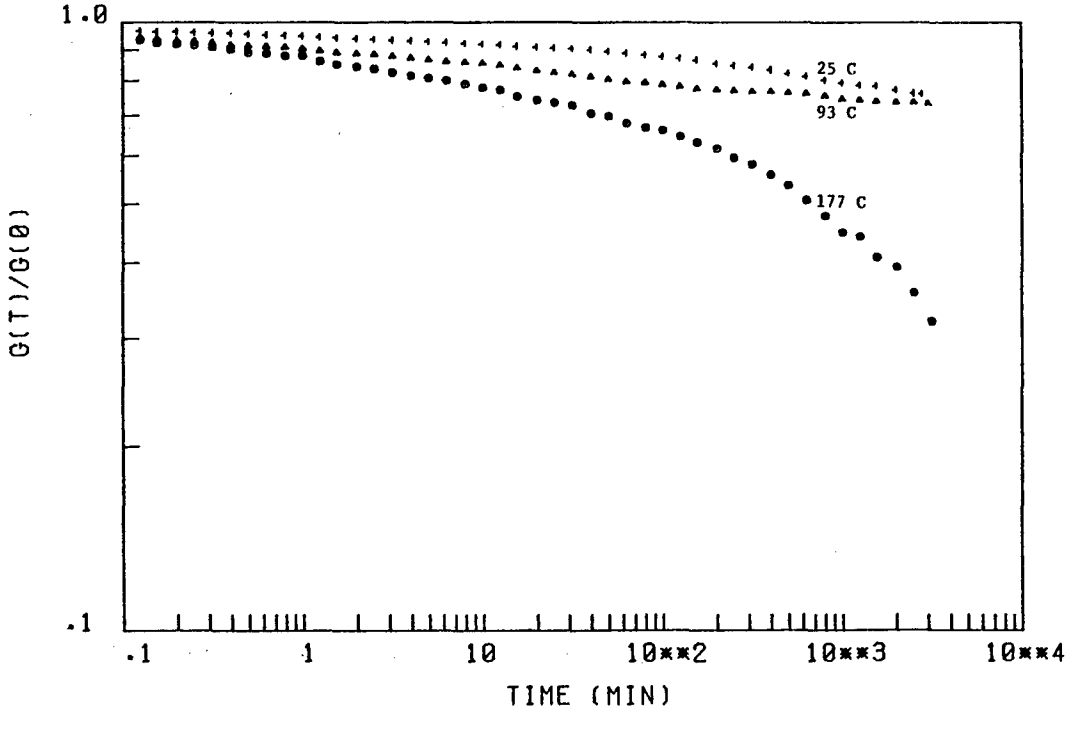

Fig. 25.d Torsional Relaxation Curve For 3501-5A (16KV4) Epoxy Resin

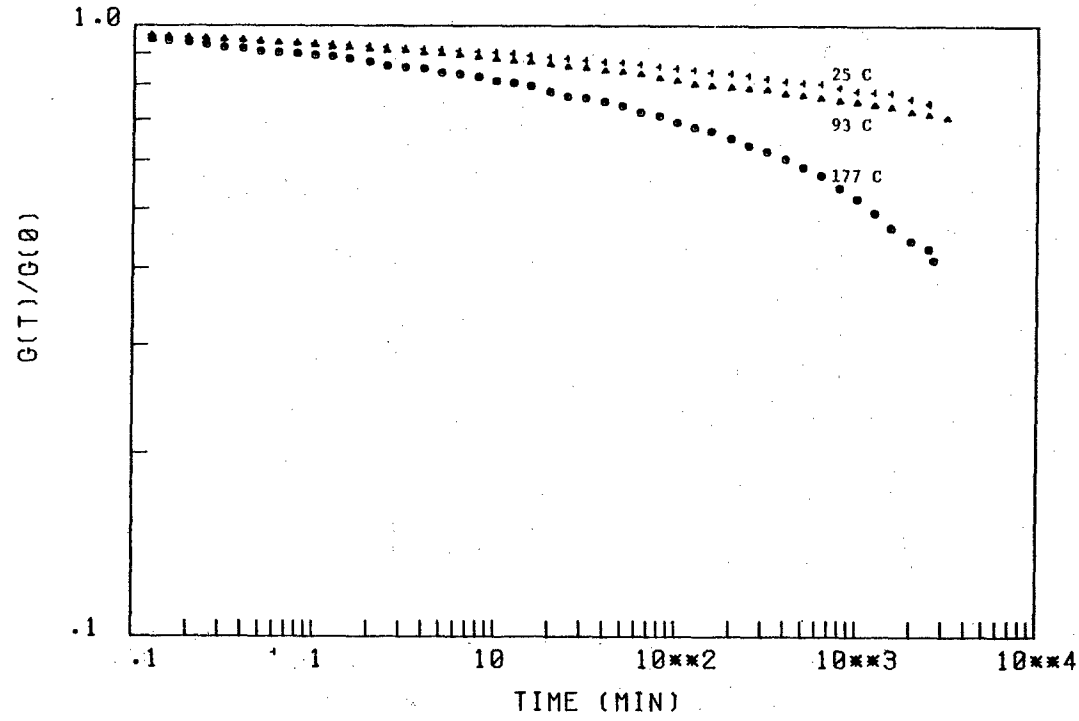

Fig. 25.e Torsional Relaxation Curve For 3501-5A (12KV5) Epoxy Resin

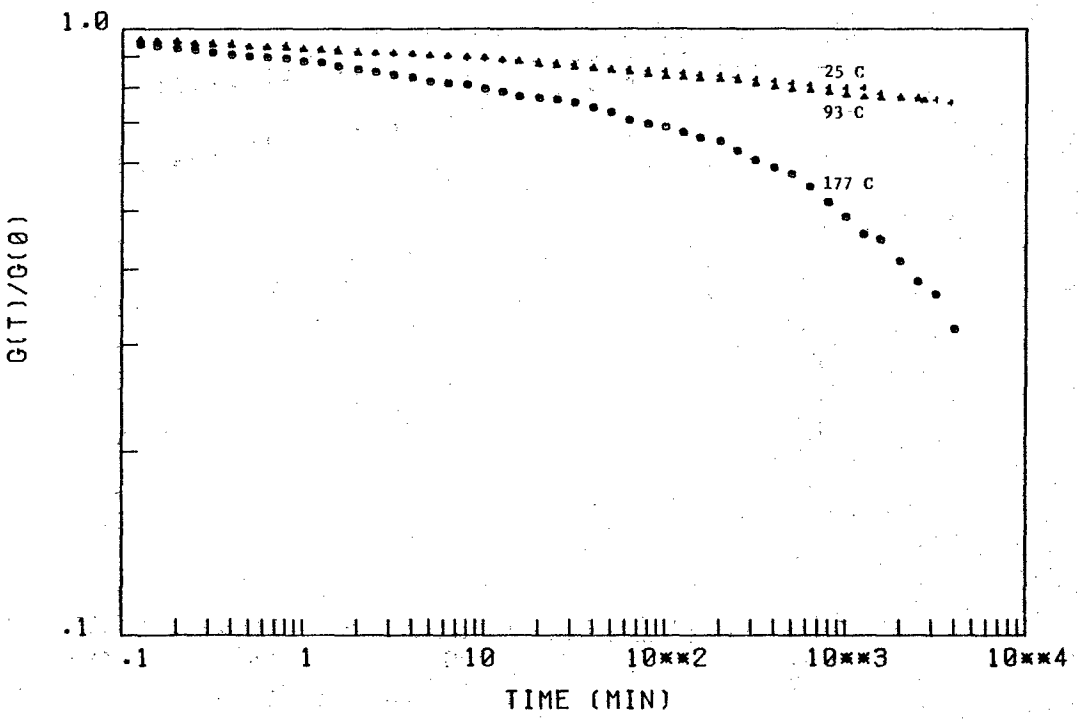

Fig. 25.f Torsional Relaxation Curve For 3501-5A (12KV6) Epoxy Resin

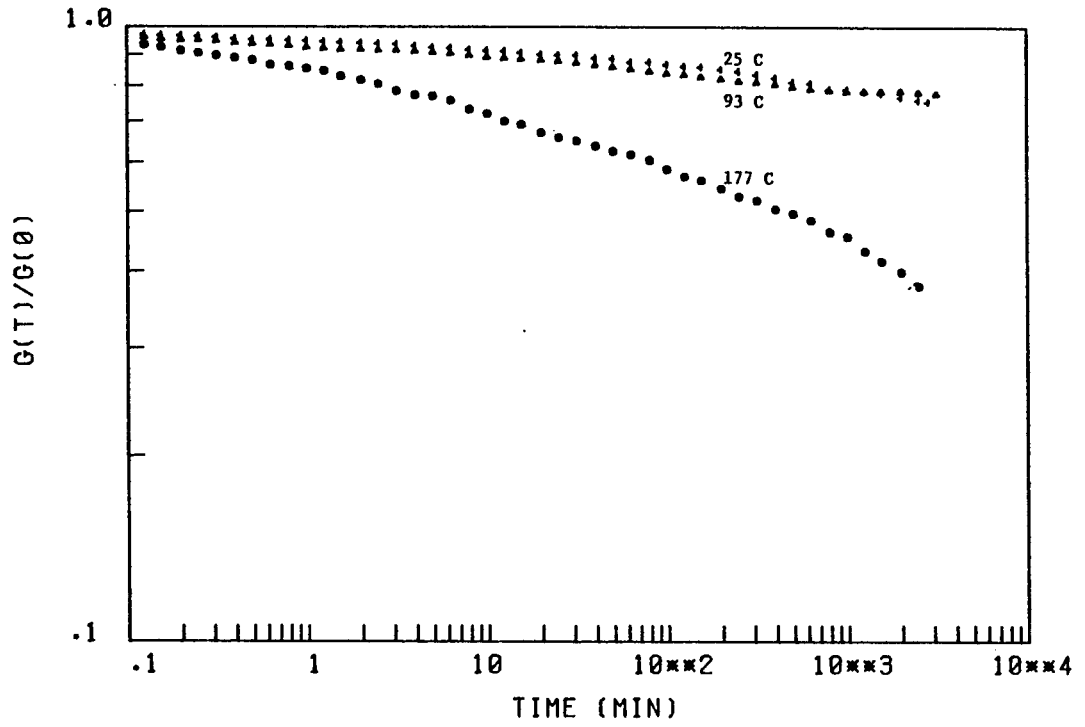

Fig. 25.g Torsional Relaxation Curve For 3501-5A (12KV7) Epoxy Resin

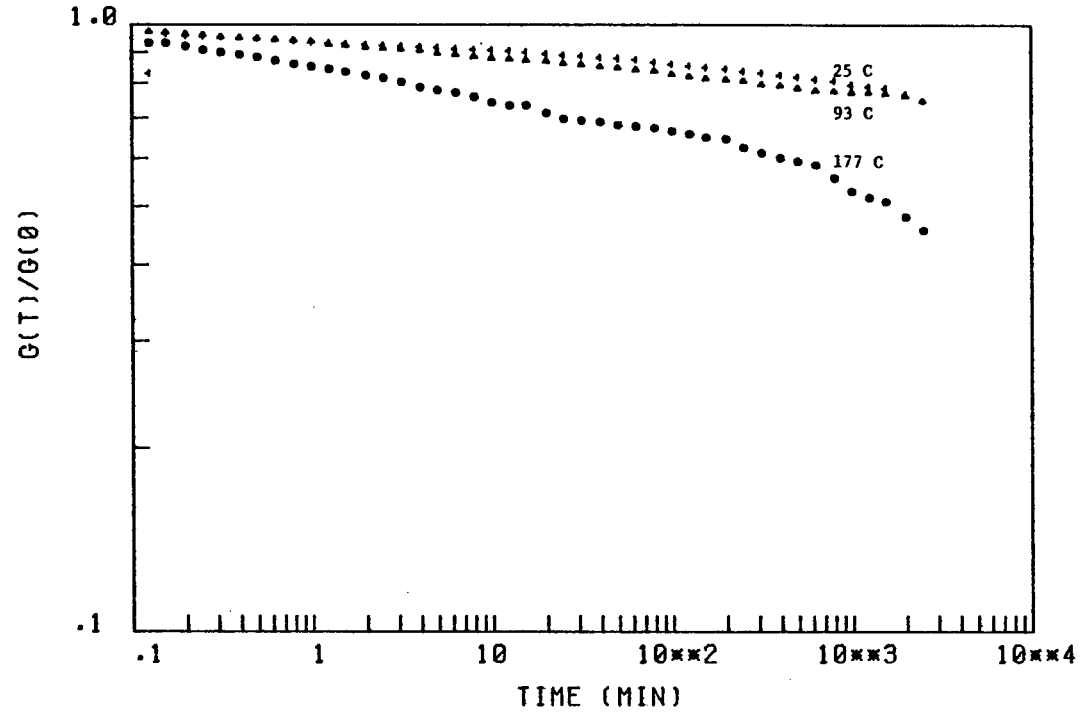

Fig. 25.h Torsional Relaxation Curve For 3501-5A (12KV8) Epoxy Resin

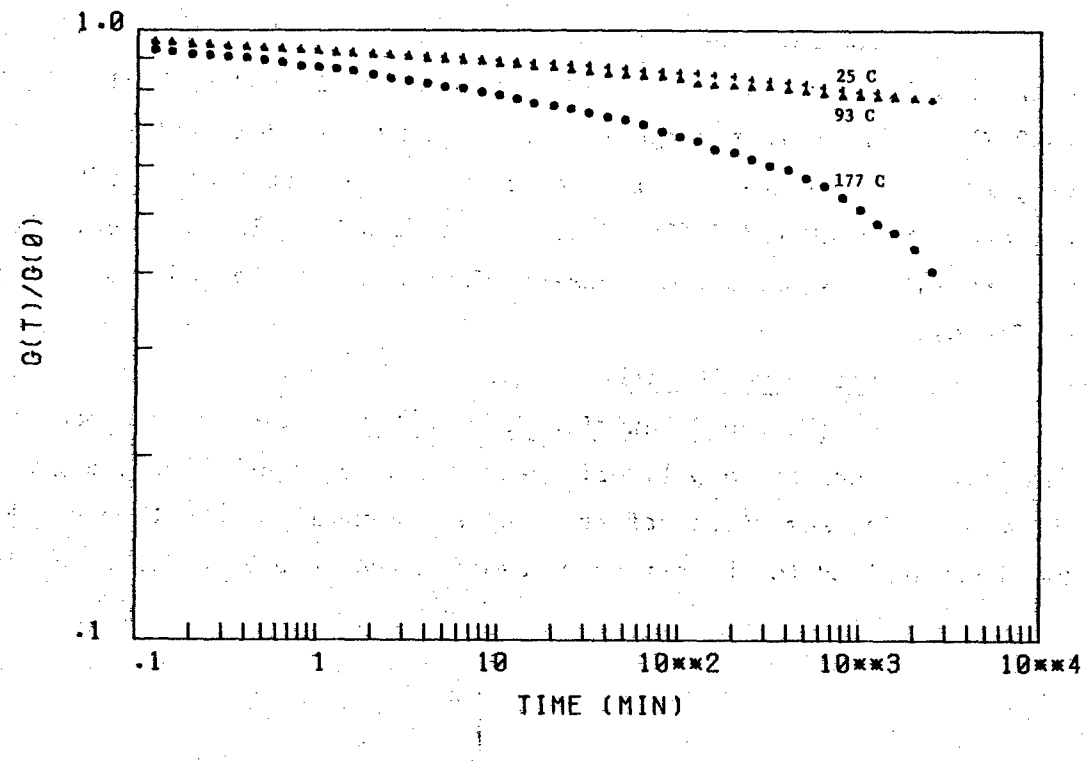

Fig. 25.i Torsional Relxaation Curve For 3501-5A (12KV9) Epoxy Resin

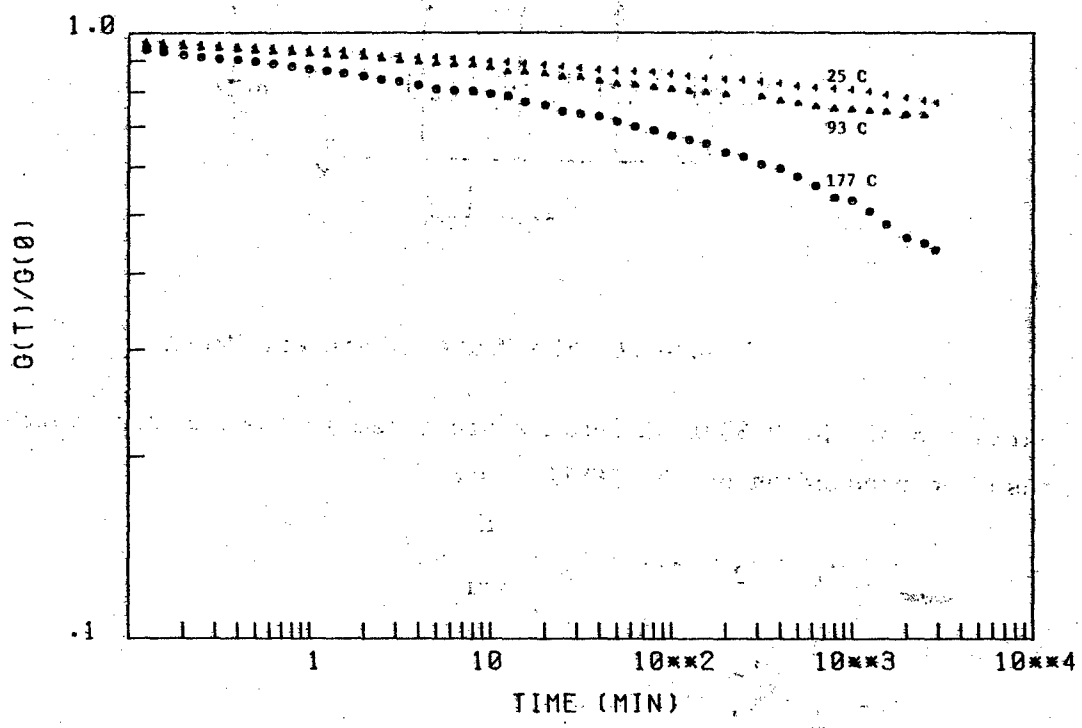

Fig. 25.j Torsional Relaxation Curve For 3501-5A (12KV10) Epoxy Resin

behave approximately the same and lose approximately 20% of their original stiffness in shear at room temperature and up to 93 C (200 F). At 177 C (350 F) they have lost slightly more than 50% of their stiffness in shear KV1, KV2, KV4 and KV6 have lost about 60% to 65% of their stiffness. On the other hand at 177 C (350 F) the so called Brittle batch 8KV3 falls off very rapidly. After three thousand minutes it has lost 90% of its shear stiffness.

b. The Maxwell-Weichert Model

(1) The Relaxation Modulus Data Fit - To accommodate a complex response spectra for a polymeric material such as H-3501-5A, a generalized Maxwell chain, sometimes referred to as a Maxwell-Weichert model, Figure 26, has been applied to the stress relaxation response behavior of a single

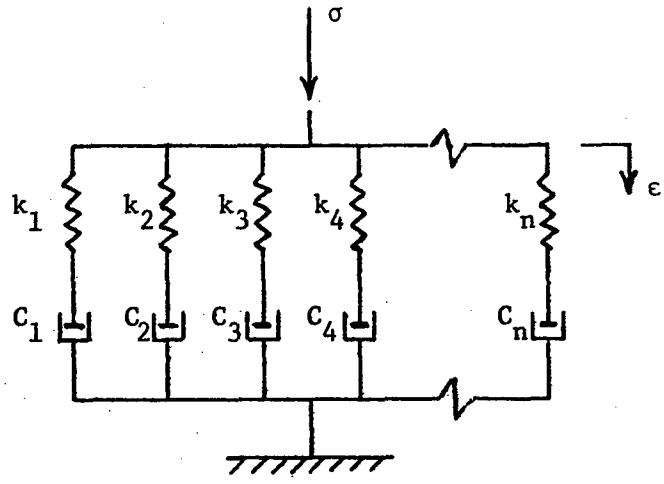

Figure 26 The Maxwell-Weichert Model

variation of the H-3501-5A resin system, namely the standard batch, in this case the production batch 12KV11. Here

$$\sigma = \sigma_1 + \sigma_2 + \ldots + \sigma_n = \sum_{i=1}^{n} \sigma_i$$

and

$$\varepsilon = \varepsilon_1 = \varepsilon_2 = \ldots = \varepsilon_n$$

It can be shown that the differential equation of motion for this model is

$$\sigma = \frac{d\varepsilon}{dt} \sum_{i=1}^{n} C_i + \sum_{i=1}^{n} \frac{C_i}{k_i} \frac{d\sigma_i}{dt} \tag{23}$$

and that the response to a fixed strain ε^* and an intital condition σ_o thus

$$\varepsilon = \varepsilon^* \text{ for all time } t$$

$$\sigma = \sigma_{o_i} \text{ for time } t = 0$$

results in a solution

$$\sigma(t) = \sum_{i=1}^{n} \sigma_{o_i} \exp\left(-k_i t/C_i\right) \tag{24}$$

If equation (24) is divided by the fixed strain and defining

$$G_i = \sigma_{o_i}/\varepsilon^*$$

$$\tau_i = C_i/k_i$$

then

$$G(t) = \sum_{i=1}^{n} G_i \exp\left(-t/\tau_i\right) \qquad \text{Ref.(16)\&(17)} \tag{25}$$

which represents the Maxwell-Weichert response of the shear modulus to a shear stress.

Christensen[18] states that an isotropic viscoelastic solid, when subjected to a stress of constant shear deformation will have a component of stress which will remain non-zero as long as the shear is maintained. By substituting a rigid link for one of the dashpots (or, in the model, by setting one of the damping terms equal to zero), this criterion is met and equation (25) becomes

$$G(t) = G_o + \sum_{i=1}^{n} G_i \exp\left(-t/\tau_i\right) \tag{26}$$

which is a Dirichlet series. The corresponding model for tensile relaxation modulus is

$$E(t) = E_o + \sum_{i=1}^{n} E_i \exp(-t/\tau_i) \tag{27}$$

In addition to the normalized shear relaxation modulus data presented in the previous section 3.a experiments were conducted to obtain normalized tensile relaxation modulus data for several temperatures for the standard variation of this epoxy resin. These data were curve fit to a four term Dirichlet series of the form

$$f(t) = f_o + \sum_{i=1}^{3} f_i \exp(-t/\tau_i) \tag{28}$$

Coefficients for the curve fit are tabulated in Appendix B, Table B1. For this curve fit the coefficients τ_i were fixed and f_o, f_1, f_2, and f_3 evaluated. Figures B1 and B2 of Appendix B are curves plotted using these coefficients.

(2) The Prediction of Uniaxial Tension Behavior - Using linear small deformation viscoelastic theory it is possible to predict uniaxial tension behavior from tensile or shear relaxation response information. For simple uniaxial extension and taking into account the "memory" effects of viscoelastic materials the constitutive relation becomes

$$\sigma(t) = \int_o^t E(t - \tau) \frac{d\varepsilon(\tau)}{d\tau} d\tau \tag{29}$$

and therefore if the tensile relaxation function is known, the state of stress may be determined for any strain rate condition. If on the other hand the shear relaxation function is known, the tensile relaxation function may be determined from

$$E(t) = 2\{1 + \nu(0)\} G(t) + \int_o^t G(t - \tau) \frac{d\nu(\tau)}{d\tau} d\tau \tag{30}$$

Figures B3 and Figures B4 of Appendix B show a good correlation between the shear and tensile relaxation generated stress-strain properties for three temperatures at two strain rates of the standard batch resin.

(3) The Temperature-Time Shift - The basic postulate of a simple thermorheological material is that the effect of temperature on the mechanical properties is to shift them by a constant along the logarithmic time axis. Mathematically this is expressed

$$\log_{10} t_T = \log_{10} t_{T_o} + \log_{10} \{a(T)\} \tag{31}$$

where a(T) is the shift function. The tensile relaxation may then be written

$$E(T_o,t) = E(T,t/a(T)) \tag{32}$$

Obviously the shift function a(T) must have a value of unity when the reference temperature and the shift temperature are the same. Suh and Turner[19] determined that a suitable form for the shift function may be written as

$$\log_{10} \{a(T)\} = -\lambda \left(\frac{1}{T_o} - \frac{1}{T}\right) \tag{33}$$

where λ is a constant over a given temperature regime and may be determined from the equation

$$\lambda = -\left\{\frac{1}{T_o} - \frac{1}{T}\right\}^{-1} \log_{10} \left(t_T/t_{T_o}\right) \tag{34}$$

By substituting a number of sets of values of temperature and time into this equation an equal number of constants, λ, may be evaluated. The arithmetic average of these is then used. For this material λ was determined to have an average value of 658.8 and therefore equation (33) becomes

$$\log_{10} \{a(t)\} = -658.8 \left(\frac{1}{T_o} - \frac{1}{T}\right) \tag{35}$$

Values for the shift function a(T) are tabulated in Table B2 of Appendix B for a reference temperature of 177 C (350 F). Figure B5, Appendix B, shows how data from tensile relaxation experiments at 25 C (77 F) and 177 C (350 F) were shifted to 135 C (275 F) and compared to an actual relaxation test run at that temperature.

c. The Dynamic Modulus - In linear viscoelastic behavior, it is well known that if a steady state sinusoidal stress is applied to a material the strain will also vary sinusoidally but will lag behind the stress. The phase lag depends on the viscous damping nature of the material and therefore becomes another useful parameter, along with the modulus, to describe the response of the material to a dynamic stress. Thus it can be shown[20] that

$$E = E' + i\,E'' \tag{36}$$

where: E' represents the elastic portion of the tensile modulus which is in phase with the applied force (stress) frequently referred to as the storage modulus.

E'' represents the portion of the tensile modulus which is 90^o out of phase with the applied force (stress) and represents the dissipation of energy or damping characteristics and is therefore referred to as the loss modulus.

It follows that

$$\frac{E''}{E'} = \tan \phi \tag{37}$$

where: ϕ is the phase lag (angle) of the strain with respect to the stress and therefore tan ϕ is frequently referred to as the loss tangent.

A direct analogy between the complex modulus and creep and stress relaxation may be shown[20] and therefore it is necessary to express E' and E" (or tan ϕ) as a function of temperature and time (frequency) if it is desired to specify the viscoelastic behavior of this material.

To investigate the complex properties of this material a clamped-clamped beam 4-1/2 inches long by 5/8 inches wide by 1/8 inch thick was driven sinusoidally at mid-span. The test fixture, Figure 27, consisted of a clamping frame attached solidly to a very large mass at the same time bridging an MB Electronics Model PM 25 driving head which is also attached to the mass. The clamping frame is extended above the driving head so that the beam specimen may be placed inside an oven while the shaker head remains outside. A stiff 12 inch long lightweight drive rod ties the armature of the driver to a force transducer which in turn is connected to the mid-span of the beam. A Bently Nevada proximity probe Type 300, Model 304 LR with Proximitor was used to monitor the armature displacement.

The equation of the elastic curve[21] of a clamped-clamped beam with the sinusoidal loading $P_o \sin \omega t$ at the mid-span may be written

$$y(\frac{L}{2}, t) = \frac{P L^3 \sin \omega t}{EI} \{5038 \beta_1 + 135 \beta_3 + 22 \beta_5 + \ldots\} \times 10^{-6} \tag{38}$$

where

$$\beta_i = \frac{1}{1 - (\frac{\omega}{p_i})^2}$$

and

$$p_i = k_i^2 a = k_i^2 \sqrt{\frac{EI}{\rho A}}$$

and

k_i = clamped-clamped beam eigenvalues

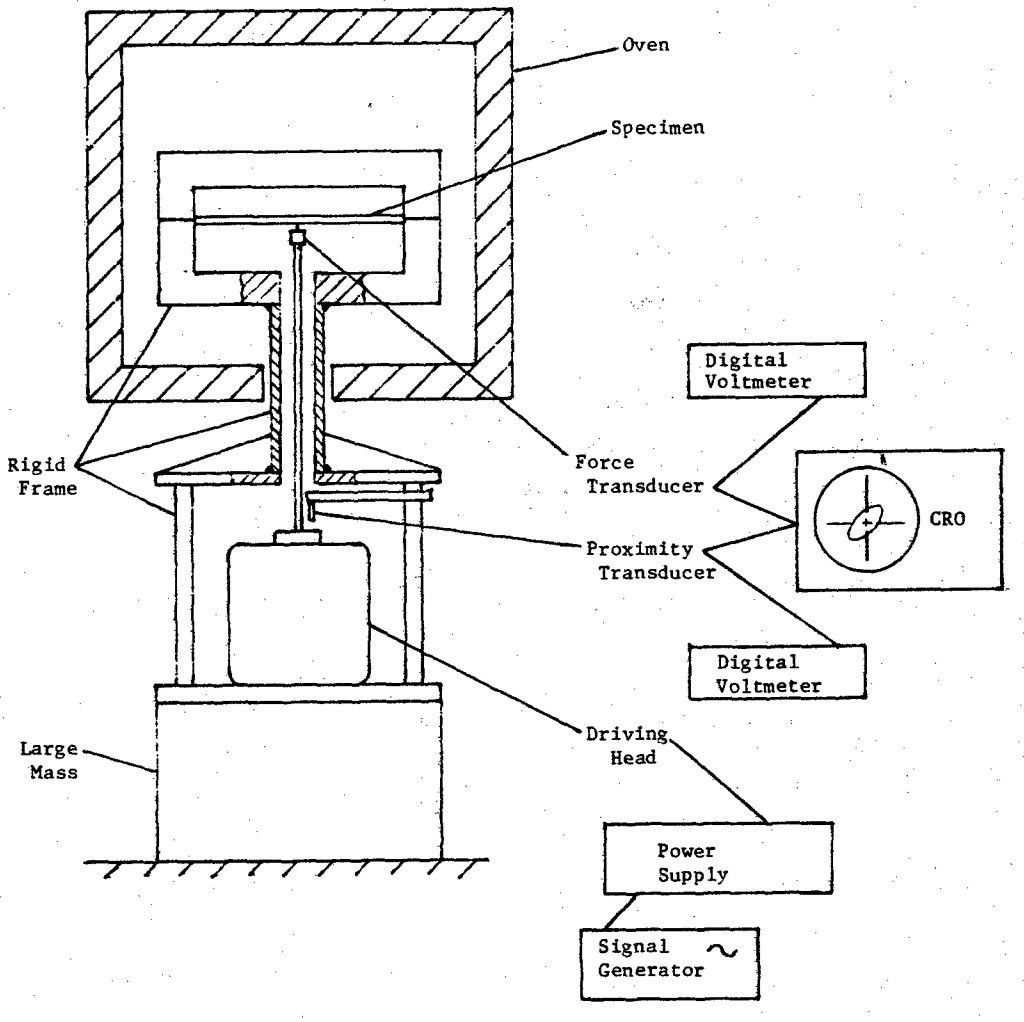

Fig. 27 Schematic of Dynamic Modulus Apparatus

It can be shown that the first term of the series contributes over 97% to the solution. As a good approximation only the first term was used to obtain an expression for the complex modulus E in terms of frequency, load and center span displacement, thus:

$$E = \frac{5038\ L^3\ P_o\ x\ 10^{-6}}{I\ y_o} + \frac{4\pi^2\ \rho\ bt\ L^4\ f}{k_1^4\ I} \qquad (39)$$

where: b = beam width

t = beam thickness

f = frequency

$k_1 = 4.73$ (22)

Peak to peak load P_o, peak to peak center span displacement y_o, frequency f, phase angle ϕ, and temperature were recorded. The phase angle was obtained by Lissajous pattern formed by the load and displacement waveforms.

Figures 28.a through 28.j are graphs of the Storage Modulus and the Loss Tangent showing variations with frequency and temperature in both the dry and the wet state. Data was recorded 1 Hz, 5 Hz and 10 Hz although only 1 and 10 Hz are shown. The data at 5 Hz was bracketed by that of the 1 Hz and 10 Hz. Temperatures ranged from 25 C to approximately 200 C for dry specimens but only up to 120 C for the wet specimens because of drying effects during the fairly long runs.

There is very little difference among the ten variations in their dynamic behavior. All show about the same sensitivity to frequency, temperature, and moisture state. In the frequency range 1 Hz to 10 Hz the storage modulus E' is reduced by about 10% over the temperature range, dry or wet. Over the temperature range 25 C to 204 C the dry state loses about 50% of its storage modulus regardless of frequency. In the wet state 50% is lost in the temperature range 25 C to only 121 C. At any frequency or temperature about 20% is lost due to moisture. The loss tangent shows similarity among the ten variations. Temperature seems to have little effect on the loss tangent in the dry state up to about 180 C at which point there is a sharp increase. On the other hand in the wet state this increase occurs at 90 C.

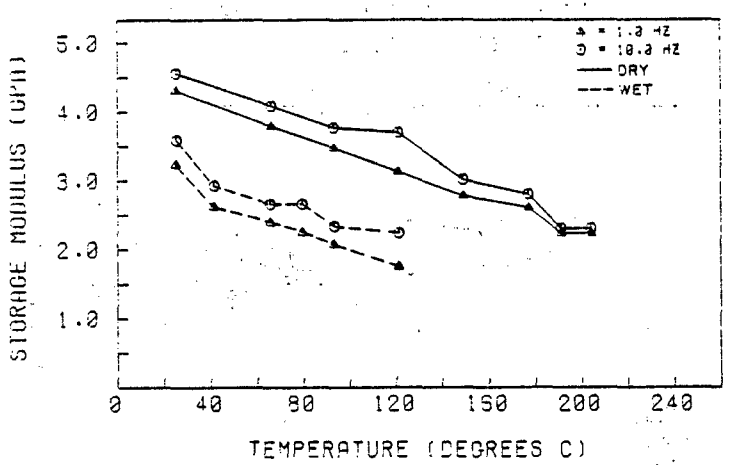

Fig. 28.a(1) Storage Modulus vs Temperature
Hercules 3501-5A Epoxy Resin
(Variation: 16KV1)

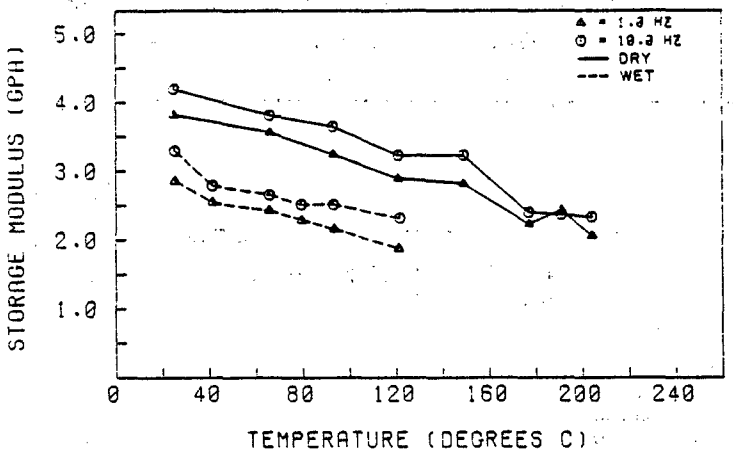

Fig. 28.b(1) Storage Modulus vs Temperature
Hercules 3501-5A Epoxy Resin
(Variation: 8KV2)

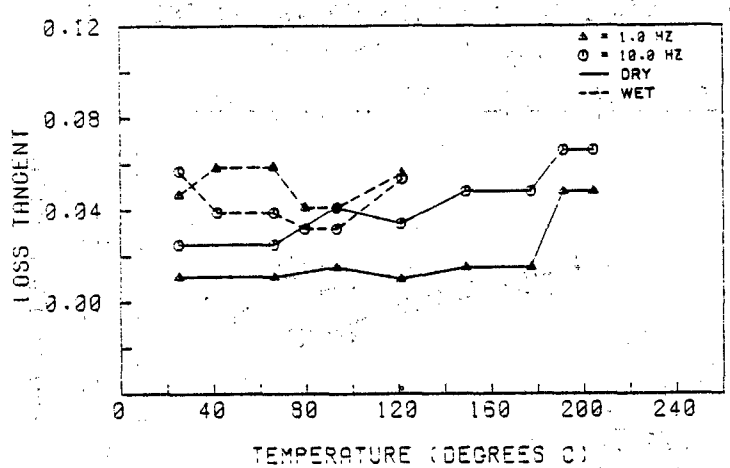

Fig. 28.a(2) Loss Tangent vs Temperature
Hercules 3501-5A Epoxy Resin
(Variation: 16KV1)

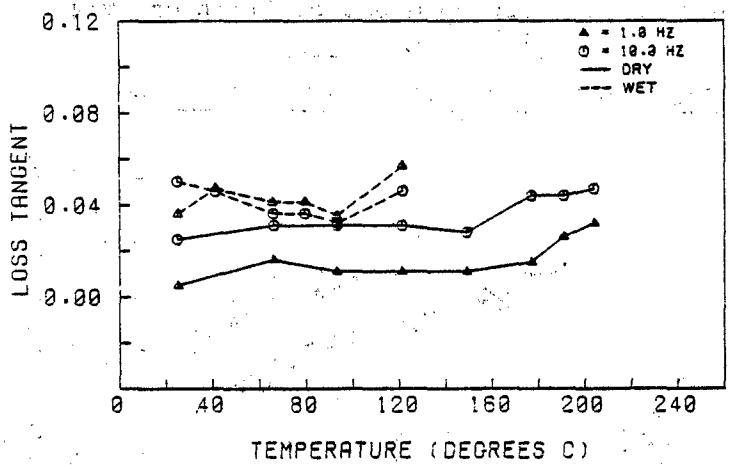

Fig. 28.b(2) Loss Tangent vs Temperature
Hercules 3501-5A Epoxy Resin
(Variation: 8KV2)

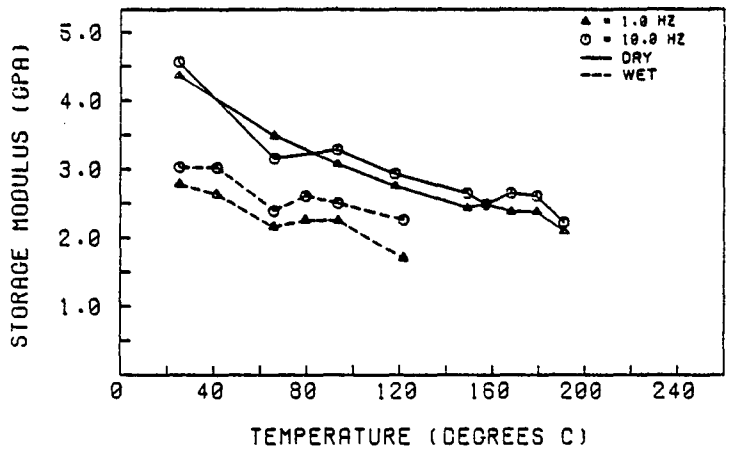

Fig. 28.c(1) Storage Modulus vs Temperature Hercules 3501-5A Epoxy Resin (Variation: 8KV3)

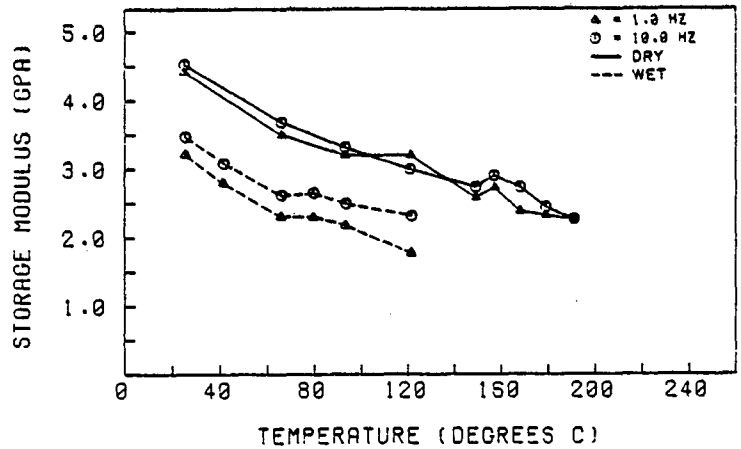

Fig. 28.d(1) Storage Modulus vs Temperature Hercules 3501-5A Epoxy Resin (Variation: 16KV4)

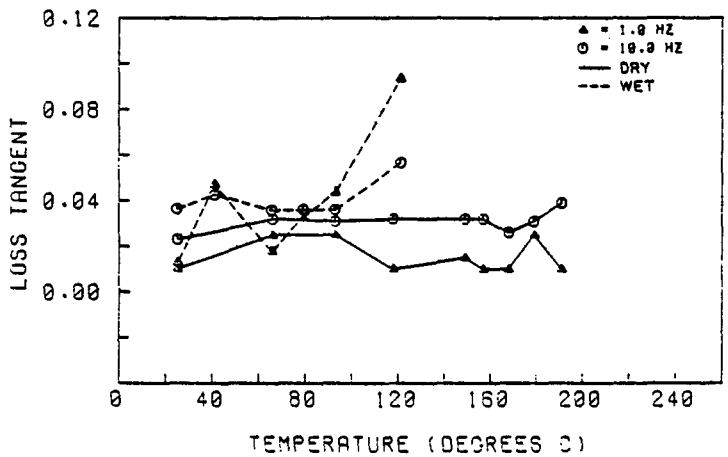

Fig. 28.c(2) Loss Tangent vs Temperature Hercules 3501-5A Epoxy Resin (Variation: 8KV3)

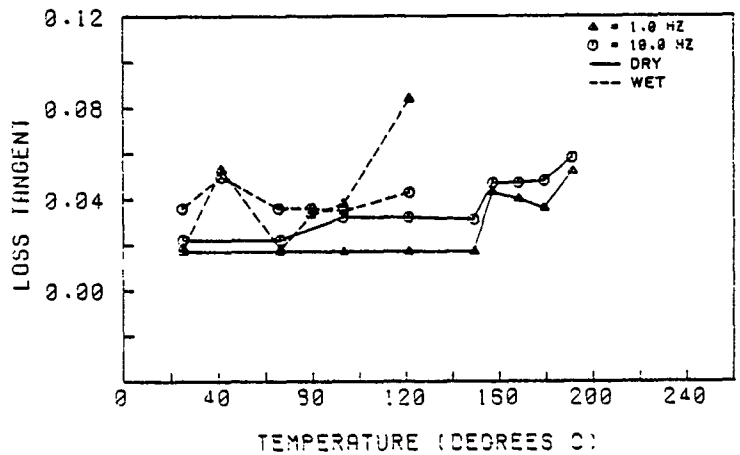

Fig. 28.d(2) Loss Tangent vs Temperature Hercules 3501-5A Epoxy Resin (Variation: 16KV4)

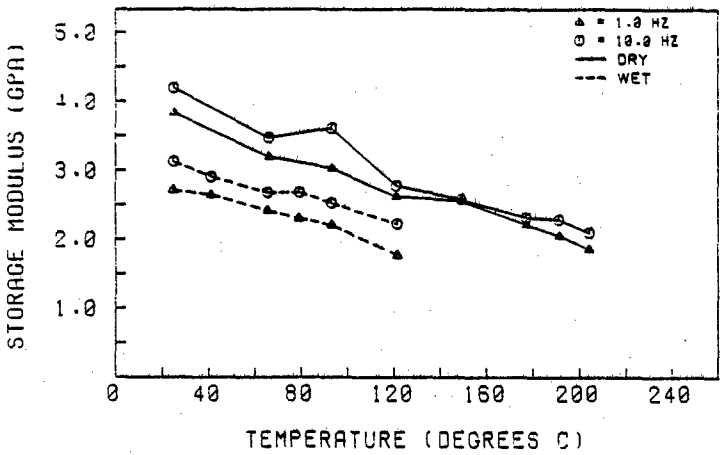

Fig. 28.e(1) Storage Modulus vs Temperature Hercules 3501-5A Epoxy Resin (Variation: 12KV5)

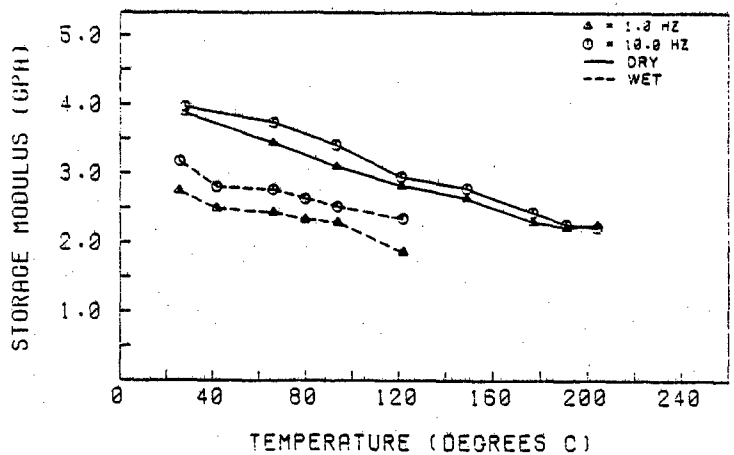

Fig. 28.f(1) Storage Modulus vs Temperature Hercules 3501-5A Epoxy Resin (Variation: 12KV6)

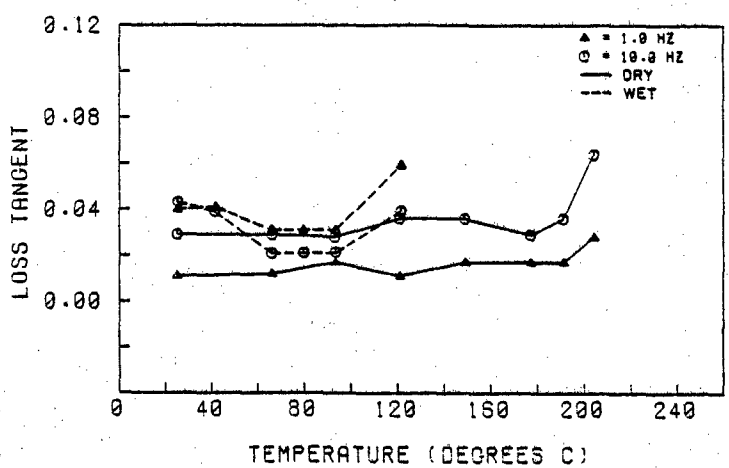

Fig. 28.e(2) Loss Tangent vs Temperature Hercules 3501-5A Epoxy Resin (Variation: 12KV5)

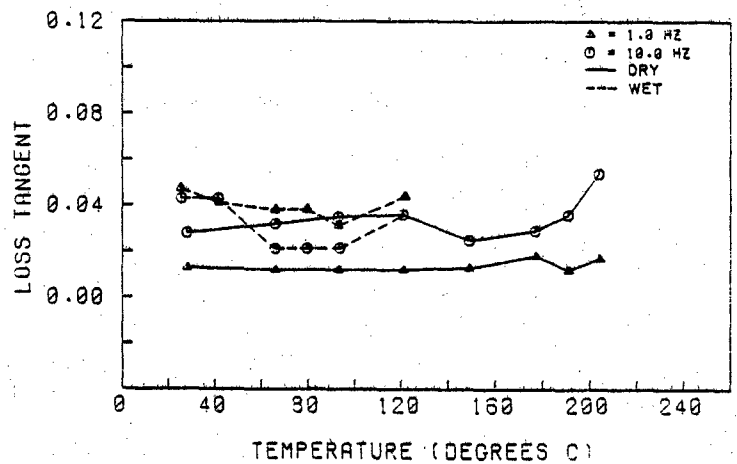

Fig. 28.f(2) Loss Tangent vs Temperature Hercules 3501-5A Epoxy Resin (Variation: 12KV6)

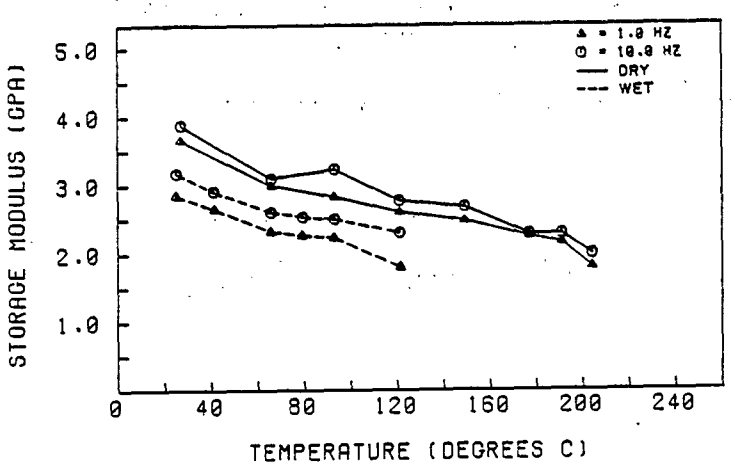

Fig. 28.g(1) Storage Modulus vs Temperature
Hercules 3501-5A Epoxy Resin
(Variation: 12KV7)

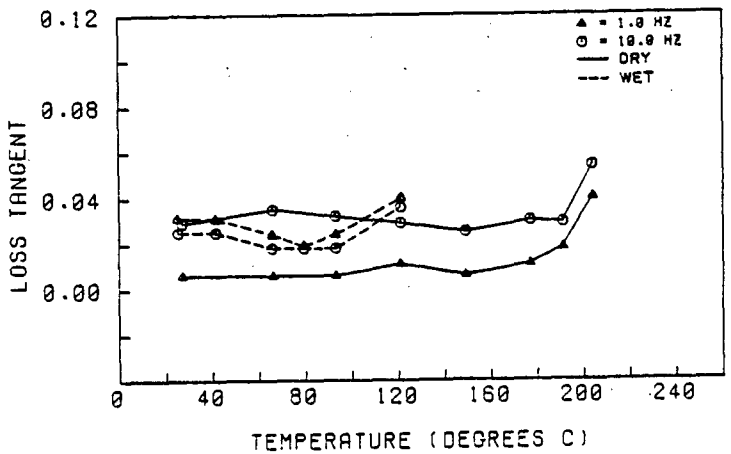

Fig. 28.g(2) Loss Tangent vs Temperature
Hercules 3501-5A Epoxy Resin
(Variation: 12KV7)

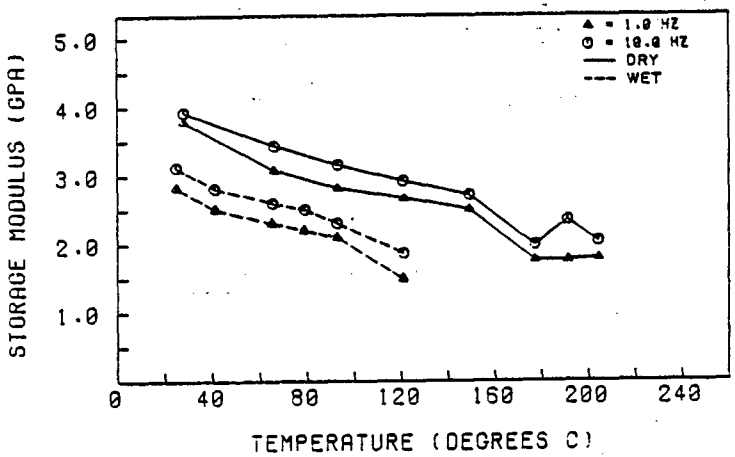

Fig. 28.h(1) Storage Modulus vs Temperature
Hercules 3501-5A Epoxy Resin
(Variation: 12KV8)

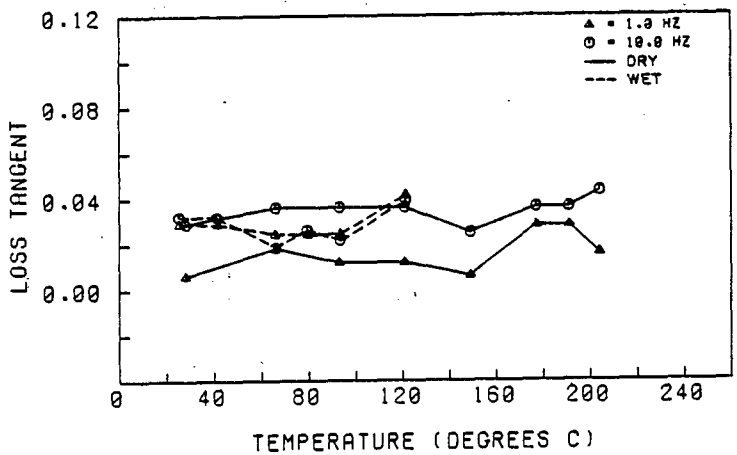

Fig. 28.h(2) Loss Tangent vs Temperature
Hercules 3501-5A Epoxy Resin
(Variation: 12KV8)

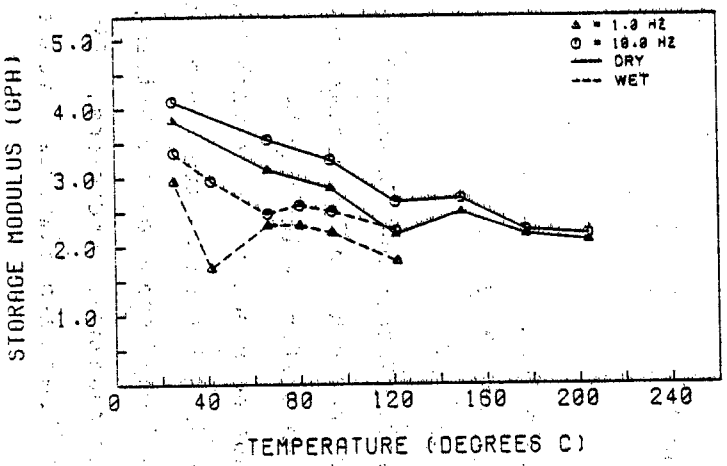

Fig. 28.i(1) Storage Modulus vs Temperature
Hercules 3501-5A Epoxy Resin
(Variation: 12KV9)

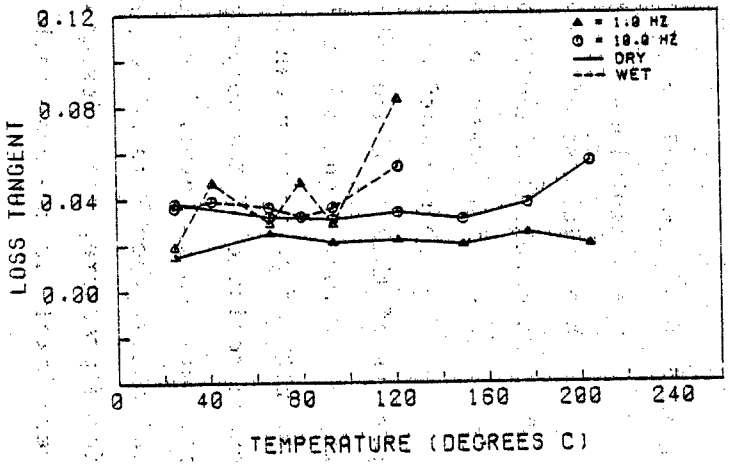

Fig. 28.i(2) Loss Tangent vs Temperature
Hercules 3501-5A Epoxy Resin
(Variation: 12KV9)

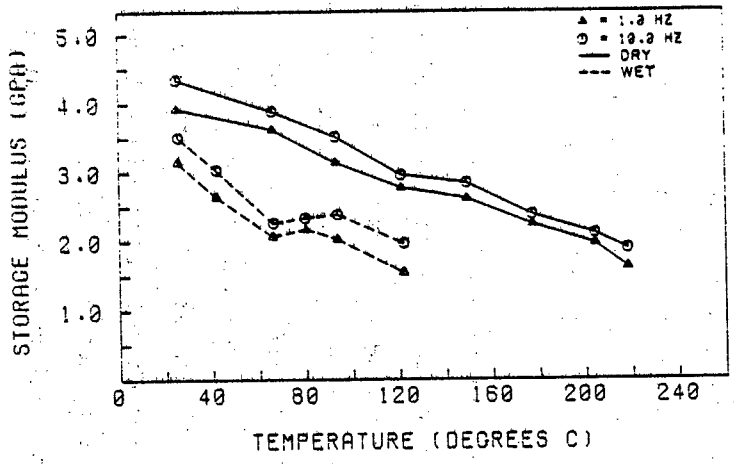

Fig. 28.j(1) Storage Modulus vs Temperature
Hercules 3501-5A Epoxy Resin
(Variation: 12KV10)

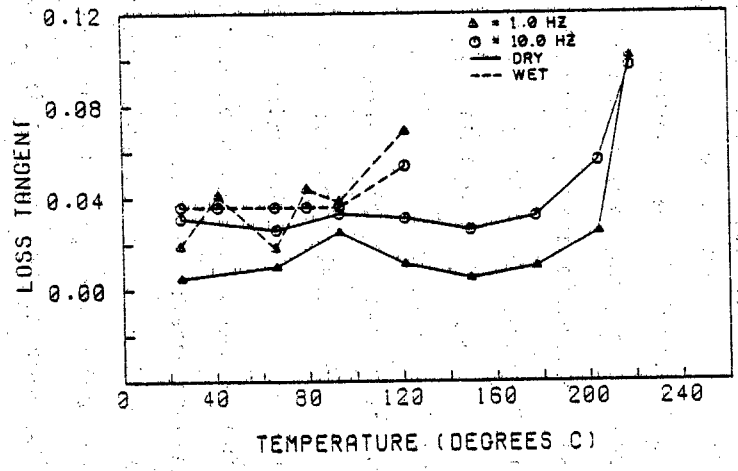

Fig. 28.j(2) Loss Tangent vs Temperature
Hercules 3501-5A Epoxy Resin
(Variation: 12KV10)

4. PHYSIOCHEMICAL PROPERTIES

A limited number of physiochemical tests were performed on the ten variations of the H-3501-5A resin system. Water permeability and solubility tests were run from which diffusion coefficients were determined for all ten variations. Thermal degredation and cure kinetics were investigated for the standard batch 12KV10 only.

a. Permeability Coefficient - Each variation of the H-3501-5A resin system was cast in 1/32 inch thick sheets for determination of the permeability of the material. 2-7/16 inch diameter disks were routed from the sheets and clamped in place on standard Payne Permeability Cups (Fisher No. 13-338) which were partially filled with distilled water. The assembly was then placed in a desiccator at room temperature. Weight measurements were recorded every day or two always at the same time of day using a Mettler H51AR Analytical Balance with automatic digital readout. The data was plotted and after stabilization a slope determined. Following the general method outlined by ASTM[23] Permeability is then evaluated using the relation

$$P = \frac{wh}{p(R_1 - R_2)a} = 4.959 \times 10^{-7}\ wh \qquad (40)$$

where: P = permeability (gm cm/day m^2(mm Hg))

w = weight loss per day (gm/day)

h = thickness of sheet (mm)

$R_1 - R_2$ = relative humidity difference (%) = 100%

p = vapor pressure (mm Hg) = 23.754 mm Hg @ 77F

a = exposed surface area (cm^2) = 9.825 cm^2

Results of this test are tabulated in Table 9. Yasuda and Stannett[24] point out that when small molecules permeate through a polymer membrane, the rate of permeation can be expressed by parameters which may be characteristic of the polymer if the permeant does not interact with the polymer. On the other hand if the permeant does interact with the polymer molecules, then P is no longer a constant and may depend on the driving force pressure, the thickness, and other environmental conditions. This very likely is the case with this material. They also summarize trends

in permeability as related to some influencing factors. The summary is repeated here.

Density can be regarded as a measure of "looseness" of the polymer structure and, in general, the lower the density the higher the permeability.
Molecular weight of a polymer has been found to have little effect on the permeability of polymer, except in the very low range of molecular weights.
Crystallinity of a semi-crystalline polymer reduces the permeability significantly from the value of the corresponding amorphous polymer, i.e., the higher the degree of crystallinity, the lower the permeability.
Orientation of polymer molecules reduces the permeability.
Crosslinking decreases the permeability, especially for large molecular size permeants.
Plasticizers usually, but not always, increase the permeability.
Humidity increases the permeability of some hydrophillic polymers
Liquid permeants have slightly higher permeabilities than the corresponding saturated vapor under many practical conditions.
Solution-cast films have variable permeabilities depending upon the kind of solvent and the drying technique. Poor solvents tend to yield films of higher permeability.
The method of vulcanization has a significant effect on the permeability of elastomers.
Fillers generally decrease the permeability; however, the effect is complicated by the type, shape and amount of filler, and its interaction with the permeant.
Thickness of film does not, in principle, affect the permeability coefficient, the diffusion constant, and the solubility coefficient; however, different values may be obtained by films of identical sample but of various thickness due to the difference of morphology and to the effect of asymmetry introduced in the preparation of films of various thickness.

b. Water Solubility - Disks of each variation 2.00 inches diameter by 1/8 inch thick were fabricated. Two diametric lines 90 degrees apart were carefully scribed on the surface. These diameters provided locations for measuring the diameter of the disk at two places and the thickness at four places both of which were average and used in volume calculations. After thoroughly desiccating the disks for about 60 days they were placed in a room temperature water vapor saturated glass container (desiccator jar with distilled water). Volume and weight were carefully recorded weekly for twenty-five weeks using a precision micrometer (.001 inch resolution estimate to .0002 inch) and the H 51 AR Mettler analytical balance. Both weight and volume were plotted against time. There was not sufficient time to reach an equilibrium state of water absorption, however the time was sufficient to show a definite leveling off but not an asymptotic value. Therefore it was felt that the data could be quite accurately extrapolated

to a finish by assuming that the process of moisture absorption causing weight increase and volume expansion is a first order process following the differential equation

$$\frac{df}{dt} + \frac{1}{\tau} f = \frac{1}{\tau} f_{\infty} \tag{41}$$

For two time periods t_1 and t_2 and defining the first derivative as

$$\frac{df}{dt} = \frac{f_{t+\Delta t} - f_{t-\Delta t}}{2\Delta t} \tag{42}$$

it can be shown that

$$\frac{1}{2\Delta t} (f_{t_1+\Delta t} - f_{t_1-\Delta t} - f_{t_2+\Delta t} + f_{t_2-\Delta t})/(f_{t_2} - f_{t_1}) = \frac{1}{\tau} \tag{43}$$

which can be used to evaluate the process time constant τ on the basis of values of f at two arbitrary times t_1 and t_2 and a Δt.

The solution to equation (41) is

$$f/f_{\infty} = 1 - \exp(-t/\tau) \tag{44}$$

from which it can also be shown that

$$f_{\infty} = (f_{t_2} - f_{t_1})/\exp(-t_1/\tau) - \exp(t_2/\tau) \tag{45}$$

which was used to determine the asymptotic value of the function at t_{∞}. Values of f_{∞} (i.e., maximum weight increase and maximum volume increase) were used to determine the percent weight and percent volume increase. They are tabulated in Table 9 along with corresponding time constants. The maximum weight increase was also used to evaluate the water solubility coefficient also listed in Table 9 where

$$S = \frac{\Delta w}{pv(R_1 - R_2)} = \frac{\Delta w}{V} \tag{46}$$

and where: S = solubility coefficient (gm/cm^3 mm Hg)

Δw = weight of water absorbed (gm)

V = initial dry volume of specimen (cm^3)

c. Diffusion Coefficient - The diffusion coefficient may be evaluated from the permeability and the solubility coefficients.

$$D = P \times 10^{-4}/S \tag{47}$$

where: D = diffusion coefficient (cm^2/day)

Values of the diffusion coefficient are also tabulated in Table 9.

TABLE 9

PERMEABILITY, SOLUBILITY AND DIFFUSION COEFFICIENTS
FOR WATER PENETRANT IN H 3501-5A EPOXY RESIN

Permeability; Specimen 2 in. x 1/32 in. (5 cm x 0.8 mm), Std. Payne Cup, 25 C, 100% RH inside, 0.0 % R.H. outside

Solubility; Specimen 2 in. x 1/8 in. (5 cm x 3.2 mm), 25 C, in 100% R.H. environment

Variation	Permeability Coefficient	Solubility					Diffusion Constant
		By Weight		By Volume		Water Solubility Coefficient	
	P	Time Constant τ	Equilibrium Weight Increase	Time Constant τ	Equilibrium Volume Increase	S	D = P/S
	(g cm/sec m^2 mm Hg)	(days)	(%)	(days)	(%)	(g/cm^3 mm Hg)	(cm^2/sec)
16KV1	1.379×10^{-7}	127	5.46	65	3.01	2.95×10^{-3}	4.67×10^{-9}
8KV2	1.109	120	5.14	105	2.60	2.79	3.97
8KV3	2.304	122	5.40	38	6.26	2.91	7.92
16KV4	1.786	142	5.74	112	3.22	3.12	5.72
12KV5	1.609	122	5.37	61	2.96	2.91	5.53
12KV6	1.258	145	6.02	40	5.79	3.25	3.87
12KV7	1.243	216	5.44	31	5.84	2.92	4.25
12KV8	0.946	103	5.18	56	3.83	2.80	3.38
12KV9	1.646	131	5.50	91	3.41	2.96	5.56
12KV10	0.948	154	5.77	112	3.06	3.09	3.07

d. Thermal Gravimetric Analysis

A thermal gravimetric analysis (TGA) was performed on the standard sub-scale 12KV10 using a Perkin-Elmer TGS-2 system. Six runs were performed at heating rates of 2.5, 5, 10, 20, 40, and 80 centigrade degrees per minute from which the rate of thermal degradation in Nitrogen by weight as a function of temperature at each heating rate was continuously determined. Simultaneous differentiation of the data also indicated the temperature when the degredation rate is greatest. Table 10 summarizes the temperatures at various weight losses for the six heating rates. Appendix C, Figures C-1 through C-6 are the thermograms of the material at the six heating rates. A cross plot of these curves provides data from which the activation energy of chemical decomposition of the resin system may be determined following the method of Flynn and Wall[25]. They showed that the thermogravimetric conversion rate dC/dT followed the Arrhenius equation

$$dC/dT = (A/\beta)\, f(C) \exp(-E/RT) \tag{48}$$

where C is the degree of conversion, T the absolute temperature, β the constant heating rate dT/dt, A is a pre-exponential factor, E the activation energy, R the universal gas constant and f(C) a function of the degree of conversion (weight loss). If A, f(C) and E are considered independent of C then the magnitude of E may be determined directly from equation (1) and

$$E = -4.34\, d(\log \beta)/d(1/T) \tag{49}$$

Figure 29 shows this cross plot for three different degrees of conversion (C). Note that the slope of each is the same and is constant over the full range of temperatures (i.e., 1/T) thus

$$\text{Slope} = d(\text{Log } \beta)/d(1/T) = -9.49 \times 10^3$$

and therefore the activation energy of chemical decomposition is

$$E = 41.3 \text{ K cal/mole}$$

e. Differential Scanning Calorimeter

Three cured samples of H-3501-5A standard sub-scale variation 12KV10 weighing 6.856 mg, 4.949 mg and 6.848 mg were tested in a Perkin-Elmer Differential Scanning Calorimeter. This equipment monitors and controls the

TABLE 10

THERMAL GRAVIMETRIC ANALYSIS (TGA) OF
HERCULES 3501-5A CODE 12KV10 (STANDARD SUB-SCARE)

	Rate of Temperature Rise (°C/min)					
	2.5	5	10	20	40	80
Temperature at 1% Weight Loss (°C)	239	280	303	307	325	333
Temperature at 10% Weight Loss (°C)	329	340	348	360	374	384
Temperature at Maximum Rate of Degradation (°C)	375	386	405	422	439	450
% Weight Remaining at Maximum Rate of Degradation	62	60	57	53	53	50

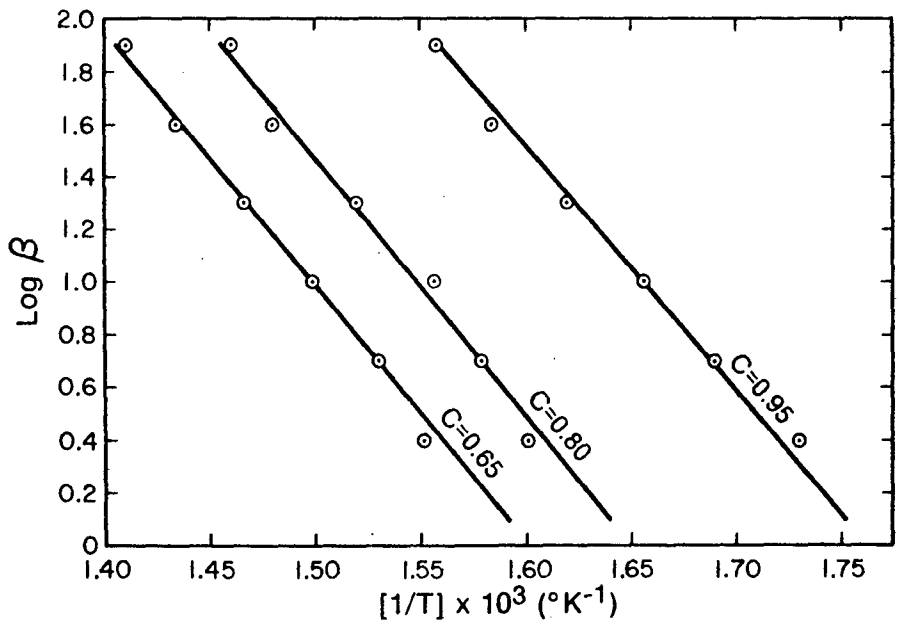

Fig. 29 Log β versus 1/T Plot for Determination of Activation Energy of Chemical Decomposition of 12KV10 Standard Sub-Scale of H 3501-5A

power delivered to sample holders necessary to maintain a preset rate of temperature rise. If a thermal transition takes place in the sample that alters the rate of temperature rise the power is proportioned to hold the rate. With rate of temperature rise plotted versus power required to maintain the temperature rate thermal transitions such as the glass transition temperature, t_g, crystillization if present, or melting if it occurs, can be determined. Note that the slope of this record is proportional to the heat capacity of the sample. The three samples were each tested at a heating rate of 20 C^o/min with sensitivities set at 1 mcal/sec. The temperature ranged from about 17°C to 227°C which is slightly below the point at which thermal degradation starts at this heating rate. No conclusions could be drawn from the output curves regarding the glass transition temperature (T_g). This is probably to be expected with a heavily crosslinked resin system.

f. Cure Rheology

A rheological characterization of the standard sub-scale variation 12KV10 has been performed* using a torsion pendulum TBA (Torsion Braid Analysis) technique[26]. The method uses a loose glass braid about .030 inches diameter by 2 to 8 inches long made up of some 3600 filaments. The large surface area of the braid permits pickup of relatively large amounts of polymer solution and minimizes the effects of gravity. The braid supports a torsion pendulum which is intermittently set into torsional oscillation of about 1 Hz period producing a series of freely damped waves. The specimen is enclosed in a thermal chamber which can be flooded with inert gas and temperature controlled as desired. The apparatus is interfaced with appropriate sensing transducer, conditioning gear and on-line computer data acquisition and reduction to output two mechanical functions related to the in-phase shear modulus G' and out-of-phase shear modulus G'' of the complex modulus G. Because of the irregular geometry and composite nature of the specimen the actual output is the relative rigidity

*Performed under subcontract to J.K. Gillham of Plastics Analysis Consultants, Inc., Princeton, NJ.

$1/P^2$ (P is the period in seconds) which is directly proportional to the elastic portion G' of the shear modulus and the logarithmic decrement Δ ($\Delta = \ln (A_i/A_{i+1})$ where A_i is the ith oscillation of freely damped waves) which is directly proportional to the viscous portion G" on the shear modulus. ($\Delta = \pi\ G''/G' = \pi \tan \delta$).

The work was done in two parts as follows.

(1) TBA Task 1 - Task 1 consisted of measuring the thermo-mechanical spectra after each successive stage in the specified cure cycle (See Table 2) and relating the transitions to the cure. Procedure: A solution was formed of 12KV10 Standard Sub-Scale with methylene chloride approximately 50/50 by weight at room temperature over a 3 hour period. The glass braid was impregnated with the solution and mounted in the TBA apparatus. Air was displaced by Helium. The specimen was then heated from room temperature to 90°C at a high heating rate and the following TBA Torsional Pendulum experiments were performed, data recorded (See Figures D-1 through D-9 of Appendix D) and interpretations made.

RT to 90°C high heating rate
Figure D-1. 90°C/2.5 hour.
Cool to 5°C.
Figure D-2. 5°C to 120° to 5° to 120°C/hold 1 hour.
Figure D-3. 120°C to -115° to 180° to -190° to 180°C/hold 0.5 hour.
Figure D-4. 180°C to -190° to 180°C/hold 0.5 hour.
Figure D-5. 180°C to -190° to 180°C/hold 8 hours.
Figure D-6. 180°C to -190° to 225°C.
Figure D-7. 225°C to -190° to 225°C/hold 8 hours.
Figure D-8. 225°C to -190° to 225°C.
Cool and then rapid to 250°C.
Figure D-9. 250°C to -190°C to 275°C
End

---

*Change in temperature (heating and cooling) was 1.5°C/min for all plots.

Discussion:

1. The H-3501-5A, variation 12KV10 is reactive throughout tmperature range $90^{o}C < T < 180^{o}C$.
2. Glass transition temperature, T_g, rises from below $90^{o}C$ to $180^{o}C$ on heating to $180^{o}C$.
3. Isothermal cure at $180^{o}C$ raises T_g only slightly since vitrication essentially quenches further chemical conversion.
4. Heating to higher temperatures permits devitrification and further chemical reaction.
5. On heating to $275^{o}C$ at $1.5^{o}C$/min, a distinct T_g was observed at $T_g = 267^{o}C$.
6. For a cure to $180^{o}C$ for 1 hour the system displayed slight relaxations at approximately $168^{o}C$, and approximately $-150^{o}C$ and a more distinct relaxation at $-26^{o}C$.

Opinion:

1. The T_g of a fully reacted system of highly functional branching units is likely to be above the onset of thermal degradation which for this material has been determined to be about $239^{o}C$ (at heating rate of $2.5^{o}C$/min. See Table 10).
2. It will be difficult to establish structure-property relationships with incompletely reacted systems such as occur when the system has a maximum T_g above the maximum cure temperature.

Table 11 summarizes the modulus transitions of the Standard Sub-Scale variation as a function of the thermal prehistory. These transitions were obtained from the maxima of the logarithmic decrement (Δ) versus temperature of Figures D-2 through D-9.

(2) TBA Task 2 - Task 2 requires that a general phase diagram be developed for H-3501-5A Variation 12KV10 (Standard Sub-Scale) indicating the four states liquid, ungelled glass, gelled glass, and rubber by measuring the time to reach gellation (t_{gel}) and the time to vitrification (t_{vit}) as a function of isothermal cure temperature (t_{cure})[26]. Figure 30 is a typical phase diagram for a Thermoset Resin showing these four regions. $T_{g\infty}$ is the maximum glass transition temperature of the reactive system, T_{gg} is the cure temperature at which the time to gelation and the time to vitrification are

TABLE 11

TRANSITIONS VS THERMAL PREHISTORY

EPOXY H-3501-5A LOT 12KV10 STD. SUBSCALE

Effective Prehistory	Figure Number*	Temp. Change**	T > Tg °C	Tg °C	T' < Tg °C	T < Tg °C	T << Tg °C
93°C/2.5 hr	D-2		61	40 (2.2290)			
T_{max} 120°C	D-2	-	72	47 (2.1450)			
		+	71	48 (2.0720)			
T_{max} 120°C/1 hr	D-3	-		82 (1.6040)		-51	
		+	114	82 (1.5230)		-47	
T_{max} 180°C	D-3	-		180 (1.1540)		-30	∿-150
		+		>180		-32	∿-150
T_{max} 180°C/0.5 hr	D-4	-		>180		-26	∿-150
		+		>180		-28	∿-150
T_{max} 180°C/1 hr	D-5	-		>180		-26	∿-150
		+		>180		-27	∿-150
T_{max} 180°C/9 hr	D-6	-		>180		-26	∿-156
		+		>250		-25	∿-156
T_{max} 225°C	D-7	-		>250		-23	∿-156
		+		>250		-26	∿-156
T_{max} 225°C/8 hr	D-8	-		>250	168	-31	∿-156
		+		>250	168	-32	∿-156
T_{max} 250°C	D-9	-		>250	168	-31	∿-156
		+		267	168	-34	∿-156

*Appendix D

**$\Delta T/\Delta t$ = 1.5°C Min. Positive +
Negative -

equal ($t_{gel} = t_{vit}$). T_{gg} is significant because curing a material below T_{gg} results in vitrification (essentially a quenched chemical conversion) and therefore an ungelled glass which can be stored or used for molding or prepreg material. If the system is cured above T_{gg} then the material gels before it vitrifies producing a material which cannot flow and therefore has limited processibility. The phase diagram should be independent of the experimental method for obtaining it. However it does assume that the material has vitrified at its glass transition, the validity of which does depend on the method of measurement. The Torsion Pendulum TBA technique used here[27] distinguishes between the glass transition and vitrification in that T_g is measured by the maximum in a loss peak, whereas vitrification is measured by the leveling off of the rigidity.

Procedure: Sample preparation followed the method previously described in Section 4.f.1 "Procedure". The following runs were made to develop the phase diagram.

1. Cure isothermally (80°C to 180°C) through "gelation" and "glass transition" loss peaks to leveling off of relative rigidity due to vitrification. Read off time to gel (t_{gel}) and time to isothermal glass transition (t_{T_g}) versus cure temperature (T_{cure}) (See Table 12). The following figures appearing in Appendix D are original data of the isothermal cures.
   - Figure D-10A. 60°C/401 hour.
   - Figure D-11A. 80°C/119 hour.
   - Figure D-12A. 100°C/72 hour.
   - Figure D-13A. 120°C/14.9 hour.
   - Figure D-14A. 140°C/8.6 hour.
   - Figure D-15A. 160°C/5.4 hour.
   - Figure D-16A. 180°C/6.8 hour.
   - Figure D-17A. 200°C/3.4 hour.
2. After each isothermal cure, and after cooling to less than T_g obtain thermomechanical plots (> RT to 250°C to > RT) of material cured at T_{cure}. Read off T_g versus T_{cure} (See Table 12). The following figures appear in Appendix D are the original thermomechanical data.

Figure D-10B. 25°C to 250°C, 2°C/min; 250°C/50 min

Figure D-10C. 250°C to 90°C $\leq$ 2°C/min

Figure D-11B. 50°C to 250°C to 190°C $\leq$ 2°C/min

Figure D-12B. 33°C to 250°C to 35°C $\leq$ 1.5°C/min

Figure D-13B. 70°C to 250°C to 55°C $\leq$ 2°C/min

Figure D-14B. 40°C to 250°C to 60°C $\leq$ 2°C/min

Figure D-15B. 110°C to 250°C to 75°C $\leq$ 2°C/min

Figure D-16B. 115°C to 250°C to 100°C $\leq$ 2°C/min

Figure D-17B. 25°C to 250°C to 58°C $\leq$ 2°C/min

Figure D-17C. 25°C to 270°C to 75°C $\leq$ 2°C/Min

3. Plot t_{gel} and t_{T_g} vs. T_{cure} (See Figure 31).
4. Plot Log_{10} t_{gel} and Log_{10} t_{T_g} versus $1/T(^{\circ}K)$(See Figure 32).
5. Plot T_g versus T_{cure} (See Figure 33).

Discussion:

A comparison of the results with the general phase diagram follows.

The plots of times to gelation and to isothermal T_gs vs. the isothermal cure temperature Figure 31 do not cross. Since the time to true vitrification (leveling off of the isothermal rigidity) is longer than the time to the isothermal T_g, it follows also that the gelation and vitrification curves will not cross.

It appears from a comparison of the time to gel and time to isothermal T_g versus cure temperature (Table 12) that these times are closest together at 100°C (42 minutes) and diverge at higher and lower temperatures.

The time to gelation vs. T_{cure} is approximately exponential. This leads to an apparent activation energy of 18 kcal/mole (Figure 32 and Appendix D-18). The time to isothermal T_gs vs. T_{cure} varies in a more complicated manner showing two sections, one above and one below 100°C.

The maximum glass transition is above the maximum temperature of isothermal cure investigated. Note that the thermomechanical plots on cooling from 250°C indicate that there is a T_g above 250°C.

The plot (Figure 33) of T_g after isothermal cure to vitrification vs. T_{cure} shows that T_g of the material cured essentially to its maximum at T_{cure} is 34-47°C higher than the cure temperature. This temperature difference is a

measure of the difference in viscoelasticity between the vitrified state and the state at the glass transition temperature. It should be translated into a time difference at T_{cure} by time-temperature superposition if knowledge of the relationship between T_g and time was available for each cure temperature. An approximation for the shift factor can be obtained, in principle, from the time for leveling off of rigidity vs. T_{cure}: however a more extensive program would have to be undertaken to develop these ideas.

TABLE 12

INFLUENCE OF TEMPERATURE OF CURE (T_{cure}) ON TIME TO GELATION (t_{gel}), TIME TO ISOTHERMAL T_g (tT_g), AND GLASS TRANSITION (T_g) OF VITRIFIED MATERIAL

T_{cure} °C	Order of Experiment	t_{gel} (min)	tT_g (min)	T_g (time of cure hr) °C
60	8	3960	8400	91* (401)
80	6	1140	2160	114 (119)
100	5	363	405	142 (72)
120	1	116	233	165 (14.9)
140	2	41.5	134	184 (8.6)
160	3	11.9	53.6	207 (5.4)
180	4	3.1	20.5	227 (6.8)
200	7	-	7.8	>250** (3.4)

*After heating to 250°C and 250°C/50 min, the T_g was above 250°C, as observed on cooling.

**After cooling from 250°C, the thermomechanical behavior from 25° to 270° to 60°C ($\Delta T/\Delta t \leq 2$°C/min) revealed T_g = 262°C on heating, and T_g = 256°C on cooling (the decrease is presumably the result of thermal degradation).

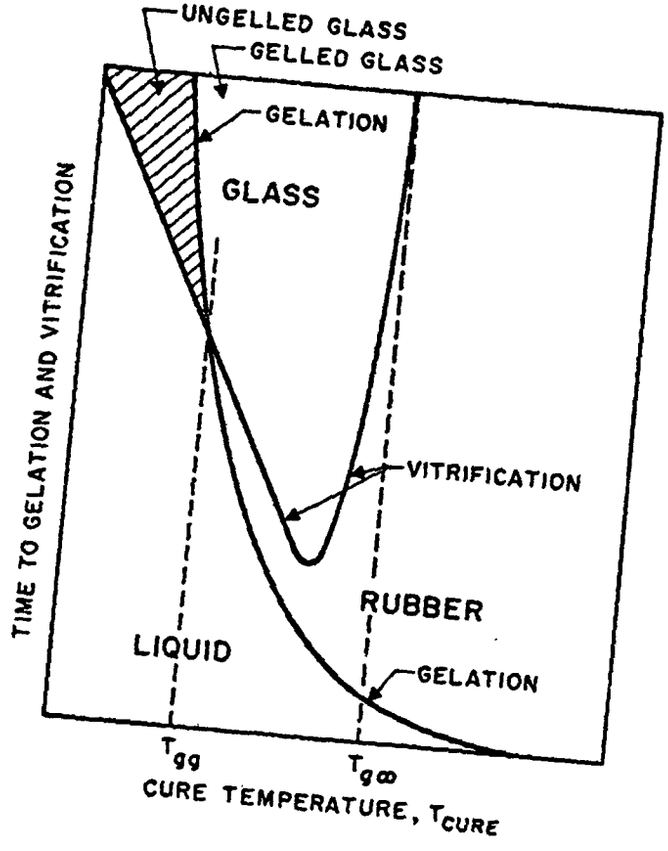

Fig. 30 Typical Phase Diagram for a Thermoset Epoxy Resin(27)

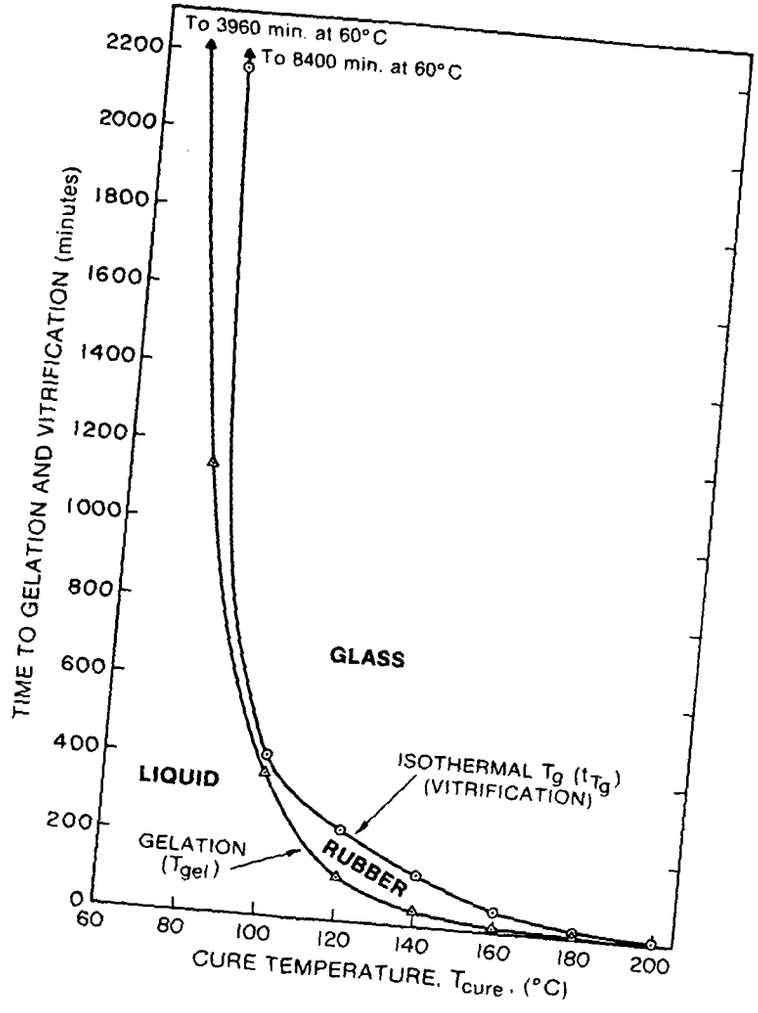

Fig. 31 Phase Diagram for H 3501-5A Epoxy Resin Variation 12KV10 Standard Sub-Scale

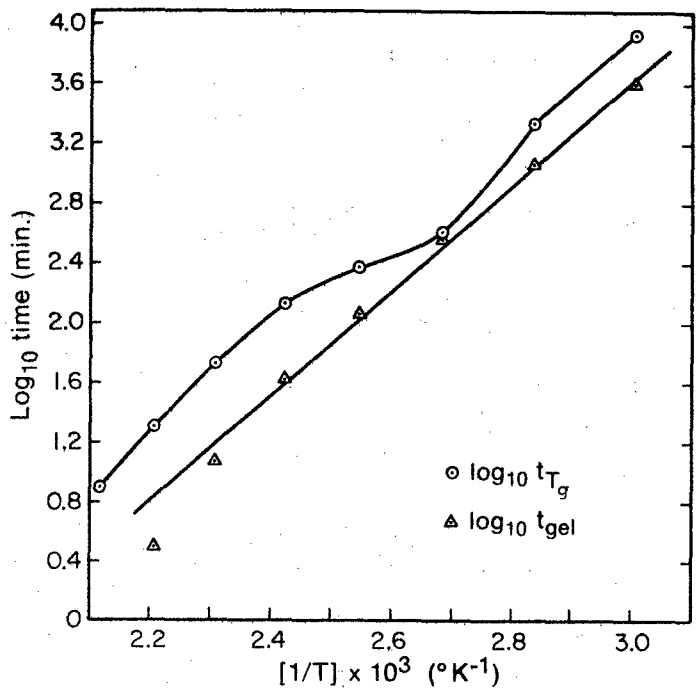

Fig. 32 Log_{10} t_{gel} and Log_{10} t_{T_g} versus 1/T for H 3501-5A Variation 12KV10

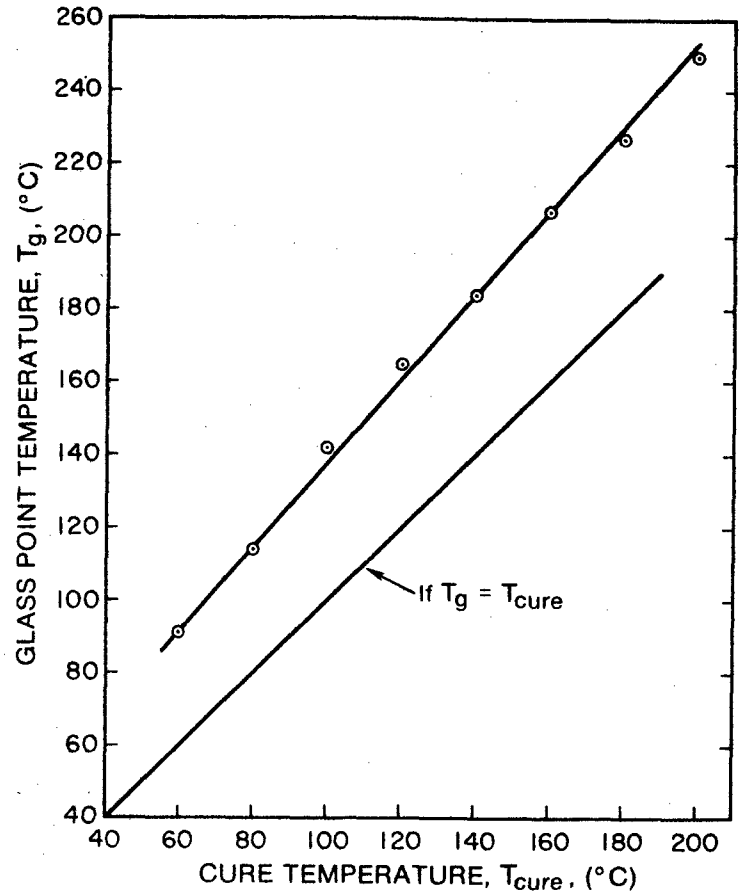

Fig. 33 Glass Transition Temperature versus Cure Temperature for H 3501-5A Variation 12KV10 Standard Sub-Scale

g. Cure Dilatometry

The relationship between the density, temperature, and pressure of polymers is a concern to polmer chemists, physists, and engineers. Experimental data is useful in verifying theoretical equations of state[28,29] of thermoplastics in their liquid, liquid-solid and solid states necessary for high pressure injection molding and the solidification phase. Certain other physiomechanical properties such as the bulk modulus of elasticity and Poisson's[30] ratio can be determined from the experimental pvT data for both thermoplastics and thermosets in their solid states, although the time effects of viscoelastic materials such as these require careful interpretation.[31] Studies of glass transitions and secondary transitions can be studied[29,31] during the cure process of either class of polymer, and in the case of thermosets related to crosslinking rates. For the reactive adhesives the degree of shrinkage during cure effects the localized surface stresses at the interface of the substrate as well as the stresses in the adhesive material. This includes reinforced composites for which shrinkage during cure causes regions of tensile stresses in the matrix and compressive stresses in the filler material. This is probably contrary to the generally desired effects.

It is for these latter reasons that a dilatometer has been developed to measure the shrinkage of high performance epoxy resins during their cure process. The apparatus makes use of a bellows to translate the volume change of a mercury confined polymer sample into a measurable linear displacement. This technique was first employed by Bridgeman[32] for his study of liquids and later by Quach and Simha[31] and by Zoller et al[33] for their studies of polymers. Figure 34 is a drawing and Figures 35a and 35b photographs of the basic test instrument.

A polymer sample which has been previously degassed and consolidated at as low a temperature as possible into a cylinder about 16 millimeters in diameter and 20 millimeters long (about 4 cc volume) is enclosed in a presized aluminum foil wrapper and placed in the sample cup which in turn is placed in the sample cell.

The upper closure of the sample cell is a bellows sub-assembly (Fulton Sylphan Ref. 43527, BB ends) threaded into the sample cell. The

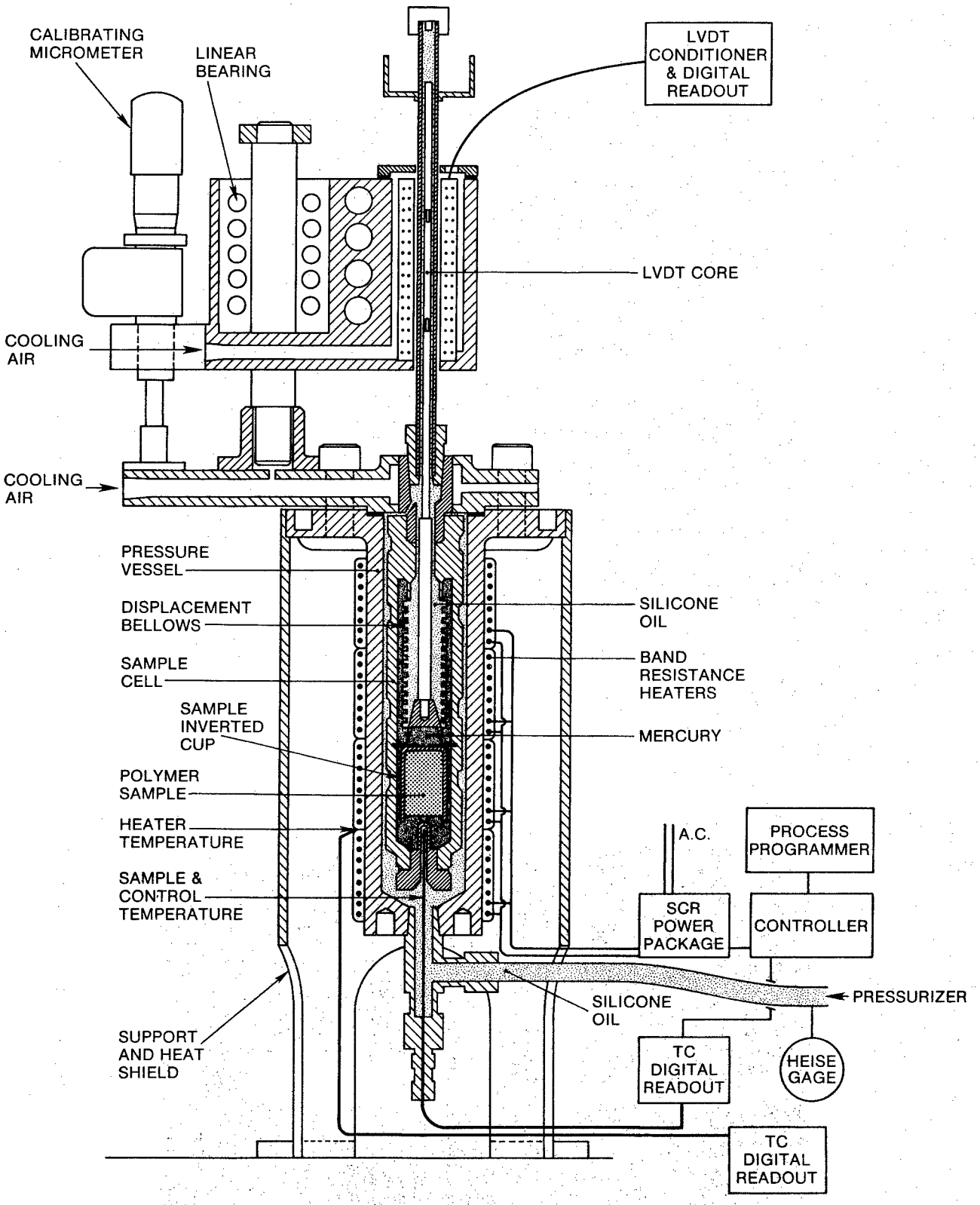

Fig. 34. Polymer Cure Dilatometer

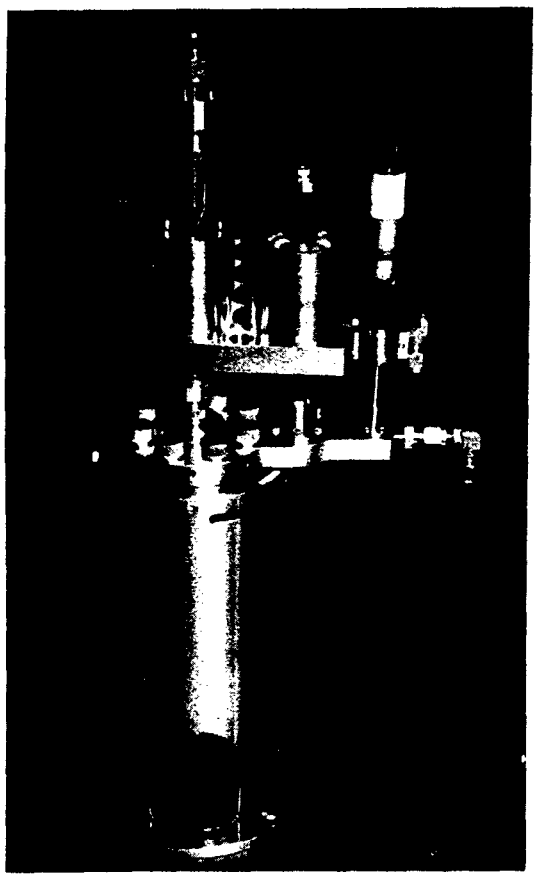

Fig. 35a Assembled Dilatometer

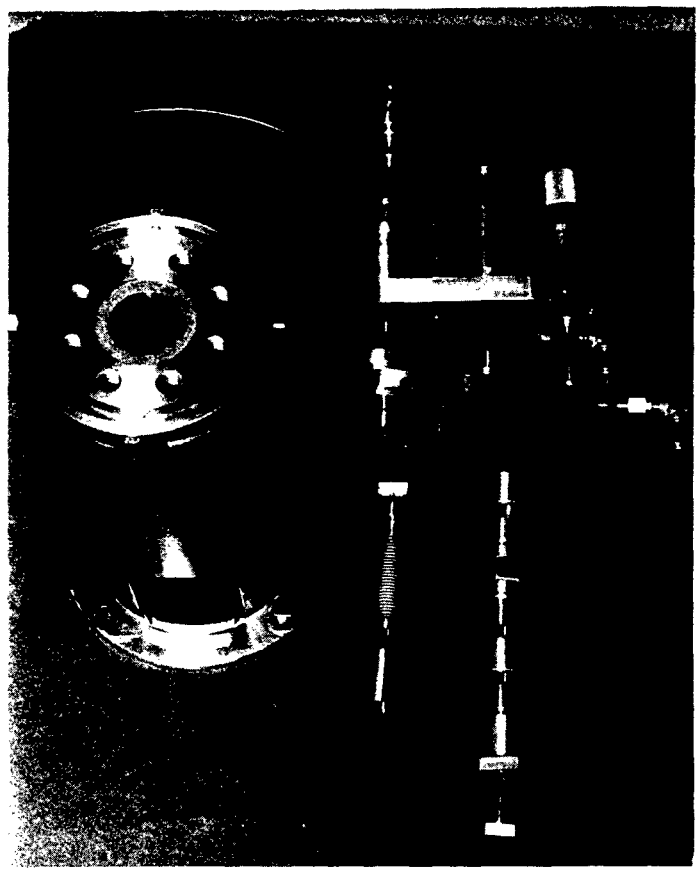

Fig. 35b Disassembled Dilatometer showing sample cell.

cell assembly is filled with mercury in an inverted position in a separate apparatus under a high vacuum to eliminate all voids. The bellows are pre positioned in a slightly compressed state during the mercury vacuum fill and until the lower closure, which doubles as a thermocouple well, is threaded into position completely sealing the sample and the mercury inside the cell forming a void free "solid" interior. Appropriate bleed holes permit mercury to escape while threading in the lower closure up to the point of gasket seal. A long thin displacement rod, part of which is a small diameter core (Schaevitz Engineering core from MHR series) of a Linear Variable Differential Transformer (LVDT) (Schaevitz Engineering 200HR) is threaded into the inside of the bellows to complete the sample cell sub assembly.

The reactor pressure vessel closure consists of a flange, a section of ¼ inch O.D. seamless tubing which receives the core of the LVDT and a splined inner race "pedistal" of a linear ball bearing (Saginaw 0625-6-0187-SSR) supporting a floating head which carries the LVDT coil and digital micrometer (Starrett Tool Co. 363 MRL). The micrometer is used to calibrate and to zero the LVDT.

The sample cell is then threaded on to the pressure vessel closure and the assembly fitted into the vessel observing care while slipping the thermocouple well over the previously placed control thermocouple. Note that prior to assembly the T.C. well is packed with a high temperature silicone grease (Dow Corning Molykote 33, Light Consistancy). This eliminates air pockets and provides better heat transfer from thermocouple well to thermocouple.

With the unit completely assembled a high temperature silicone oil (Dow Corning 210 H Fluid) is slowly pumped into the reactor vessel from the bottom using the pressurizer hand pump (Century-Fox Model CPI-4) until oil appears at the top of the ¼ inch LVDT tube at which point the system is tightly capped off.

Four band heaters (Watlow 3843 HX) provide a maximum of 1200 watts at 240 volts AC for the cure cycle. Power is programmable in accordance with the required cure cycle of a particular polymeric system using a Process Programmer (Leeds & Horthrup Modle 1300-11-00-0-0-0-1-000) controlling the set point of a current adjusting universal controller (L & N Electromax III

Model 6432-5-4099-520-2-20-407-422) with proportional reset rate and approach which modulates a silicone control rectifier power package (L & N Model LN 1-2430, 220 VAC, 30 Amp). Control and sample temperature is monitored by a type K thermocouple with digital readout (L & N Model 025601 with Auxiliary Unit BCD and Analogue Output Model 025685). Heater temperature is also monitered with a type K thermocouple using a similar digital type readout.

Displacement, monitered by the LVDT, is indicated on the digital readont of a transducer-conditioner-readout with 100% zero and temperature compensation (Schaevitz Model DTR -450-030) with BCD and 0 to 10 VDC analogue capabilities.

Although as previosuly mentioned, the sample must be degassed and consolidated prior to placing it in the dilatometer the entire system must still be pressurized to assure that any solvents and/or water dissolved in the sample remain in solution during cure heating. A precision pressure gage (Heise Model 8½ -CM-DQ-TC-SL) with a range 0 to 50 MPa (0 to 7500 psig) is used to moniter this pressure. It is contemplated that the system will be pressurized to about 35 MPa (5000 psig), well above the critical pressure of water.

Air cooling is provided to the reactor vessel flange closure and to the floating head to maintain the LVDT coil temperature at an acceptable level (less than 150 C, 300 F).

All components have been fabricated from type 304 stainless steel. The band heaters, the linear bearing and inner race, and the micrometer however are made of appropriate materials other than stainless steel.

The consolidated uncured sample wrapped in "Frekoted" aluminum foil is floated over mercury inside the inverted sample cup. As the epoxy resin sample cures and bonds itself to its containment surface the foil will wrinkle and/or free itself providing minimum surface constraint to the volume cure shrinkage process. The foil also isolates the sample from the bellows and cell wall during the liquid phase of the cure cycle.

The initial volume of the consolidated epoxy resin sample must be determined. The two fluid (air & distilled water) bouyancy method[34] will

be used to determine both the epoxy resin sample volume and its density. This method of determining volume and density may also be used as a check of instrument calibration by working with sample volume before and after cure.

To use this apparatus for studies of the cure kinetics of polymeric materials the apparatus must be calibrated. The output variable of this dilatometer is simply a relative displacement between the coil and the core of the LVDT. The coil is indirectly attached to the body of the reactor. The core indirectly senses the volume change of the sample through the bellows however the LVDT readout is influenced by such things as the volume of the mercury in the cell, the volume of the hydraulic silicone pressurizer fluid, the volume of the "rigid" sample cell, the interior volume of the reactor pressure vessel, the length of the LVDT displacement rod, the length of the micrometer stem etc, all of which are functions of either pressure, temperature or time or any combination of all three.

For the study of the crosslinking kinetics during an isothermal-isobaric cure, instrument calibration and sample testing are fairly straight forward following the method outlined by Zoller.[33] For a calibration run the sample cell is filled with mercury plus foil wrapping but without a polymer sample. The dilatometer is then completely assembled. The instrument is stabilized at an appropriate reference pressure and temperature (p_r, T_r) and the LVDT readout zeroed at $d_r(p_r, T_r)$. The dilatometer is then stabilized at a sufficient number of pressures and temperatures over its full operating range above p_r and T_r to establish a calibration function $d_1(p,T)$ which is the LVDT displacement from $d_r(p_r, T_r)$ and which will probably be a linear function of pressure and temperature of the form

$$d_1(p,T) = a_o + a_1 p + [a_2 + a_3] T. \tag{50}$$

For a sample test predetermined volume of the consolidated polymeric material replaces an equal volume of mercury in the sample cell at some ambient temperature T_a. Then

$$V_{Hg}(T_a) = V_s(T_a) \tag{51}$$

from which

$$m_{Hg} = m_s \, v_s(T_a)/v_{Hg}(T_a) \tag{52}$$

where

m_{Hg} is the mass of the mercury

m_s is the mass of the sample

$v_{Hg}(T_a)$ is the specific volume of the mercury at the ambient temperature determined from handbook tables[35, 36]

$v_s(T_a)$ is the specific volume of sample experimentally determined by the two fluid weighing method.

To make a sample run the assembled dilatometer is again stabilized at p_r and T_r and the LVDT zeroed at $d_r(p_r,T_r)$. For an isothermal cure run the sample displacement function $d_2(p,T)$ which is again the LVDT displacement from $d_r(p_r,T_r)$ is recorded as a function of time. The difference in the volume change between the sample and the mercury which it replaced is caused by the difference in their pvT characteristics and therefore it can be shown that

$$A(T)[d_2,(p,T) - d_1(p,T)] = m_s \, [v_s(p,T) - v_s(p_r,T_r)] - m_{Hg} \, [v_{Hg}(p,T) - v_{Hg}(p_r,T_r)] \tag{53}$$

where

$A(T)$ is the effective cross sectional area of the bellows. Substituting equation (52) into (53) and rearranging, the change in specific volume of the sample referenced to a pressure and temperature (p_r,T_r) is

$$v_s(p,T) - v_s(p_r,T_r) = A(T)/m_s\,[d_2(p,T) - d_1(p,T)]$$

$$+ [v_s(T_a)/v_{Hg}(T_a)]\,[v_{Hg}(p,T) - V_{Hg}(p_r,T_r)] \qquad (54)$$

The effective cross sectional area $A(T)$ of the bellows is assumed to be a function of temperature only and not pressure. Applying the linear thermal coefficient of expansion for type 304 stainless steel to the area, the function is found to be

$$A(T) = A(T_a)\,[1 + (3.46 \times 10^{-5})\,(T - T_a)] \qquad (55)$$

From work done by Zoller[33] using data from Carnazzi[36] the specific volume of mercury at pressures p and temperatures T may be found from

$$\phi(p,T) = b_1 + b_2 p + [b_3 + b_4 p]T \qquad (56)$$

where

$$\phi(p,T) = v_{Hg}(p,T)/v_o(p = 0,\ T = 0^oC)$$

$$b_1 = 0.99981$$

$$b_2 = -0.3508 \times 10^{-5}\ cm^2\ kg^{-1}$$

$$b_3 = 0.1838 \times 10^{-3}\ C^{-1}$$

$$b_4 = -0.5674 \times 10^{-8}\ cm^2\ kg^{-1}\ C^{-1}$$

All quantities on the right hand side of equation (54) are now either experimentally determined or determined from available references. This equation may be used to experimentally moniter the change in specific volume of a polymer during an isobaric-isothermal cure process.

In the special case of end point shrinkage, viz allowing the dilatometer to cool down to the reference pressure and temperature equation (54) reduces to

$$v_r(p_r,T_r) - v_s(p_r,T_r) = A(T_r)/m_s[d_2(p_r,T_r) - d_1(p_r,T_r)] \qquad (57)$$

For studies of cure kinetics based on a ramp-dwell-ramp-dwell transient cure heating schedule the calibration function becomes time dependent and

$$d_1 = d_1(p,T,t)$$

Each sample run would at least be isobaric, nevertheless because of the thermal characteristics of the apparatus the calibration function $d_1(p,T,t)$ must be determined for each cure heating schedule and then the sample function $d_2(p,T,t)$ run at precisely the same cure heating schedule. Equation (54) then takes on the form

$$v_s(p,T,t) - v_s(p_r,T_r) = A(T)/m_s[d_2(p,T,t) - d_1(p,T,t)]$$

$$= v_s(T_a)/v_{Hg}(T_a)[v_{Hg}(p,T) - v_{Hg}(p_rT_r)] \qquad (58)$$

It is apparent that temperature and time are coupled variables for a transient cure cycle and for any meaningful cure kinetic studies it is necessary that the relationship between temperature and time be reproducable from calibration run to sample run.

APPENDIX A

Tabulation of Coefficients for

Least Square Exponential Fit to Tensile Data

TABLE A-1

LEAST SQUARE EXPONENTIAL FIT FOR TENSILE DATA

VALUES OF COEFFICIENTS A AND B

$$\sigma = A\{1 - \exp(-B\varepsilon)\} \qquad \sigma(\text{psi});\ \varepsilon(\text{in/in})$$

State	Cross Head Speed in/min	Temp (°F)	H-3501-5A Variations 16KV1 A	16KV1 B	8KV2 A	8KV2 B	8KV3 A	8KV3 B	16KV4 A	16KV4 B	12KV5 A	12KV5 B
Dry	0.02	-67	-	-	-	-	34220	24.85	15594	89.34	-	-
		77	25773	27.83	24922	27.11	24307	27.58	33480	20.84	25074	25.28
		200	23427	21.30	35318	13.04	21881	24.14	26410	20.48	19657	26.38
		275	17837	24.80	19930	21.54	23266	17.88	19638	23.59	22085	19.73
		350	7178	56.43	9131	45.36	9034	50.19	8747	50.96	7765	56.20
	0.20	77	29567	24.66	27029	26.09	27544	24.99	23430	36.27	24402	28.58
		350	13560	34.31	14715	32.07	14444	30.47	11430	38.61	11687	40.08
	2.00	77	24872	31.93	29977	23.03	13965	79.42	27631	28.74	33168	20.03
		350	13672	33.01	14888	29.14	11319	38.91	14000	35.32	16710	25.51
Wet	0.02	-67	-	-	-	-	22920	33.01	19275	44.10	-	-
		77	21428	22.47	19519	25.50	12568	44.20	14705	36.45	17252	28.84
		200	9987	37.59	6985	60.15	13598	26.49	11806	33.42	8525	45.33
		275	1230	123.85	1490	47.35	1511	54.35	1589	68.99	2382	106.55
		350	739	35.08	814	23.12	1362	12.20	1764	9.79	651	40.45
	0.20	77	23049	22.20	21186	24.30	16273	34.73	16790	32.48	32931	13.97
		350	785	68.67	686	64.92	637	65.73	734	58.56	917	42.75
	2.00	77	17968	32.09	20243	26.46	12460	49.49	15746	39.46	14793	40.53
		350	1468	38.47	884	46.48	1167	47.30	969	49.56	771	42.92

State	Cross Head Speed in/min	Temp (°F)	H-3501-5A Variation 12KV6 A	12KV6 B	12KV7 A	12KV7 B	12KV8 A	12KV8 B	12KV9 A	12KV9 B	12KV10 A	12KV10 B
Dry	0.02	-67	-	-	-	-	-	-	-	-	32134	26.49
		77	22957	30.41	25270	26.95	26355	25.31	27141	23.49	28711	21.30
		200	26939	18.48	22317	24.35	28044	18.41	17178	33.38	22038	23.66
		275	18492	25.09	20214	22.40	17710	26.98	17843	26.10	16099	30.36
		350	9319	51.56	9970	43.17	10035	46.62	9735	44.91	9319	45.94
	0.20	77	27400	25.74	26857	26.85	22659	34.83	26863	25.25	36065	17.00
		350	12919	36.27	14676	31.82	13348	35.23	13375	35.00	13957	30.49
	2.00	77	23473	34.03	25248	29.12	25810	29.05	26192	28.14	24662	30.64
		350	13211	35.37	13828	34.30	14290	33.63	14193	36.01	16884	24.31
Wet	0.02	-67	-	-	-	-	-	-	-	-	11802	81.92
		77	16396	30.22	22007	22.00	20190	23.96	24033	19.77	32736	14.07
		200	15457	22.43	10507	37.83	10350	36.02	8232	51.42	12548	29.45
		275	1494	92.01	1950	101.41	1466	119.49	1620	84.10	1737	70.16
		350	958	34.97	640	62.58	772	24.00	1137	18.16	885	24.68
	0.20	77	23742	21.22	16544	33.52	20853	24.61	8976	71.73	27173	18.39
		350	805	96.31	1031	50.46	683	69.89	840	61.12	1147	128.76
	2.00	77	12164	50.16	17641	30.95	18055	30.11	13610	44.04	15593	40.87
		350	766	49.02	1005	39.70	881	38.23	1011	49.70	1025	50.31

APPENDIX B

The Maxwell Weichert Model

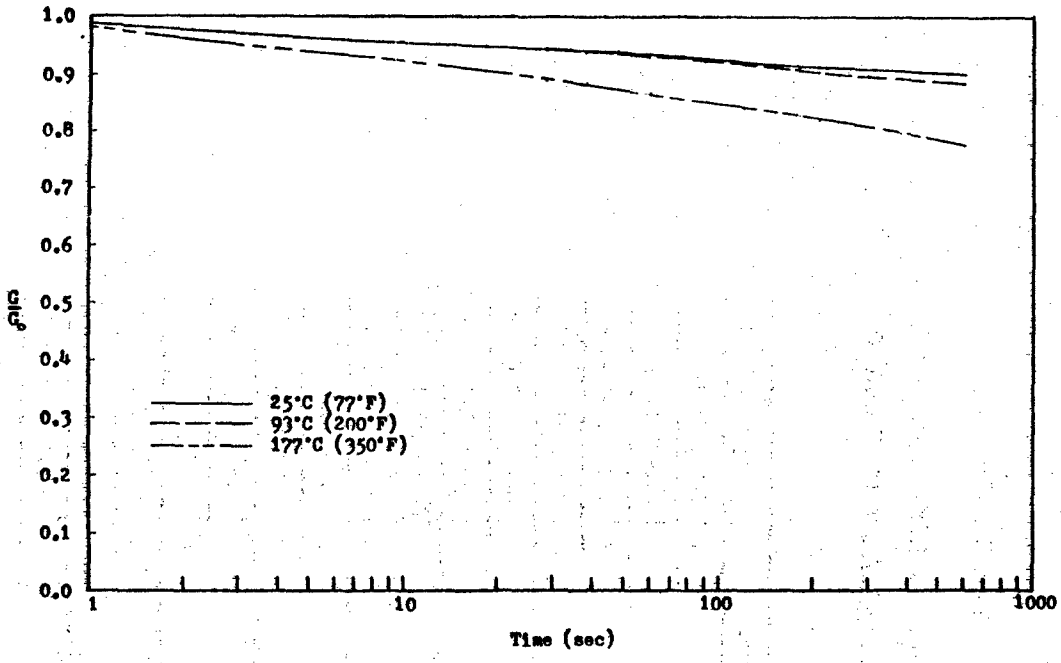

Fig. B-1 Normalized Shear Relaxation Function vs Time For Epoxy Resin

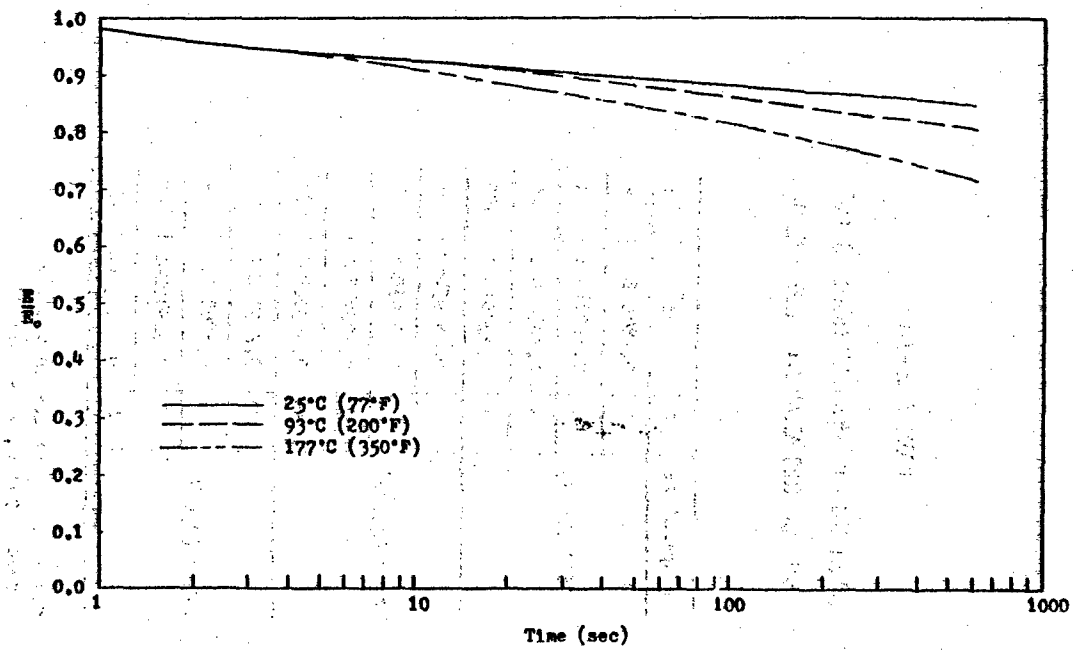

Fig. B-2 Normalized Tensile Relaxation Function vs Time For Epoxy Resin

TABLE B-1a

DIRICHLET SERIES MODELS OF
SHEAR RELAXATION BEHAVIOR

Temperature	i	G_i†	τ_i
25°C (77°F)	1	0.88404E+0	∞
	2	0.38021E-1	4
	3	0.29847E-1	40
	4	0.45209E-1	400
93°C (200°F)	1	0.86295E+0	∞
	2	0.37096E-1	4
	3	0.30874E-1	40
	4	0.68300E-1	400
177°C (350°F)	1	0.74723E+0	∞
	2	0.67826E-1	4
	3	0.62540E-1	40
	4	0.12023E+0	400

Note: All τ_i values in seconds
† Based upon equation (2.20)

TABLE B-1b

DIRICHLET SERIES MODELS OF
TENSILE RELAXATION BEHAVIOR

Temperature	i	E_i†	τ_i
25°C (77°F)	1	0.83540E+0	∞
	2	0.69053E-1	4
	3	0.32046E-1	40
	4	0.58985E-1	400
93°C (200°F)	1	0.78424E+0	∞
	2	0.60567E-1	4
	3	0.58135E-1	40
	4	0.95253E-1	400
135°C (275°F)	1	0.68475E+0	∞
	2	0.72774E-1	4
	3	0.80095E-1	40
	4	0.16138E+0	400
177°C (350°F)	1	0.72251E+0	∞
	2	0.63979E-1	4
	3	0.61201E-1	40
	4	0.15143E-1	400

Note: All τ_i values in seconds
† Based upon equation (2.20)

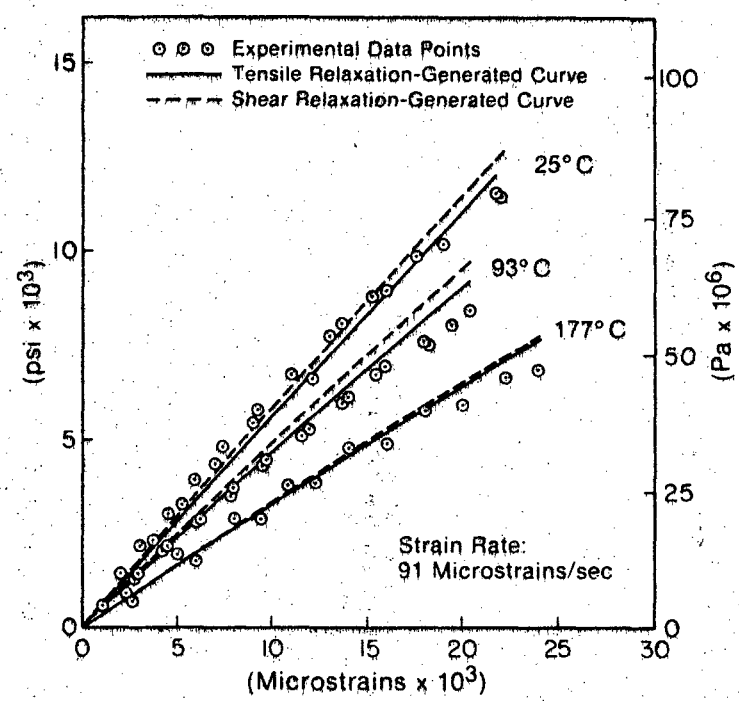

Fig. B-3 Comparison of Relaxation Generated Curves with Actual Stress-Strain Curves

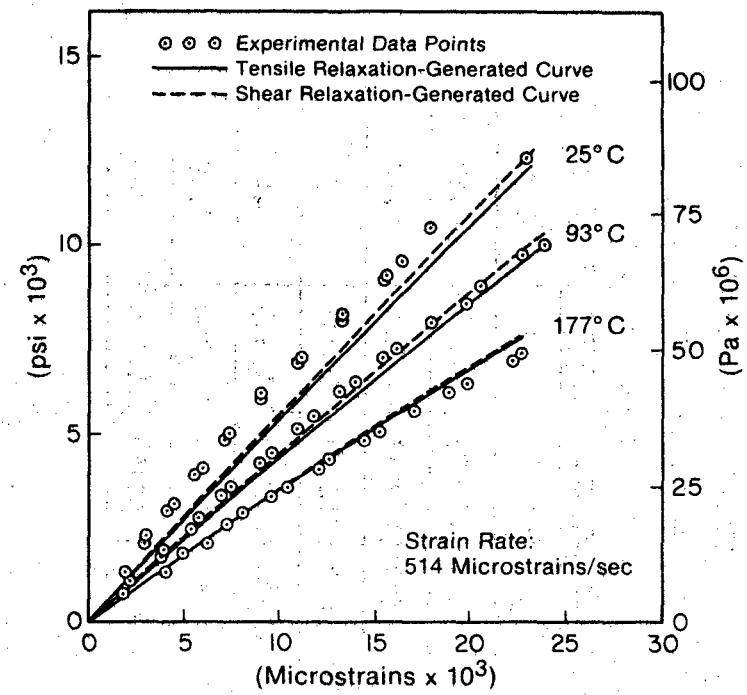

Fig. B-4 Comparison of Relaxation Generated Curves with Actual Stress-Strain Curves

TABLE B-2

TIME-TEMPERATURE SHIFT

VALUES FOR EPOXY RESIN

(See Equation (35)

Temperature	a(T)	Log(a(T))
25°C (77°F)	5.581	0.747
50°C (122°F)	3.764	0.575
75°C (167°F)	2.686	0.429
100°C (212°F)	2.006	0.302
125°C (257°F)	1.553	0.191
150°C (302°F)	1.240	0.093
177°C (350°F)	1.000	0.000

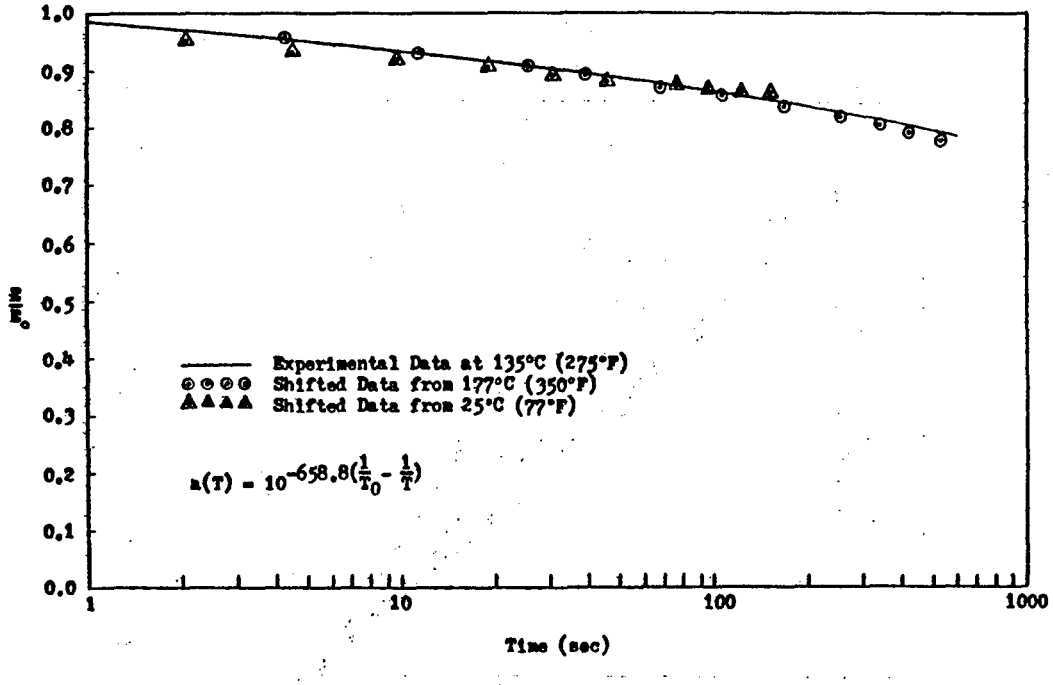

Fig. B-5 Comparison Of Shifted Tensile Relaxation Data To Actual Response Curve

APPENDIX C

Thermograms of H-3501-5A Variation 12KV10 Resin

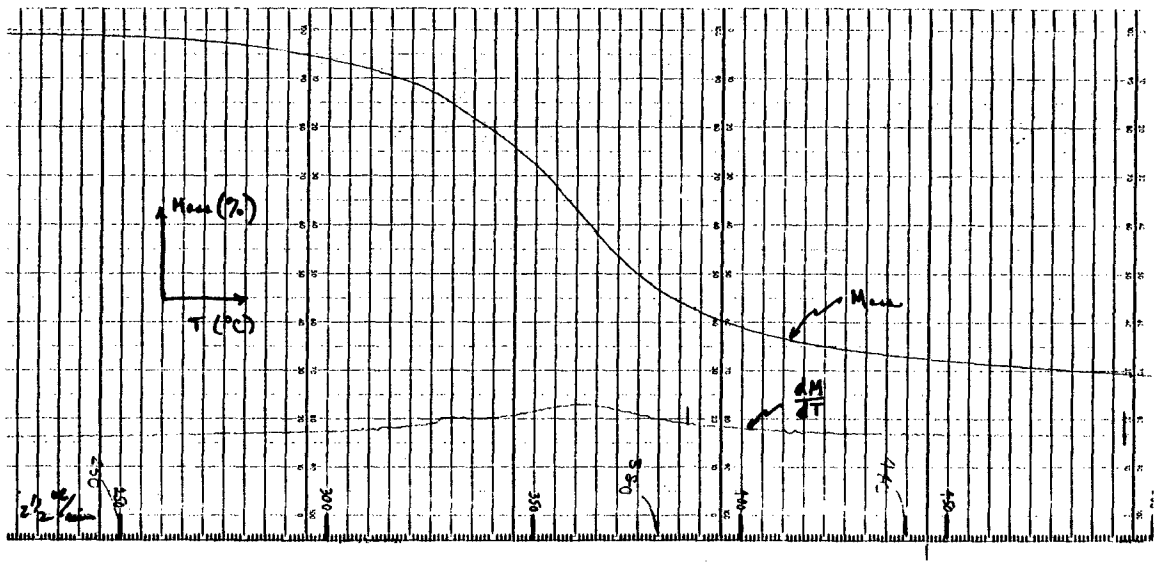

Figure C1 Thermogram (TGA) of H3501-5A Variation 12KV10 Std. Subscale Heating Rate 2-1/2°C/min

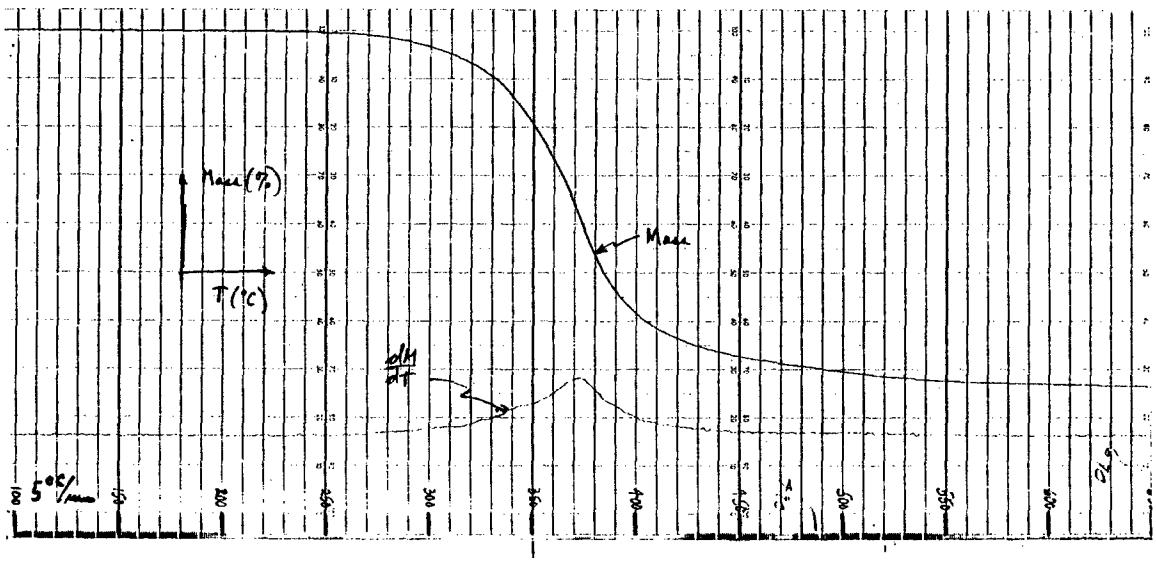

Figure C2 Thermogram (TGA) of H3501-5A Variation 12KV10 Std. Subscale Heating Rate 5°C/min

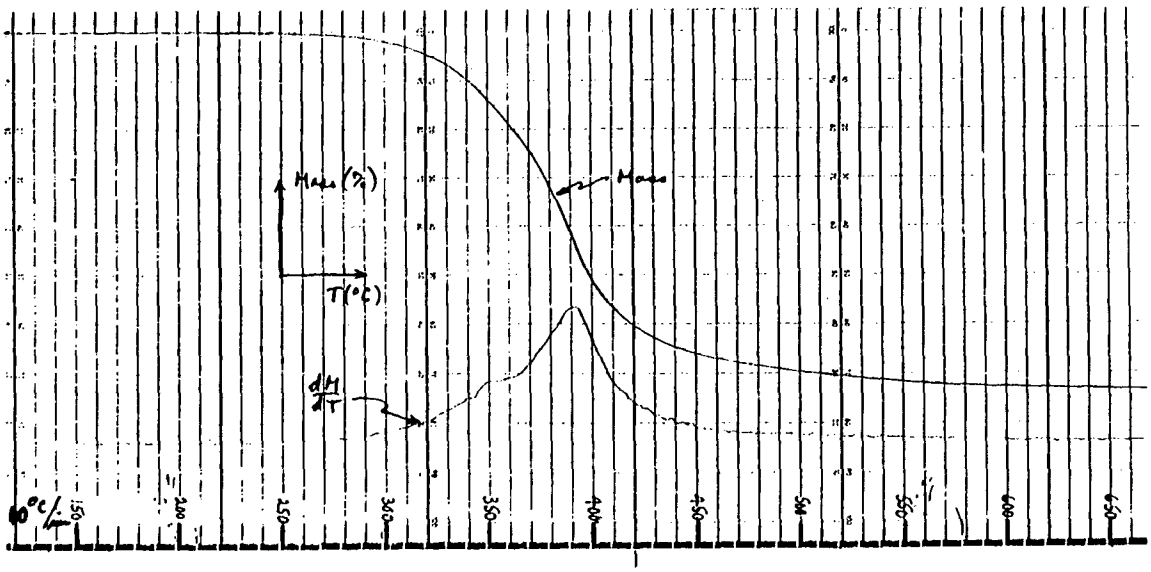

Figure C3 Thermogram (TGA) of H3501-5A Variation 12KV10 Std. Subscale Heating Rate 10°C/min

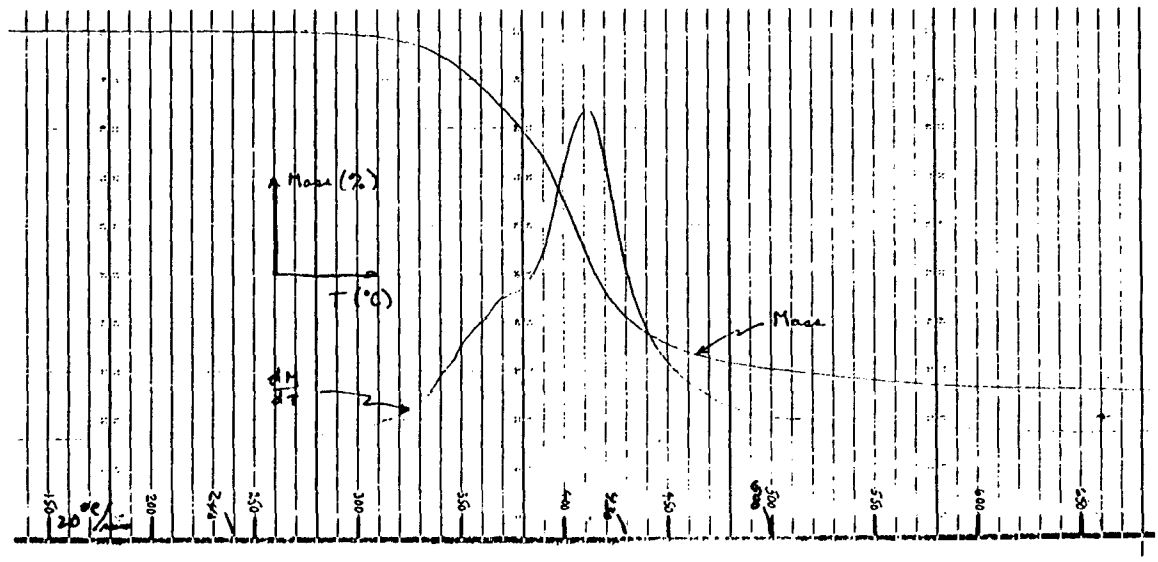

Figure C4 Thermogram (TGA) of H3501-5A Variation 12KV10 Std. Subscale Heating Rate 20°C/min

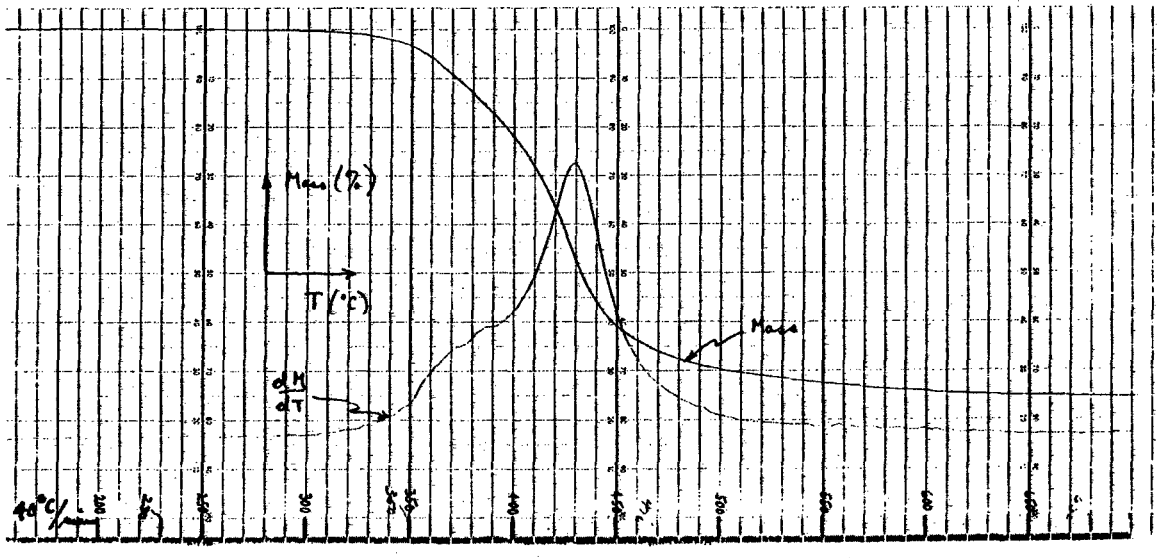

Figure C5 Thermogram (TGA) of H3501-5A Variation 12KV10 Std. Subscale Heating Rate 40°C/min

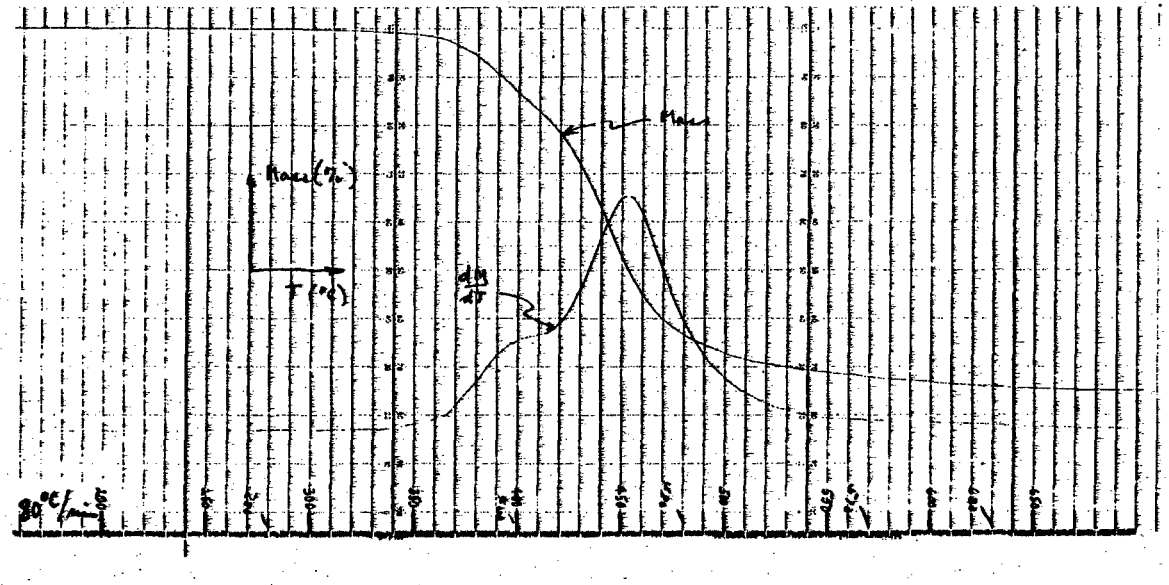

Figure C6 Thermogram (TGA) of H3501-5A Variation 12KV10 Std. Subscale Heating Rate 80°C/min

APPENDIX D

Cure Rheology; Torsion Braid Analysis Task 1 and Task 2

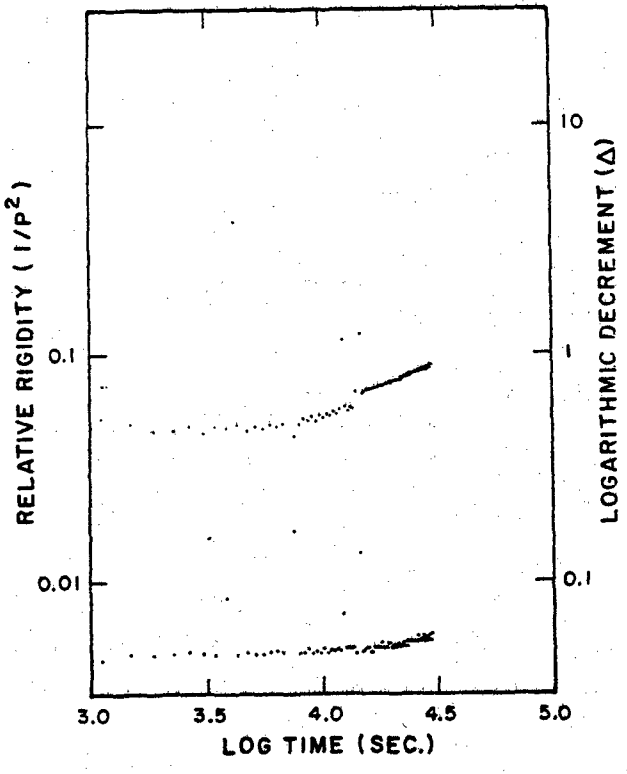

Fig. D-1 TBA Cure Spectra
RT to 90°C hold 2.5 hour to 5°.

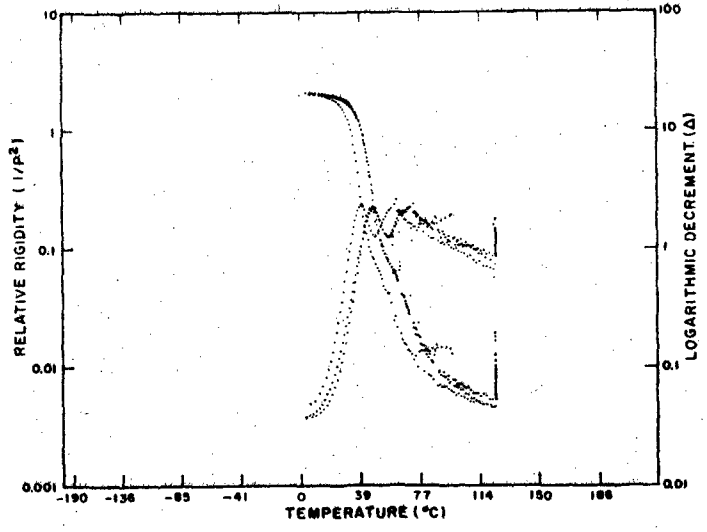

Fig. D-2 TBA Cure Spectra
5°C to 120° to 5° to 120° hold 1 hour.

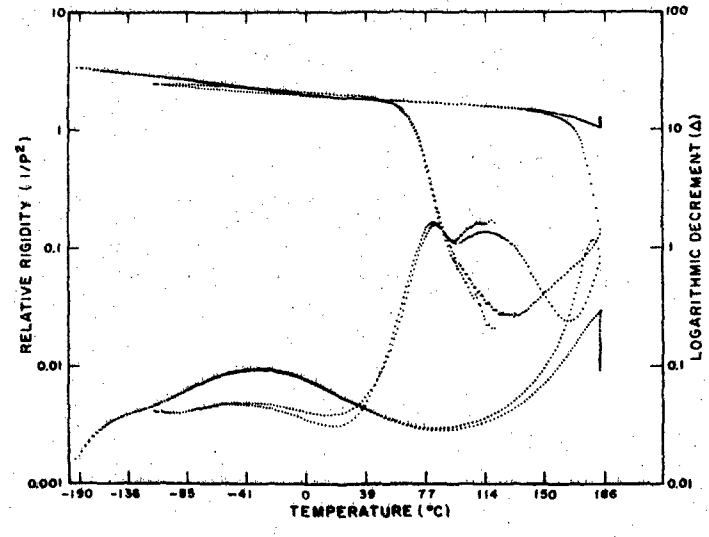

Fig. D-3 TBA Cure Spectra
120°C to -115° to 180° to -190° to 180° hold 0.5 hour.

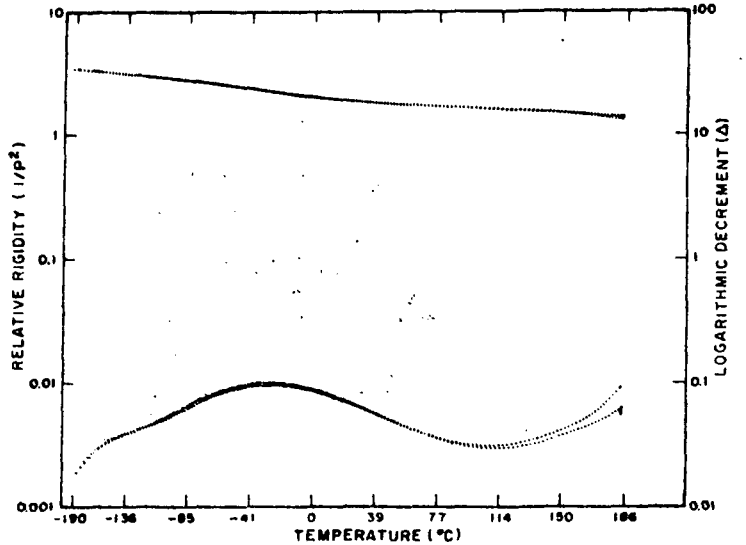

Fig. D-4 TBA Cure Spectra
180°C to -190° to 180° hold 0.5 hour.

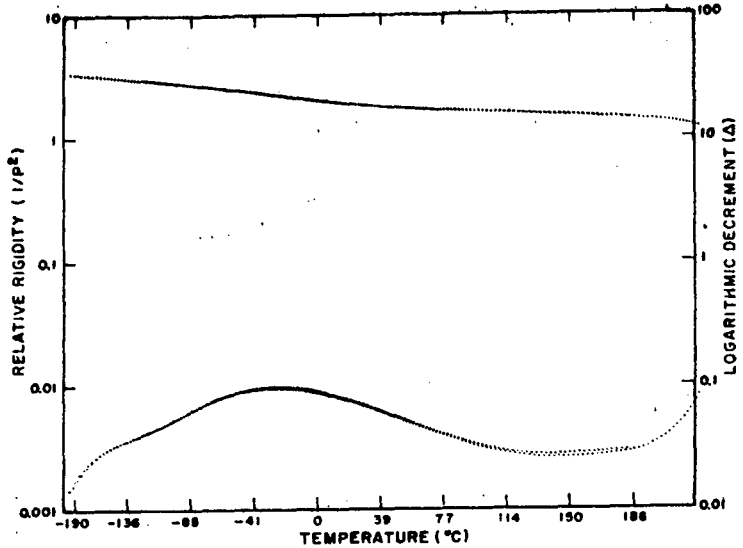

Fig. D-6 TBA Cure Spectra
180°C to -190° to 225°.

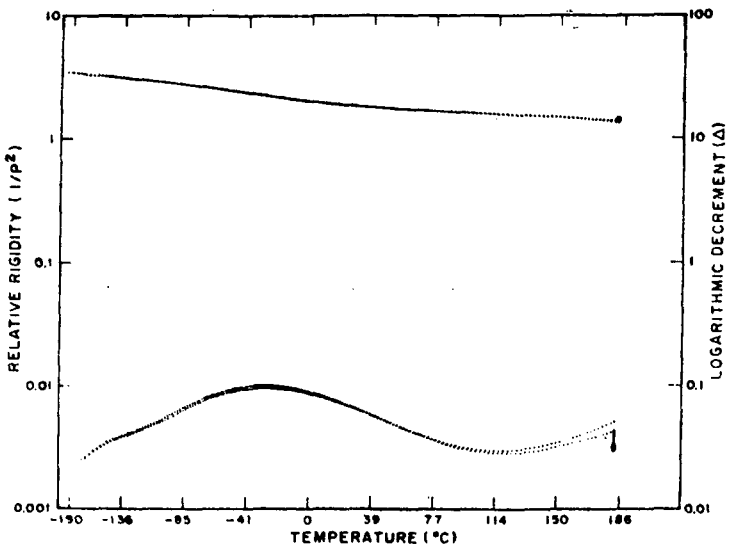

Fig. D-5 TBA Cure Spectra
180°C to -190° to 180° hold 8 hours.

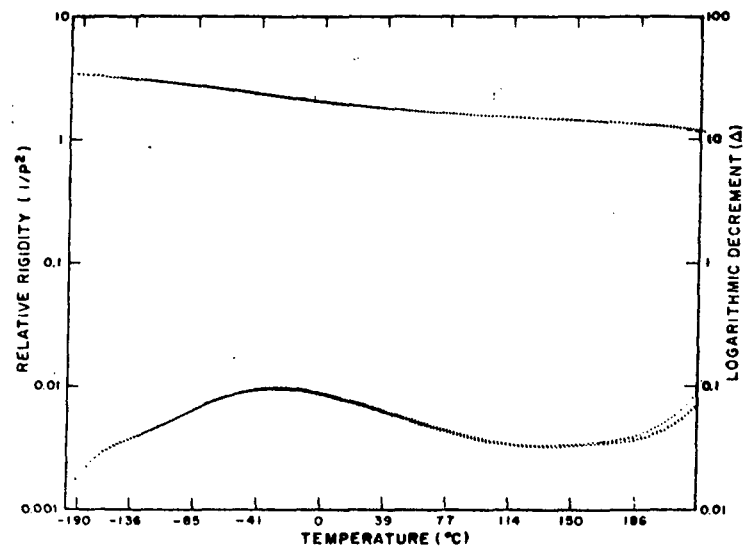

Fig. D-7 TBA Cure Spectra
225°C to -190° to 225°C hold 8 hours.

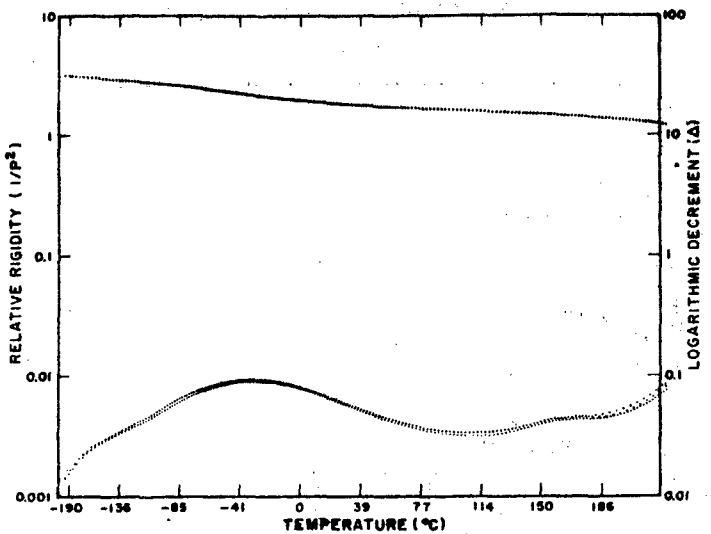

Fig. D-8 TBA Cure Spectra
225°C to -190° to 225°C to RT to 250°.

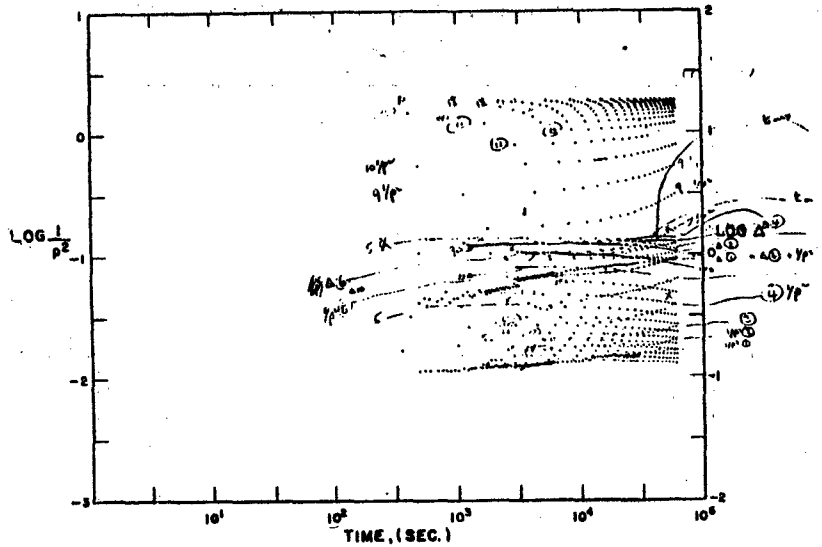

Fig. D-10A TBA Isothermal Cure
401 hours at 60°C.

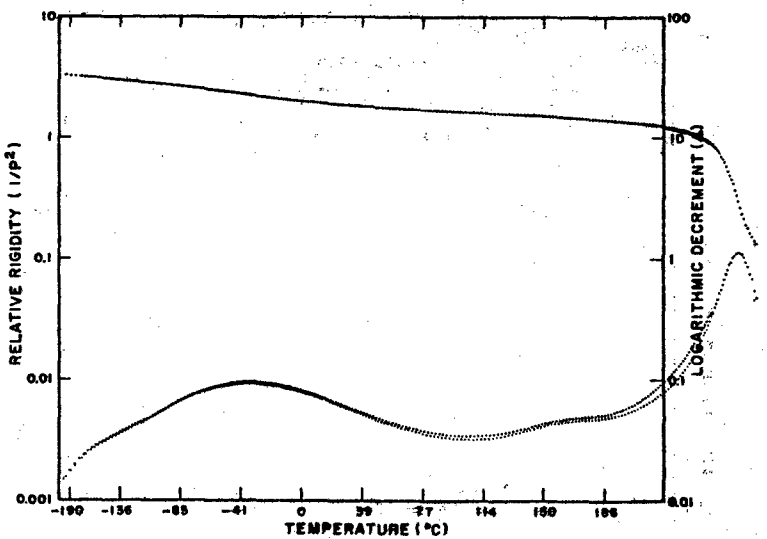

Fig. D-9 TBA Cure Spectra
250°C to -190° to 275°.

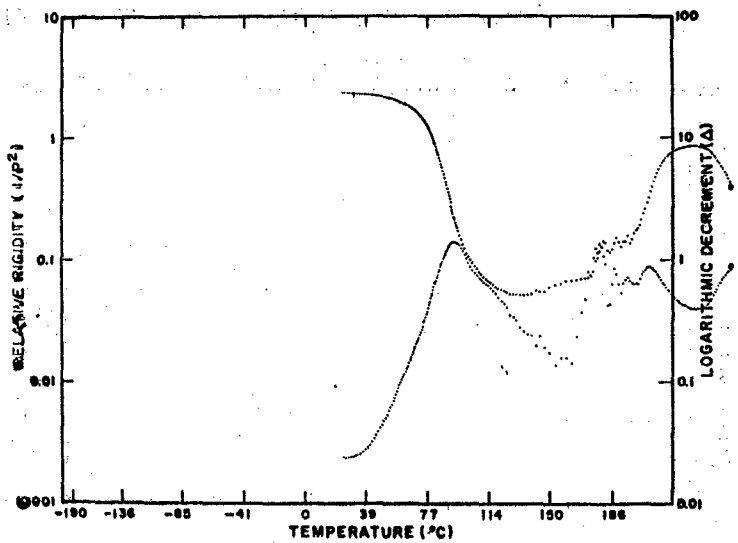

Fig. D-10B TBA Spectra Post Isothermal Cure
60°C to 25° to 250°, 2°C/min, hold 50 min.

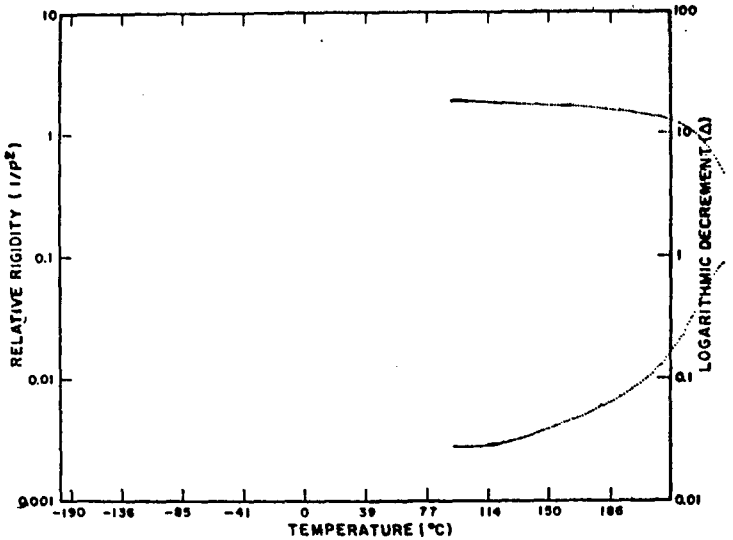

Fig. D-10C TBA Spectra Post Isothermal Cure 250°C to 90°, ≤ 2°C/min.

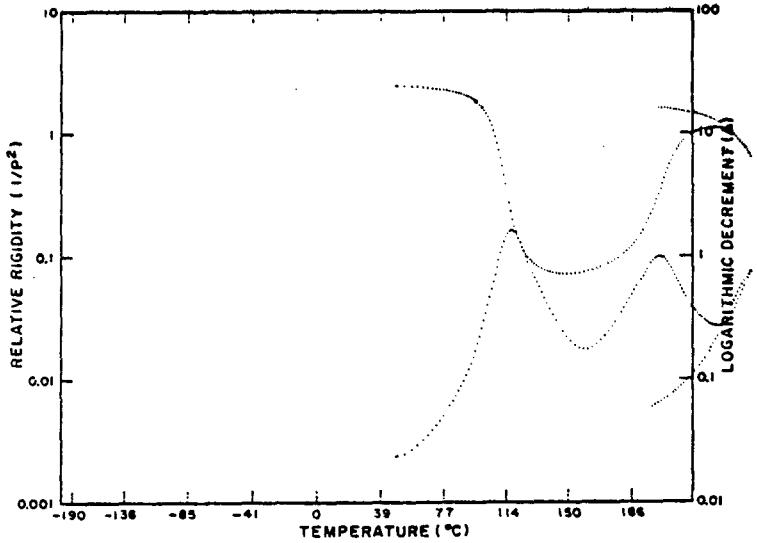

Fig. D-11B TBA Spectra Post Isothermal Cure 80°C to 50° to 250° to 190° . ≤ 2°C/min.

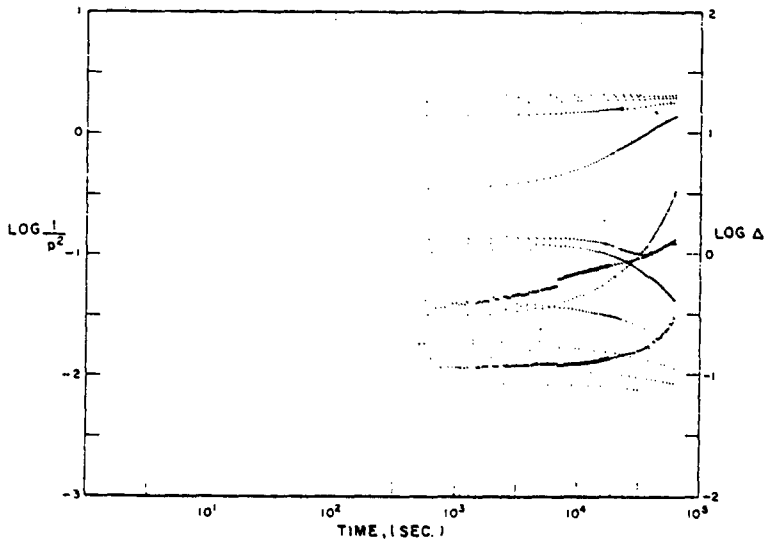

Fig. D-11A TBA Isothermal Cure 119 hours at 80°C.

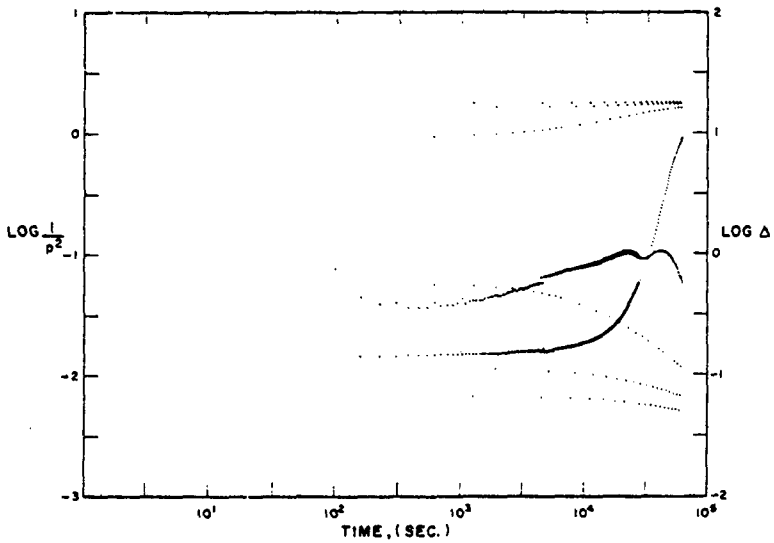

Fig. D-12A TBA Isothermal Cure 72 hours at 100°C.

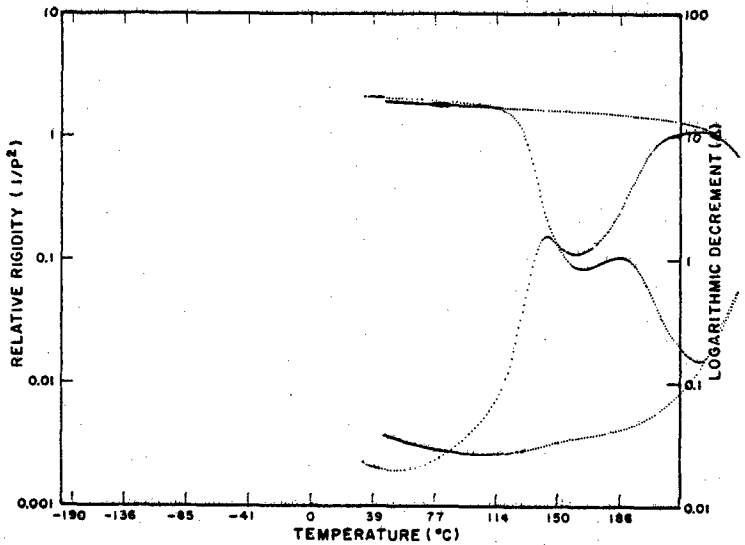

Fig. D-12B TBA Spectra Post Isothermal Cure
100°C to 33°C to 250° to 35° • ≤ 1.5°C/min.

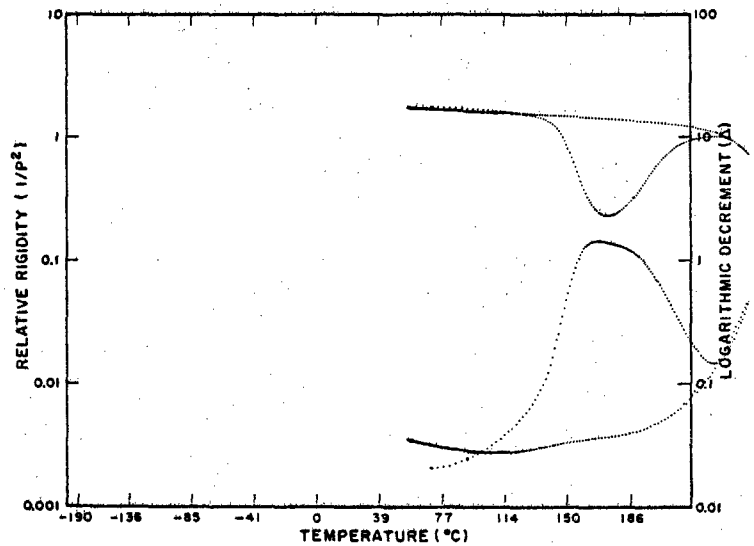

Fig. D-13B TBA Spectra Post Isothermal Cure
120°C to 70° to 250° to 55° • ≤ 2°C/min.

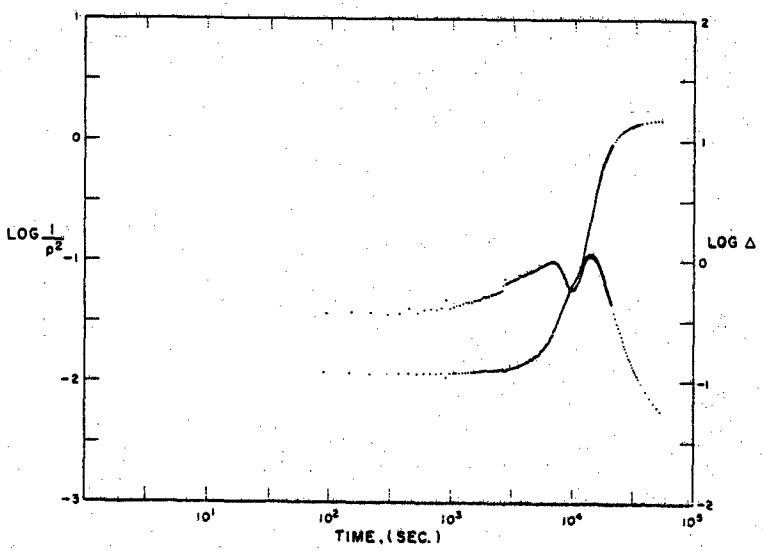

Fig. D-13A TBA Isothermal Cure
14.9 hours at 120°C.

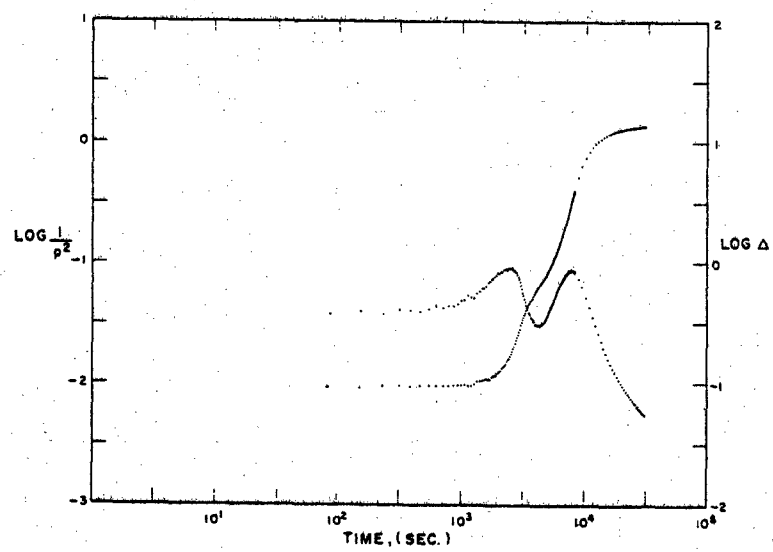

Fig. D-14A TBA Isothermal Cure
8.6 hours at 140°C.

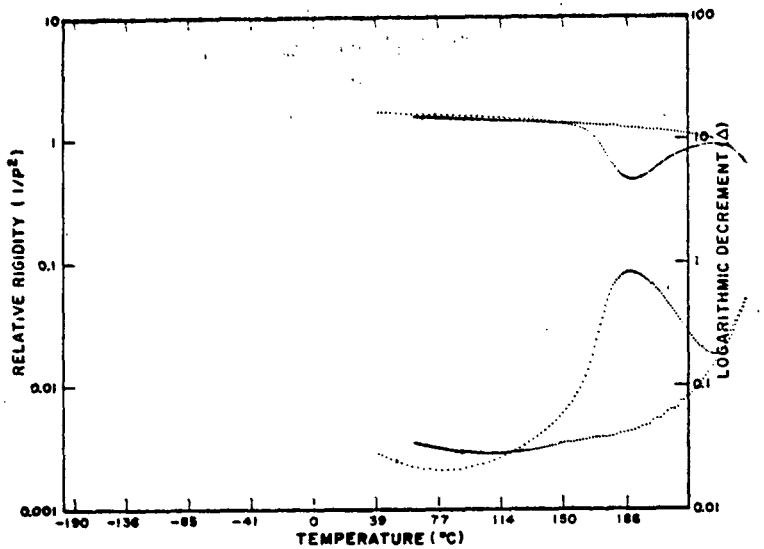

Fig. D-14B TBA Spectra Post Isothermal Cure 140°C to 40° to 250° to 60° . ≤ 2°C/min.

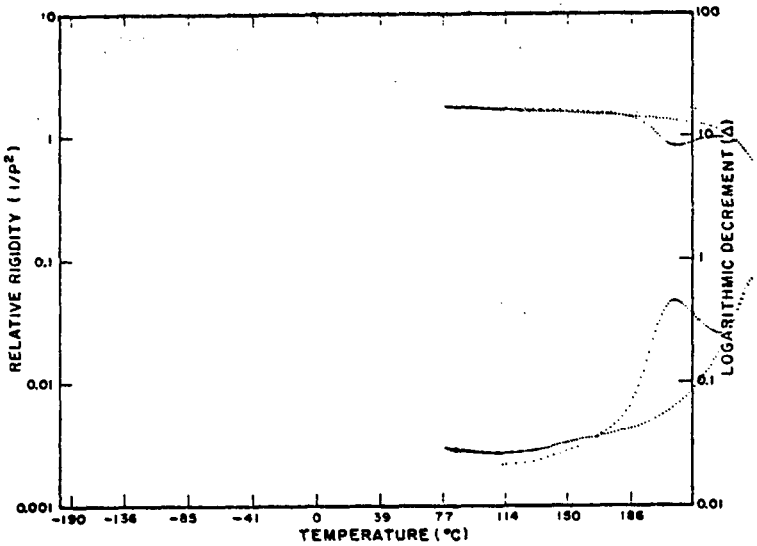

Fig. D-15B TBA Spectra Post Isothermal Cure 160°C to 110° to 250° to 75°. ≤ 2°C/min.

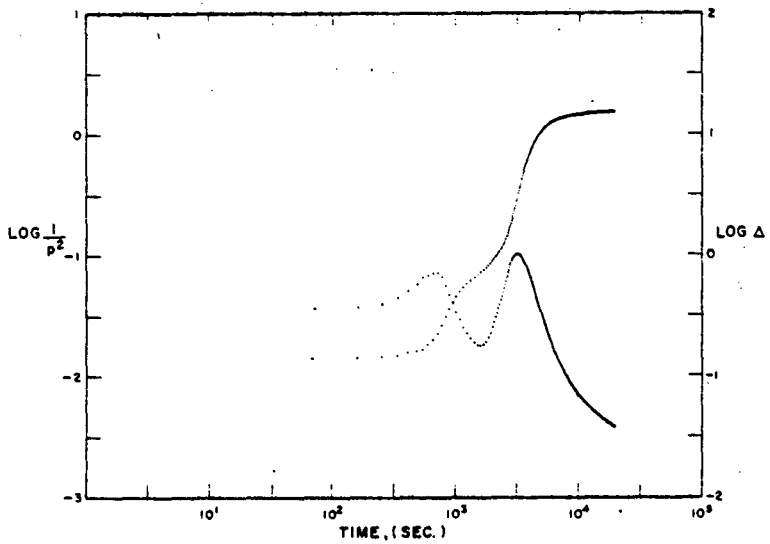

Fig. D-15A TBA Isothermal Cure 5.4 hours at 160°C.

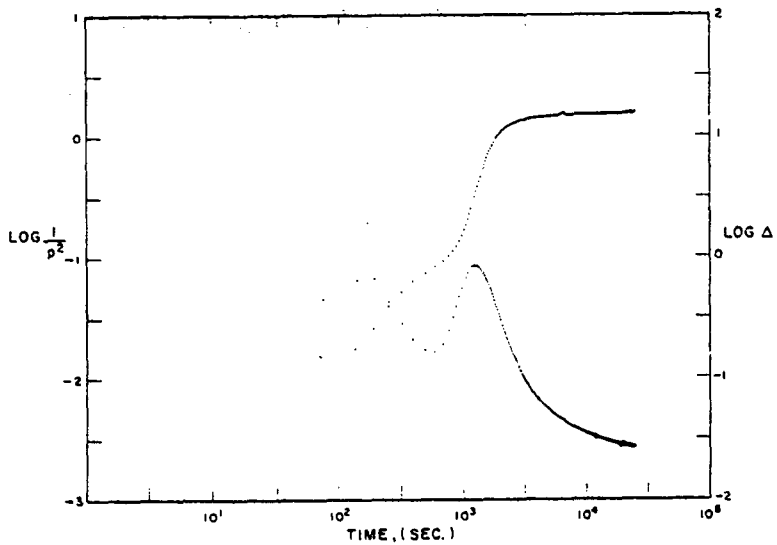

Fig. D-16A TBA Isothermal Cure 6.8 hours at 180°C.

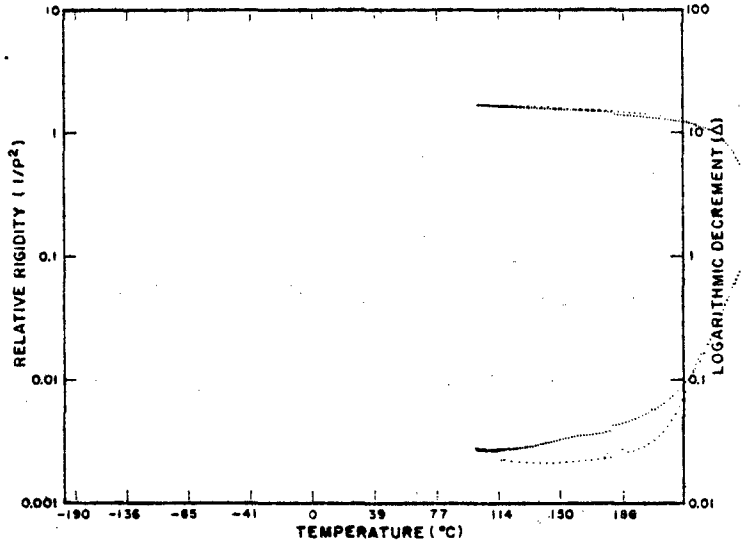

Fig. D-16B TBA Spectra Post Isothermal Cure
180°C to 115° to 250° to 100° • ≤ 2°C/min.

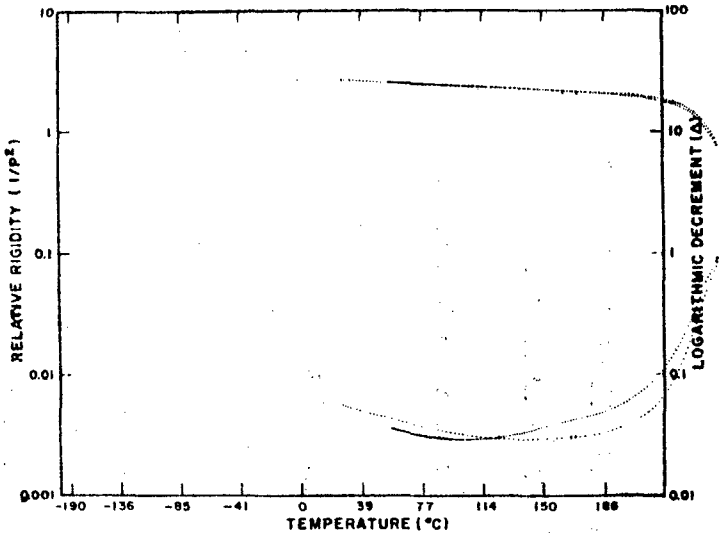

Fig. D-17B TBA Spectra Post Isothermal Cure
200°C to 25° to 250° to 58° • ≤ 2°C/min.

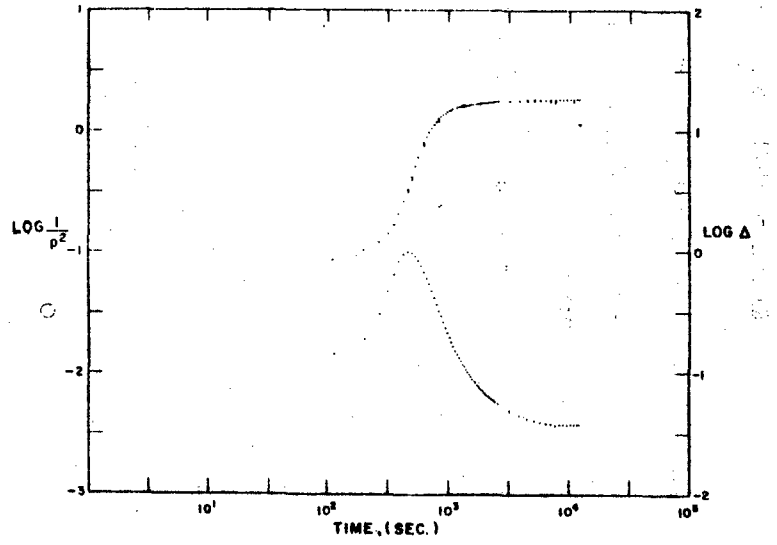

Fig. D-17A TBA Isothermal Cure
3.4 hours at 200°C.

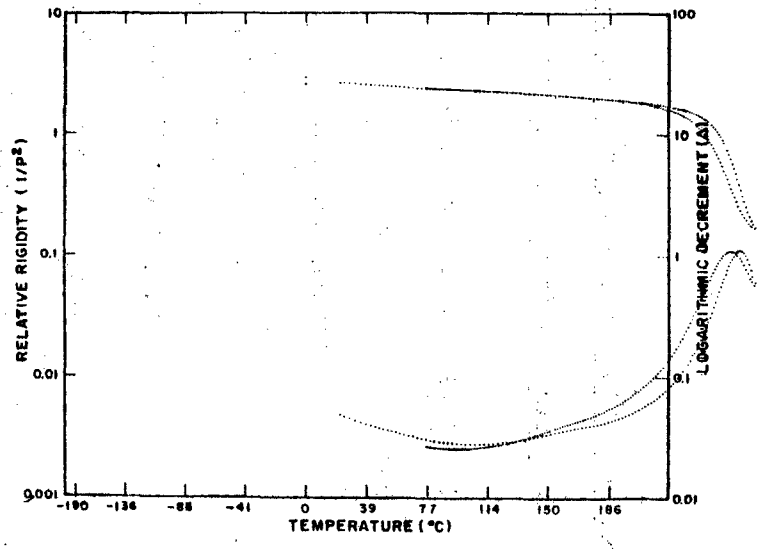

Fig. D-17C TBA Spectra Post Isothermal Cure
200°C to 25° to 270° to 75°. ≤ 2°C/min.

Determination of the Apparent Activation Energy for Reactions Leading to Gelation from the Time to Gelation vs Temperature of Cure

If gelation occurs at a fixed chemical composition then it follows that the

$$\text{Rate constant} = \text{Constant}/\text{time to gelation}$$

$$\text{Constant}/t_{gel} = A\, e^{-\Delta H/RT}$$

$$t_{gel} = (\text{Constant}/A)\, e^{\Delta H/RT}$$

$$\log_e t_{gel} = \text{Constant}' + \Delta H/RT$$

$$\log_e 10 \log_{10} t_{gel} = \text{Constant}' + \Delta H/RT$$

Plot of $\log_{10} t_{gel}$ vs $1/T$

$$\text{Slope} = \Delta H/R \log_e 10$$

From (Figure 21) Slope = 3.96×10^3

$$\Delta H = (3.96 \times 10^3) \times 1.987 \times 2.3025$$

units T cal mol^{-1} T^{-1}

$$= 18.05 \text{ kcal/mole}$$

REFERENCES

1. ASTM Standards, 1976 Annual Book of, Part 36, Plastics-Materials, Film, Reinforced and Cellular Plastics; Fiber Composites.

2. ASTM Standards, 1976 Annual Book of, Part 35, Plastics-General Test Methods; Nomenclature.

3. Schmitz, J.V., Brown, W.E. et al, Edited by, Testing of Polymers, Vol. 1, 2, 3, and 4; John Wiley & Sons, Inc.

4. Kelley, F.N., and Williams, M.L. "The Engineering of Polymers for Mechanical Behavior", Rubber Chemistry and Technology, Vol. 42, No. 4; September 1969.

5. Ragland, W. "A Technique for Preparing Void-Free Cast Resin Test Specimens", University of Dayton Research Institute UDRI-TM-77-18; October 1977.

6. Smith, T.L. "Dependence of the Ultimate Properties of an SBR Rubber on Strain Rate and Temperature," Journal of Polymer Science, Vol. 32, p. 99, 1958.

7. Smith, T.L. "Stress-Strain-Time-Temperature Relationships for Polymer." ASTM Special Technical Publication No. 325, American Society for Testing Materials, p. 60-89, 1962.

8. ASTM Designation E 399-78, Standard Test Method for Plane Strain Fracture Toughness of Metallic Materials, Annual Book of ASTM Standards Part 10, pp. 512-531, 1978.

9. Tada, H., Paris, P.C. and Irwin, G.R., The Stress Analysis of Cracks Handbook, Del Research Corporation, Hellertown, Pennsylvania, p. 1.2 and p. 2.13-2.14, 1973.

10. Kausch, H.H., Polymer Fracture, Springer-Verlag, New York, 1978, p. 267.

11. Kausch, H.H., op. cit., p. 254.

12. Tada, H. et al, op. cit., p. 1.12.

13. Orr, L. "Fracture Analysis in Glass", Proceedings of the Fifth U.S. National Congress of Applied Mechanics, Univ. of Minnesota, June 1966, American Society of Mechanical Engineers, N.Y., p. 580.

14. Sneedon, I.N., Lowengrub, M., Crack Problems in the Classical Theory of Elasticity, John Wiley & Sons, Inc., N.Y., 1969, p. 7, 130.

15. Tada, H. et al, op. cit., p. 24.1.

16. Eirich, F.R. (Edited by) Rheology, Vol. I, Academic Press, Inc., N.Y., 1956, p. 397.

17. Ward, I.M., Mechanical Properties of Solid Polymers, Wiley-Interscience, N.Y., 1971, p. 94.

18. Christensen, R.M., Theory of Vicsoelasticity, an Introduction, Academic Press, N.Y., 1971, p. 11.

19. Suh, N.P., and Turner, A.P.L., Elements of the Mechanical Behavior of Solids, Scripta Book Co., Washington, D.C., 1975, pp. 320-325.

20. Ward, I.M., op. cit., p. 96-105.

21. Timoshenko, S.P., Young, D.H., and Weaver, W., Jr., Vibration Problems in Engineering, 4th Ed., John Wiley & Sons, N.Y., 1974, p. 442.

22. Timoshenko, S.P. et al, op. cit., p. 424.

23. ASTM Designation E 99-66 Reapproved 1972, Standard Test Methods for Water Vapor Transmission of Materials in Sheet Form, Annual Book of ASTM Standards, Part 18, pp. 743.

24. Yasuda, H., Stannett, V., "Permeability Coefficients", Polymer Handbook, Edited by J. Brandrup and E.H. Immergnt, Wiley Interscience, N.Y. (1975) p. 111-229.

25. Flynn, J.H. and Wall, L.A., J. Polymer Sci., Part B, Polymer Letters, 4, 323, (1966).

26. Gillham, J.K. et al, Chemistry and Properties of Crosslinked Polymers, Academic Press, N.Y. 491 (1977).

27. Gillham, J.K., "A Semimicro Thermochemical Technique for Characterizing Polymeric Materials: Torsional Braid Analysis", AIChE Journal, Vol. 20, No. 6, Nov. 1974, p. 1066-1079.

28. Somcynski, T., Simha, R.,"Hole Theory of Liquids and Glass Transition" J. Appl. Phys. Vol 42, No. 12, Nov. 1971, p 4545.

29. Quach, A., and Simha, R.,"Statistical Thermodynamics of the Glass Transition and the Glassy State of Polymers", J. Phys. Chem. Vol. 76, No. 3, Feb. 1972, p. 416.

30. Timoshenko, S., Strength of Materials, Part 1, D. Van Nostrand, Inc., N.Y., 1960, p. 67.

31. Quach, A., and Simha, R., "Pressure-Volume-Temperature Properties and Transitions of Amorphous Polymers, Polystyrene and Poly(orthomethylstyrene)", J. Ap. Phys. Vol. 42, 1971, p. 4592.

32. Bridgman, P. W., "The Physics of High Pressure", Proc. Am. Acad. Arts Sci., Vol. 66, 1931, p. 185; (Bell and Sons, London, 1952)

33. Zoller, P., Bolli, P., Pahud, V., and Ackermann, H., "Apparatus for Measuring Pressure-Volume-Temperature Relationships of Polymers to 350°C and 2200 kg/cm^2", Rev. Sci. Instrum., Vol. 47, No. 8, Aug. 1976.

34. ASTM Designation C693-74, Density of Glass by Buoyancy, 1978 Annual Book of Standards, Part 17, p. 695-697.

35. Handbook of Chemistry and Physics, edited by R. C. West, 60th Ed., The Chemical Rubber Co, Cleveland, 1979-80.

36. Carnazzi, P., Nuovo Cimento 5, 180 (1903)

☆U.S.Government Printing Office: 1981 — 559-006/5040